UNIVERSITY OF CALIFORNIA
RIVERSIDE

Investigating the Mechanism of MicroRNA Turnover and Characterizing the Role of RCD1 During Small RNA Metabolism in *Arabidopsis*

A Dissertation submitted in partial satisfaction
of the requirements for the degree of

Doctor of Philosophy

in

Plant Biology

by

Yu Yu

September 2017

Dissertation Committee:
Dr. Xuemei Chen, Chairperson
Dr. Julia Bailey-Serres
Dr. Ted Karginov

The Dissertation of Yu Yu is approved:

Committee Chairperson

University of California, Riverside

Acknowledgements

I am deeply grateful to everyone around me without whom this work would not have been possible.

First and foremost, I would like to express my deepest gratitude to my advisor Dr. Xuemei Chen. I am indebted to her for her continuous guidance, sound advice and patient encouragement throughout my PhD study. From her, I have not only learned how to think critically and work efficiently, but also learned what is a real scientist. Her constant passionate to science has helped me through many challenging times. I earnestly appreciate her mentorship and support that would provide a strong foundation for my future career.

I would also like to thank the other members in my dissertation committee: Dr. Julia Bailey-Serres and Dr. Ted Karginov for their valuable comments, thoughtful advice, and positive feedback, keeping me on track toward my dissertation work. My sincere thanks additionally go to other faculties who were in my qualify examination committee and guidance committee for their time and insightful suggestions including Dr. Linda Walling, Dr. Patricia Springer, Dr. Thomas Eulgem, Dr. Eugene Nothnagel and Dr. Wenbo Ma.

Furthermore, I am thankful for all the professors who taught me during my PhD study at UC Riverside and during my master and undergraduate study at Shenzhen University in China. I am especially grateful to my master degree advisor, Dr. Beixin Mo, who opened me the window to plant science and who further paved me the odyssey to work in Dr. Chen's lab.

In addition, I wish to thank every member in Dr. Chen's lab. I am fortunate to have such fabulous people around me, allowing me to work in an inspiring and homelike environment. They not only brought me many happy memories, but also supported me to

overcome challenges. I would particularly like to thank Dr. Shengben Li for passing on a lot of background knowledges and experimental skills during my early PhD study. His constant suggestions and help motivated me to partake in this long journey successfully.

The second chapter of this dissertation, in full, is a reprint with some rearrangements and minor alternations of a published article. I gratefully acknowledge the approval for using the article published in PLoS Biology (PLoS Biol. 2017 Feb 23;15(2):e2001272). Dr. Xuemei Chen directed and supervised the research that formed the basis for Chapter 2 of this dissertation. Drs. Xiaofeng Cao, Beixin Mo, Jinbiao Ma and Blake C. Meyers offered some molecular and genetic materials and bionomical assistance. Drs. Lijuan Ji, Brandon Le, Jixian Zhai, Jiayi Chen, Elizabeth Luscher, Lei Gao and Chunyan Liu provided their technical expertise in different aspects.

Last but not least, I want to express my sincere gratitude to my family and friends. Without their love and support, I would not be able to have delivered this work. In particular, I feel deeply beholden to my parents for their unconditional love, for their understanding that I could not accompany them for so many years, and for their constant encouragement during those challenging times.

Author Contributions

The following is a document stating the author contributions for each section of this dissertation.

The whole Chapter One was written and organized by myself.

For Chapter Two, a former postdoc Dr. Vanitha Ramachandran performed the cross between the *sdn1* and *sdn2* mutants, a former graduate student Dr. Yuanyuan Zhao performed the cross between the *heso1-1* and *hen1-8* mutants, a fellow graduate student Elizabeth Luscher performed the cross between the *hen1* and *sdn1 sdn2* mutants. A former graduate student Dr. Lijuan Ji generated the transgenic lines, including *AGO10 OE S1*, *AGO10 OE 4mAGO1* and *AGO10 OE sdn1 sdn2*. I constructed the small RNA libraries for *hen1* vs. *hen1 sdn1 sdn2*, Col vs. *sdn1 sdn2*, *hen1* vs. *hen1 heso1*, *AGO10 OE lines S2*, *M1*, *M2* and *W1*. All the sequencing data was analyzed by a current postdoc Dr. Brandon Le. The small RNA libraries for Col, *AGO10 OE S1*, *AGO10 OE 4mAGO1* and *AGO10 OE sdn1 sdn2* were constructed by Dr. Lijuan Ji. The sequencing data was coordinately analyzed by a former graduate student Dr. Jixian Zhai in Dr. Blake Meyers' lab, a former postdoc Dr. Lei Gao and Dr. Brandon Le in Dr. Xuemei Chen's lab. I expressed and purified the SDN1 proteins, and performed the SDN1 assay with AGO immunoprecipitates followed by small RNA library construction. All the sequencing data was analyzed by Dr. Brandon Le. I performed all the experiments in two *ago10* mutants and some experiments in *AGO10 OE* lines, and the rest experiments in *AGO10 OE* lines were performed by Dr. Lijuan Ji. The *YFP-ZLL* and *His-Flag-AGO10* lines were provided by Dr. Thomas Laux and Dr. Xiuren Zhang, respectively. The *SDN1* constructs and anti-AGO1 antibody were provided by a graduate student Jiayi Chen in Dr. Jinbiao Ma's lab

and Dr. Chunyan Liu in Dr. Xiaofeng Cao's lab, respectively. This project was supported by a funding to Dr. Xuemei Chen and Dr. Beixin Mo.

For Chapter Three, the *int51* mutant was provided by Dr. Jian Hua. I performed the small RNA libraries construction, northern blotting, qPCR, McrBc treatment and western blotting. A former postdoc Dr. Lin Liu performed the bisulfate sequencing. All the bioinformatic analysis was performed by Dr. Brandon Le.

For Appendix A, the mutants in double-stranded RNA binding proteins *DRB2*, *DRB3* and *DRB5* were ordered from Arabidopsis Biological Resource Center (ABRC). I performed the genotyping to isolate homozygous mutants. The *SUC2::amiR-SUL* and *SUC2::siR-SUL* reporter lines were provided by Dr. Olivier Voinnet and Dr. Detlef Weigel, respectively. I performed the crosses between the *drb* mutants and the two reporter lines to generate a series of mutants in reporter line backgrounds. I also performed all other experiments as mentioned.

ABSTRACT OF THE DISSERTATION

Investigating the Mechanism of MicroRNA Turnover and Characterizing the Role of RCD1 During Small RNA Metabolism in *Arabidopsis*

by

Yu Yu

Doctor of Philosophy, Graduate Program in Plant Biology
University of California, Riverside, September 2017
Dr. Xuemei Chen, Chairperson

Small RNAs are a class of non-coding RNAs that mediate gene silencing at both transcriptional and post-transcriptional levels in eukaryotes. In plants, microRNAs (miRNAs) and small interfering RNAs (siRNAs) are two core types of small RNAs, which play essential roles in diverse biological processes. Both the metabolism and activities of small RNAs contribute to the regulation of their targets. Even though many on small RNA pathway have been reported, the detailed mechanism on its metabolism is still lacking. To address this issue, my thesis research has employed multidisciplinary approaches and techniques. The achieved results and conclusions can be closed as the following. First, it was found in this research that an Argonaute protein AGO10 represses the accumulation of miR165/6 without affecting its biogenesis. AGO10 overexpression results in a reduction in full-length miR165/6 species accompanied with an elevated 3’

truncation of miR165/6, which is rescued by losses of two exonucleases SDN1 and SDN2. An enzymatic assay between SDN1 and AGO10 immunoprecipitates *in vitro* was carried out, which confirms that AGO10 represses the accumulation of miR165/6 through promoting its degradation via SDN1. A similar assay between SDN1 and AGO1 immunoprecipitates was also performed, allowing the proposal of a model on miRNA degradation. This is the work reported in the Chapter Two of this dissertation. Second, in this research, through small RNA sequencing and comparison to wild type, many siRNAs were identified to be differentially expressed in the *rcd1* mutant (*int51)*. A whole-genome bisulfate-sequencing reveals that DNA methylation in all sequence contexts is greatly reduced on euchromatic arms in *int51*, while is not changed at heterochromatic regions. It was further found that the global level of H3K9me2 is reduced in *int51*. The changes observed in *int51* resemble those of mutants defective in DNA or histone methylation, providing a novel insightful hint to dissect the RCD1-mediated regulatory network further. My research towards elucidating this network is reported in Chapter Three. Taken together, my dissertation research has established new understanding on the mechanism of plant miRNA degradation and has also identified a novel candidate in plant siRNA metabolism.

Table of Content

Chapter 1 Introduction: Metabolism and function of miRNAs in plants..... 1

Abstract 1

Introduction..... 2

References 26

Figures 38

Chapter 2 Argonaute 10 promotes degradation of miR165/6 through exonucleases SDN1 and SDN2 in Arabidopsis 44

Abstract 44

Introduction.....45

Results 48

Discussion 61

Materials and Methods 64

References 69

Figures and Tables.....73

Chapter 3 Characterization of Arabidopsis RCD1's role in small RNA metabolism 105

Abstract 105

Introduction.....106

Results 110

Discussion 120

Materials and Methods 123

References 128

Figures and Tables 133

Conclusions and Respectives 158

Appendix A: Double-stranded RNA binding proteins in Arabidopsis 162

Appendix B: Collaborated projects and publications 180

Appendix C: Approval of using the published article in PLoS Biology 182

List of Figures

Figure 1.1 Illustrations of major steps in miRNA biogenesis in plants. 38

Figure 1.2 Overview of miRNA modes of action in plants. 40

Figure 1.3 Mechanisms of plant miRNA turnover.....42

Figure 2.1 SDN1 and 2 are responsible for miRNA 3' truncation *in vivo*. 73

Figure 2.2 Matrices representing the composition of reads for various miRNAs in *hen1* and *hen1 sdn1 sdn2* libraries.....75

Figure 2.3 A model of miRNA degradation. 77

Figure 2.4 SDN1 enzymatic assays with AGO1 and AGO10 IP as substrates. 79

Figure 2.5 Hierarchical clustering analysis showing the degree of similarity among the sRNA-seq libraries.....81

Figure 2.6 SDN1 is able to trim AGO1- and AGO10-bound miRNAs *in vitro*. 83

Figure 2.7 *ago10* mutations do not affect miR165/6 biogenesis.....85

Figure 2.8 *AGO10* over expression causes reduced miR165/6 accumulation. 87

Figure 2.9 Characterization of *AGO10* over expression lines.....89

Figure 2.10 *AGO10* over expression results in reduced levels of full-length and increased levels of 3' truncated miR165/6.....91

Figure 2.11 Matrices representing the composition of miR165/6 reads in Col, *AGO10 OE S1* and *AGO10 OE 4mAGO1* libraries. 93

Figure 2.12 *AGO10* over expression results in sequestration of miR165/6 from AGO1. 95

Figure 2.13 3' truncated miRNAs in *AGO10 OE* are preferentially bound by AGO10.....97

Figure 2.14 *AGO10* over expression-induced miR165/6 3' truncation requires SDN1 and SDN2.....99

Figure 2.15 Matrices representing the compositions of miR165/6 reads in *AGO10 OE* and *sdn1 sdn2 AGO10 OE* libraries.....101

Figure 3.1 Loss of *RCD1* does not affect the abundance or activity of miRNAs and tasiRNAs. 133

Figure 3.2 Loss of *RCD1* induces differential expression of siRNAs across the genome. 135

Figure 3.3 24-nt hyper-DSRs are mainly LTR-Gypsy TEs localized in the pericentromeric region. 137

Figure 3.4 The accumulation of 24-nt siRNAs within specific genomic locations.....139

Figure 3.5 The biogenesis of 24-nt siRNAs at *int51* hyper-DSR loci requires components of diverse pathways. 141

Figure 3.6 The biogenesis of 24-nt siRNAs at hyper-DSR loci requires components of the RdDM pathway. 143

Figure 3.7 Loss of function in *RCD1* does not affect DNA methylation at hyper-DSR loci. 145

Figure 3.8 *int51* hypo-DSRs have reduced DNA methylation in all sequence contexts. 147

Figure 3.9 H3K9me2 methylation is impaired in the *int51* mutant. 149

Figure 3.10 Histone modification is altered in *drm1 drm2 cmt2 cmt3* and *suvh4 suvh5 suvh6* mutants. 151

Figure 3.11 Global levels of histone marks in wild type (Col) and the *int51* mutant. 153

Figure A.1 Loss of *DRB2* does not affect the accumulation of miRNAs. 166

Figure A.2 DRB2 may play a role in miRNA-mediated translational repression. 168

Figure A.3 DRB2 has no effect on the expression of players involved in miRNA biogenesis. 170

Figure A.4 Losses of *DRB2* and *DRB3* enhance the photobleached phenotype of *SUC2::siR-SUL* reporter line. 172

Figure A.5 *SUL* mRNA level is impaired in both *drb2 sucsul* and *drb3 sucsul* plants. ..174

Figure A.6 DRB2 and DRB3 repress the accumulation of *SUL* siRNAs. 176

List of Tables

Table 2.1 *sdn1 sdn2* partially suppresses the developmental phenotype of *AGO10 OE*. 103

Table 2.2 Oligonucleotides used in this study. 104

Table 3.1 Number of hypo- and hyper-DSR loci identified in the *int51* mutant. 155

Table 3.2 Oligonucleotides used in this study. 156

Table A Oligonucleotides used in this study.....178

Chapter 1

Introduction: Metabolism and function of miRNAs in plants

Abstract

MicroRNAs (miRNAs) are small non-coding RNAs that regulate gene expression at post-transcriptional level through sequence complementarity. Since the identification of the first miRNA, lin-4, in the nematode *Caenorhabditis elegans* in 1993, thousands of miRNAs have been discovered in animals and plants, and their regulatory roles in numerous biological processes have been uncovered. In plants, research efforts have established the major molecular framework of miRNA biogenesis and modes of action, and are beginning to elucidate the mechanisms of miRNA degradation. Studies have implicated restricted and surprising subcellular locations where miRNA biogenesis or activity takes place. In this chapter, the current knowledge on how plant miRNAs are made and degraded and how they repress target gene expression are summarized. not only the players involved in these processes but also the subcellular sites where these processes are known or implicated to take place are discussed.

Introduction

Small RNAs are a class of non-coding RNAs 20-30 nucleotide (nt) in length that mediate gene silencing in eukaryotes [1-4]. In the past two decades since the first small RNA, lin-4, was discovered in the nematode *Caenorhabditis elegans* in 1993 [5], hundreds of thousands of small RNAs, including those at very low abundance, have been identified in diverse eukaryotes through high-throughput sequencing and bioinformatics prediction [6-8]. Due to the broad impacts of small RNAs in regulating gene expression *in vivo* and their potential as a powerful technology [1,3,4,9,10], there has been a great deal of focus on dissecting the mechanisms of small RNA metabolism and their regulatory machinery. In recent years, more and more small RNAs have been reported to function in human diseases and cancers [11-13], further underscoring the urgency and importance of deciphering small RNA-based mechanisms.

Small RNAs are classified into three major types based on their precursors, biogenesis and associated proteins: microRNAs (miRNAs), small interfering RNAs (siRNAs) and Piwi-interacting RNAs (piRNAs) [2-4,9]. MiRNAs, usually 21-24 nt in length, are generated from single-stranded RNA (ssRNA) precursors containing a stem-loop structure with usually an imperfectly base-paired stem. The processing of precursors into mature miRNAs requires the activity of RNase III-type endonucleases DROSHA and DICER in animals or DICER-LIKE (DCL) in plants. SiRNAs are 21-24 nt long, and their biogenesis also requires DICERS in animals or DCLs in plants. Unlike miRNAs, they are derived from long double-stranded RNA (dsRNA) precursors produced by RNA-DEPENDENT RNA POLYMERASE (RDR) or transcripts of inverted repeat elements with perfect sequence complementarity. Both miRNAs and siRNAs are associated with the Argonaute sub-clade of ARGONAUTE (AGO) proteins. PiRNAs are processed from

ssRNA precursors in a DICER-independent manner. Mature piRNAs are usually 24-32 nt long and bound by the Piwi sub-clade of AGO proteins. While miRNAs and siRNAs exist in both plants and animals, piRNAs are specifically found in animals [2-4,9].

Small RNAs play essential roles throughout the life of living organisms, despite their small size. They recognize target nucleic acids in a sequence-specific manner and mediate gene silencing at the transcriptional or post-transcriptional level. In transcriptional gene silencing (TGS), small RNAs guide DNA methylation or histone methylation to repress the transcription of transposons and transgenes to maintain genome stability. In post-transcriptional gene silencing (PTGS), small RNAs repress gene expression through cleavage, decay or translation inhibition of target transcripts derived from protein-coding genes, transposable elements and viral RNAs [2-4,9].

miRNAs and siRNAs are the two major types of small RNAs in plants [2]. Although miRNAs constitute only a small fraction of small RNAs, they markedly impact diverse biological processes by repressing target gene expression primarily at the post-transcriptional level. The many growth and developmental processes regulated by miRNAs include the development of rosette leaves and roots, floral morphogenesis, apical dominance of stems, and hormone signaling [1,2]. MiRNAs also mediate plant abiotic stress responses to drought and high salinity as well as plant immunity against viruses and bacteria [1,2]. Defects in miRNA metabolism or activity often lead to developmental abnormalities and compromised stress responses. Plants may even display pleiotropic phenotypes when the accumulation or function of a single miRNA is disrupted [1,2]. For example, *Arabidopsis* miR165/6 is regulated by AGO10 in the maintenance of stem cells and leaf polarity [14-16]. It is therefore essential to understand how miRNA levels are precisely maintained and dynamically regulated *in vivo* as well as the factors that mediate

and/or affect miRNA activities. The steady-state level of miRNAs depends on the balance of biogenesis and turnover. While the miRNA biogenesis pathway is well established, many aspects of miRNA turnover and mode of action remain ill-defined. Thus, new research needs to address how miRNAs are degraded and how miRNAs regulate their targets.

Biogenesis of plant miRNAs

MiRNA biogenesis is a multi-step process involving many essential proteins (Figure 1.1). Although some differences have been described, the miRNA biogenesis pathway is similar between animals and plants, and it includes transcription, processing, modification and assembly of RNA-induced silencing complex (RISC).

Transcription

MiRNAs are encoded by *MIR* genes, which are mainly located in intergenic regions and less frequently in intronic regions [17]. Hundreds of *MIR* genes have been identified in diverse eukaryotes [18,19]. Similar to protein-coding genes, *MIR* genes are transcribed by RNA POLYMERASE II (Pol II) to generate long single-stranded primary transcripts called primary miRNAs (pri-miRNAs), which are stabilized by the addition of a 5’ cap and a 3’ polyadenylated (poly A) tail [6,7,20]. Pri-miRNAs form imperfect complementary stem-loop or hairpin structures flanked by single-stranded RNA extensions, with the miRNA and miRNA* strands on opposite sides of the stem [7]. Unlike pri-miRNAs in animals, which form tandem stem-loops and give rise to several mature miRNAs from a single transcript, most plant pri-miRNA transcripts form a single hairpin structure, from which only one mature miRNA is produced [8].

Processing

The RNase III enzymes DROSHA and DICER in animals [21-23] and DCL in plants [17,24,25] mediate the processing of pri-miRNAs. Their activity releases a short duplex consisting of a miRNA guide strand (miRNA strand) and a passenger strand (miRNA* strand) via two steps. In animals, the processing requires the endonuclease activity of nuclear-localized DROSHA for the first cleavage and cytoplasmic DICER for the second cleavage [21,22,26]. No homologs of DROSHA and its cofactor DGCR8/PASHA have been found in plants; instead, both steps of pri-miRNA processing are performed by a DCL enzyme and occur only in the nucleus [4,17,24,25]. Genetic studies in the model plant *Arabidopsis thaliana* have established that DCL1 is the predominant enzyme responsible for the dicing of most pri-miRNAs, while several evolutionarily young miRNAs are produced by DCL4 [27].

DCL1, one of the four *DCL* genes in *Arabidopsis*, encodes an RNase III endonuclease with six domains: an N-terminal helicase domain, a PAZ domain, two RNase III domains and two double-stranded RNA-binding domains (dsRBDs) [28]. DCL1 first cleaves pri-miRNAs approximately 15 nt away from the base of the stem to generate precursor-miRNAs (pre-miRNAs) harboring the stem-loop. These pre-miRNAs are further processed into miRNA/miRNA* duplexes with 5' phosphate groups and 3' 2-nt overhangs on each strand [25]. Although different pri-miRNAs and pre-miRNAs vary considerably in size, from several hundred to several thousand nucleotides, mature miRNA/miRNA* duplexes are uniformly 21-22 nt, a length probably determined by the distance between the PAZ domain and RNase III domain within the DCL1 structure [25].

DCL1 is assisted by several essential cofactors that directly interact with DCL1 to form the dicing complex in nuclear Dicing-bodies (D-bodies) during MIR gene transcription

and pri-miRNA processing [29-31]. DAWDLE (DDL), a forkhead-associated (FHA) domain protein, stabilizes pri-miRNAs and facilitates their recognition by DCL1 [32,33]. The dsRNA-binding protein HYPONASTIC LEAVES 1 (HYL1) [34-37] and the C2H2 zinc-finger protein SERRATE (SE) [38-40] are required by DCL1 to ensure the accuracy and efficiency of pri-miRNA processing [31]. Mutants of these genes (*HYL1*, *SE* and *DCL1*) exhibit pleotropic developmental defects accompanied by reduced accumulation of mature miRNAs and increased levels of pri-miRNAs.

Methylation

In plants, nearly all mature miRNAs undergo 2'-*O*-methylation at the 3' end catalyzed by HUA ENHANCER 1 (HEN1), a methyltransferase that deposits a methyl group onto the 2'-OH of the 3' terminal ribose [24,41-43]. Similar to partial loss-of-function *dcl1* mutants, *HEN1* loss of function leads to developmental defects and dramatically reduced miRNA accumulation, suggesting that HEN1-mediated methylation stabilizes miRNAs *in vivo* [42,43].

HEN1 was first identified in *Arabidopsis* as an enhancer of mutations in *HUA* genes involved in floral patterning [44], and it was predicted to encode a methyltransferase (MTase) due to the S-adenosyl-L-methionine-dependent MTase domain within the protein [24]. Although the MTase domain of HEN1 is not closely related to any known RNA 2'-*O*-MTases based on phylogenetic analysis, beta-elimination assays showed that miRNAs are methylated in wild-type plants but not in *hen1* mutants. In addition, biochemical assays establish the methyltransferase activity of HEN1 and its specific role in methylating small RNAs [41-43]. HEN1 homologs have been identified in other plant species [45] and animals [46-51] and function similarly in small RNA methylation.

HEN1 contains another four domains in addition to the catalytic MTase domain: two dsRNA-binding domains (dsRBDs) at the N-terminus, a La-motif-containing domain (LCD) and a PPIase-like domain (PLD) [24,52]. Crystal structure analysis of HEN1 revealed that both dsRBDs are involved in the recognition of small RNA duplexes [52]. While the LCD binds to the 3'-end 2-nt overhang of the strand that is not methylated, the methylated 3'-end 2-nt overhang is bound by the MTase domain; the distance between the LCD and MTase domains confers the length specificity of substrate recognition [52]. *In vitro* methylation assays and crystal structure analysis also suggest that both 3' ends of miRNA/miRNA* duplexes are methylated by HEN1 separately. They also show that HEN1 recognizes the 2-nt overhangs and the lengths of RNA duplexes but not miRNA sequences [42,52].

Although HEN1 protein is detectable in both nuclear and cytoplasmic fractions, HEN1-GFP signal is only observed in the nucleus [53], suggesting that small RNAs are methylated in the nucleus before export to the cytoplasm.

RISC assembly

Methylated miRNA strands are incorporated into AGO1-containing RISC complexes to guide target mRNA recognition through sequence complementarity and to effect target repression, whereas miRNA* strands are removed [1,4]. MiRNA strand selection and loading onto AGO1 are tightly controlled processes. For strand selection, the asymmetric thermodynamic features of miRNA/miRNA* duplexes are known to play an important role in both animals and plants [54]. The strand with weaker binding at its 5' end in the duplex is more likely to be selected as the miRNA guide strand and incorporated into RISC, while the other strand becomes the miRNA* passenger strand [54,55]. Second, AGO proteins have different preferences for the first nucleotide at the 5' end of their

associated miRNAs [56]. Analysis of the ten *Arabidopsis* AGO proteins showed that AGO1 prefers to bind small RNAs with a 5'-U, AGO2 and AGO4 prefer a 5'-A, and AGO5 prefers a 5'-C [56]. Most plant miRNAs start with a 5'-U, making AGO1 the major effector in the miRNA pathway; i.e., AGO1 associates with almost all miRNAs and mediates target gene repression, which occurs by mRNA cleavage or translation inhibition. Similar regulation of miRNA loading onto AGO is also observed in *Drosophila* and humans [54]. HYL1 and its regulator CPL1 also facilitate strand selection and AGO1 loading of miRNAs [57,58]. HYL interacts and co-localizes with AGO1 in the nuclear D-bodies [30], and *HYL1* loss of function reduces the efficiency of miRNA loading onto AGO1 [57].

The *HASTY* (*HST*) gene in *Arabidopsis* is the homologue of animal exportin-5 [59,60], which exports miRNAs from the nucleus to the cytoplasm [61]. *HST* loss of function leads to reduced accumulation of most miRNAs without affecting siRNA levels [61]. The requirement of cytoplasmic protein SQUINT (SQT) and HEAT SHOCK PROTEIN 90 (HSP90) for RISC assembly [62] suggests that AGO1 loading should occur in the cytoplasm after miRNAs are exported from the nucleus. However, the observation that AGO1 localizes to the D-bodies when coexpressed with HYL1 also promotes the possibility that miRNAs are first loaded onto AGO1 in the nucleus to form functional RISCs, and then exported to the cytoplasm.

Regulation of miRNA biogenesis

Since an abnormal miRNA length or sequence could affect target gene repression, each step of miRNA biogenesis must be strictly regulated to ensure the precise and accurate production of miRNAs.

Several factors are known to regulate *MIR* gene transcription. Similar to Pol II-dependent protein-coding genes, *MIR* gene transcription requires the general

transcriptional coactivator Mediator and its interacting transcriptional activators to recruit Pol II to *MIR* promoters [63]. In the loss-of-function *mediator* mutant, the transcription of many *MIR* genes is affected, resulting in reduced accumulation of both miRNA precursors and mature miRNAs [63]. CELL DIVISION CYCLE 5 (CDC5), a DNA-binding protein, binds to Pol II and *MIR* promoters and acts as a positive transcription factor by mediating Pol II occupancy at *MIR* promoters [64]. CDC5 also interacts with PLEIOTROPIC REGULATORY LOCUS 1 (PRL1), a conserved WD-40 protein, to enhance the activity of DCL1 [65]. Subunits of Elongator were recently found to interact with DCL1 and play a role in *MIR* gene transcription, consistent with the model of co-transcriptional processing for miRNA biogenesis [66]. MiRNA transcription is also spatiotemporally regulated, as different miRNAs usually have distinct expression patterns in specific tissues. Even within a given *MIR* family consisting of several genes, the expression pattern of individual family members may vary. For example, *Arabidopsis* miR165/6 derives from the *MIR165/6* family containing nine genes, and mature miR165 and miR166 differ by only one nucleotide and target the same genes. Nevertheless, the sequences and expression patterns of the nine pri-miRNAs are distinct [67]. *MIR166A* is the most highly expressed among the nine genes and is transcribed at the abaxial side, boundary and vasculature of leaf primordia. In contrast, other *MIR165/6* genes are either expressed at lower levels than *MIR166A* [68]. Individual members of the *MIR156* and *MIR172* families, both of which play important roles in developmental timing, also exhibit different expression levels [69-71]. Some *MIR* genes are only expressed under stress conditions, such as *MIR398* [72,73] and *MIR399* [74,75]. These examples indicate that there must be some specific transcription factors or activators that facilitate and regulate the transcription of individual *MIR* genes.

DCL1 processing of pri-miRNAs is assisted and controlled by many factors. ABA HYPERSENSITIVE 1 (ABH1)/Cap-binding protein 80 (CBP80) and CBP20 are components of the nuclear cap-binding complex (CBC) that binds pri-miRNAs and facilitates the access of pri-miRNAs to D-bodies for processing [76,77]. The G-patch domain protein TOUGH (TGH) enhances the dicing activity of DCL1 [78]. The *Arabidopsis* pre-mRNA processing factor 6 homolog STABILIZED 1 (STA1) is involved in miRNA biogenesis by influencing pri-miRNA splicing and regulating *DCL1* transcript levels [79,80]. MODIFIER of SNC1 2 (MOS2), an RNA-binding protein that binds pri-miRNAs, is required for the recruitment of pri-miRNAs to the dicing complexes to promote pri-miRNA processing [81,82].

Some essential factors in miRNA biogenesis are also strictly regulated. The active hypo-phosphorylated state of HYL1 is maintained by C-terminal domain phosphatase-like 1 (CPL1) to ensure accurate miRNA processing [58]. CONSTITUTIVELY PHOTOMORPHOGENIC 1 (COP1), a RING finger-containing E3 ligase that plays an essential role in photomorphogenesis, protects HYL against an unknown endoproteinase [83]. DCL1, SE, AGO1 and AGO2 are all subjected to negative feedback regulation through the activity of miRNAs. *DCL1* transcript is targeted by miR162 for cleavage [84]; *SE* is targeted by miR863 [85]; and *AGO1* and *AGO2* are repressed by miR168 and miR403, respectively [7,86].

Modes of action of miRNAs

Plant miRNAs regulate target genes at the post-transcriptional level via two major mechanisms: transcript cleavage and translation repression [1,2,4,87] (Figure 1.2). For small RNAs in general, the degree of sequence complementarity between small RNAs and their targets influences the particular mode of action the small RNAs could engage in,

with transcript cleavage requiring a high degree of sequence complementarity [88]. In plants, miRNAs and their target mRNAs have nearly perfect complementarity, and because of this, transcript cleavage was thought to be the predominant mode of action of plant miRNAs [1,2,4,9]. However, this is a mis-conception. While a high degree of sequence complementarity is conducive to RNA cleavage, it is not necessarily refractory to translational repression. In fact, targets that have been experimentally validated to undergo miRNA-mediated translation inhibition, pair with miRNAs with a high degree of sequence complementary [89-91]. Examples are *APETALA 2* (*AP2*), *SCARECROW-LIKE PROTEIN 4* (*SCL4*), *COPPER/ZINC SUPEROXIDE DISMUTASE 2* (*CSD2*), and *SQUAMOSA PROMOTER BINDING PROTEIN-LIKE 3* (*SPL3*) targeted by miR172, miR171, miR398, and miR156, respectively [89,92-94]. In fact, the same mRNAs also undergo cleavage caused by the same miRNAs [91,95,96]. Thus, sequence complementarity is not the factor that dictates which mode of action plant miRNAs engage in. Emerging findings of miRNA target transcripts bound by ribosomes or ribosomes on the endoplasmic reticulum (ER) [95-97] imply that translation inhibition may occur at a larger number of miRNA targets than expected.

Transcript cleavage

miRNA-guided RNA cleavage, also known as slicing, occurs at a precise position in the target mRNA [98]. Genome-wide identification of RNAs with a 5' monophosphate (the 3' cleavage fragments have a 5' monophosphate) found that most plant miRNA targets undergo transcript cleavage [99]. Cleavage is accomplished by the PIWI domain of AGO proteins, which forms an RNase H-like fold and exhibits endonuclease activity; this activity has been demonstrated for *Arabidopsis* AGO1, the major miRNA effector, along with AGO2, AGO4, AGO7 and AGO10 [56,100-104].

Upon slicing, the 5’ and 3’ cleavage fragments are subsequently degraded by exonucleases. In *Arabidopsis*, EXORIBONUCLEASE 4 (XRN4), a 5’-to-3’ exonuclease, is responsible for degrading the 3’ fragments [105]. Unlike the 3’ fragments, which are usually detectable in wild-type plants, the 5’ fragments are barely detected, probably due to rapid degradation. In *Chlamydomonas reinhardtii*, the 5’ fragments are polyadenylated by the nucleotidyl transferase MUT68, followed by degradation by cytoplasmic exosome [106]. HEN1 SUPPRESSOR 1 (HESO1), an *Arabidopsis* homolog of MUT68 and its paralog UTP:RNA URIDYLYLTRANSFERASE (URT1) polyuridylate the 5’ fragments *in vivo* and *in vitro* [107,108]. The 3’-to-5’ exonuclease responsible for degrading uridylated 5’ fragments in *Arabidopsis* remains ill-defined. The cytoplasmic exosome may play a role, as its cofactor’s subunits, SKI2, SKI3 and SKI8, are required for the degradation of RISC-generated 5’ fragments [109].

Translation inhibition

miRNA-mediated translation repression was initially proposed to account for the disproportionate effects of miRNAs on target gene repression at the protein versus the mRNA levels [92-94]. In plants, translation repression is less frequently observed than transcript cleavage, possibly owing to the universal presence of miRNA-guided cleavage coupled with difficulty to determine protein levels due to the absence of high quality antibodies.

Early examples of miRNA-mediated translation inhibition in plants were *AP2* and *SPL3* regulated by miR172 and miR156/7, respectively [92-94]. When miR172 and miR156/7 accumulated abnormally, *AP2* and *SPL3* transcript levels were comparable to those of wild type, but their protein levels were altered [93,94]. Subsequently, similar observations were made for other miRNAs, including miR159 [110], miR164, miR165/6

[91], miR171, miR395, miR398 and miR834 [89]. Moreover, the Li et al. study went beyond observations of effects of miRNAs on target gene expression at transcript vs. protein levels by showing that miR398 and miR165/6 inhibit protein synthesis from their target genes *CSD2* and *PHB*, respectively [91].

Known factors required for miRNA-mediated translation inhibition include the microtubule-severing enzyme KATANIN 1 (KTN1) [89], the processing body (P body) component VARICOSE (VCS) [89], the GW-repeat protein SUO [90] and the ER membrane protein ALTERED MERISTEM PROGRAM 1 (AMP1) [91]. Mutations in these genes selectively interfere with miRNA-guided repression at the protein level, suggesting that transcript cleavage and translation repression are two independent modes of action. Based on the finding that the recruitment of miRNA target transcripts throughout the polysome fractions is enhanced in the *amp1* mutant compared to wild type [91], plant miRNAs may repress translation initiation, but other possibilities exist. Genome-wide analyses of RNA degradation through the profiling of RNAs with 5' monophosphate in *Arabidopsis* show that co-translational mRNA degradation occurs for most genes, including a large number of miRNA targets [95,96]. The cleavage of presumably ribosome-bound *AP2* and *SPL3* transcripts at the corresponding miRNA binding sites was observed [96]. An important lesson is that even for the "RNA cleavage" mode of action of miRNAs, translating mRNAs are the targets. This is consistent with findings that AGO1 and miRNAs associate with polysomes [97,111]. The molecular mechanisms underlying miRNA-mediated translation repression have yet to be determined.

Biogenesis of secondary siRNAs

In addition to mRNA cleavage and translation repression, some miRNAs also trigger the production of phased secondary siRNAs (phasiRNAs) from their target

transcripts, and this is a widespread and conserved phenomenon in plants [1,2,87]. In *Arabidopsis*, after AGO-mediated slicing, either the 5' or 3' fragment is stabilized by SUPPRESSOR OF GENE SILENCING 3 (SGS3), which associates with RISC by recognizing specific features of the 22-nt miRNA/target duplex to protect the cleavage fragment from degradation [112,113]. RNA-DEPENDENT RNA POLYMERASE 6 (RDR6) is recruited to convert the cleavage fragment into dsRNA that is later diced into phasiRNAs at a 21-nt interval [112]. This phasing requires AGO1-mediated cleavage: in an *ago1* mutant with defective slicing activity, secondary siRNAs are generated, but the phasing is disrupted [114].

The phasiRNAs generated from four families of non-coding *TAS* genes (*TAS1* to *TAS4*) in *Arabidopsis* were termed tasiRNAs at the time of discovery due to their in-*trans* mode of action similar to miRNAs [101,112,115-117]. Two mechanisms of tasiRNA production are based on the number of miRNA binding sites within the target transcripts. The predominant mechanism, known as the "one-hit model", entails one miRNA binding site in the target transcript and a 22-nt miRNA [112,115,116]. The "two-hit model" requires two miRNA binding sites within the target transcript [118]. This is observed for *TAS3* transcripts, which contain two miR390 binding sites. AGO7, instead of AGO1, mediates the cleavage at the 3' site but not at the 5' site [118].

In addition to the length of the miRNAs triggering phasiRNA biogenesis, other factors may also be influential. The asymmetric bulge structure within miRNA/miRNA* and the degree of complementarity in miRNA-target pairing affect tasiRNA production [58,113]. The position of the miR173 binding site relative to the short open reading frame in *TAS2* or a transgene containing *TAS1c* sequence was found to be important, as tasiRNA abundance decreased when premature stop codons were introduced further upstream of

the miR173 binding site [119,120], suggesting a relationship between translation and tasiRNA biogenesis.

phasiRNAs are not generated from most miRNA target transcripts. Most miRNAs are 21 nt in length and do not trigger phasiRNA biogenesis from their targets. Genome-wide small RNA sequencing and bioinformatic analysis identified a small number of protein-coding genes, including immune receptor *NUCLEOTIDE-BINDING LEUCINE-RICH REPEAT* (*NBS-LRR*) and *PENTATRICOPEPTIDE REPEAT* (*PPR*) genes, as targets of 22-nt miRNAs for phasiRNA production in *Arabidopsis* [121]. Monouridylation of miR171 catalyzed by URT1 in the *hen1* mutant leads to a 22-nt miR171 that is able to trigger the production of phasiRNAs [122]. A larger number of phasiRNAs, as well as the loci that generate them (*PHAS* loci), have been identified in many non-Brassicaceae plants [121]. The phasiRNAs are derived from transcripts of protein-coding genes, such as *NBS-LRR* and *PPR* genes, or long non-coding RNAs [121,123,124]. Although the targets of many phasiRNAs are still unclear, miRNA-triggered production of phasiRNAs is nevertheless hypothesized to act in beneficial microbial interactions or plant defense, or have other long-term evolutionary benefits [121].

Subcellular locations of miRNA activities

Several studies in *Arabidopsis* link the sites of miRNA activity to polysomes [111], the ER membrane [91] and membrane-bound polysomes [96,97].

Because AGO1 is the major miRNA effector, the subcellular localization of AGO1 is an important clue for uncovering the sites of miRNA activity. AGO1 is a peripheral membrane protein, based on fractionation experiments after high-salt or high-PH treatments [91,125]. The link between AGO1's membrane localization and the rough endoplasmic reticulum (rER) is based on fluorescence microscopy analysis showing that

AGO1 accumulates in cytoplasmic granules that colocalize with an ER marker [91]. The association of AGO1 with the rER is further supported by its interaction with AMP1, an integral membrane protein localized to the rER [91].

Subcellular fractionation detected the association of miRNAs and AGO1 with polysomes [111]. Further fractionation revealed the association of miRNAs and AGO1 with membrane-bound polysomes (MBPs) rather than polysomes in general [91,97]. AMP1 and its paralog LIKE AMP1 (LAMP1) are both required for miRNA-guided translation repression but not transcript cleavage [91]. In the *amp1 lamp1* double mutant, miRNA target transcripts are associated with total polysomes as in wild-type plants [91]. However, these transcripts are more enriched on MBPs in *amp1 lamp1* than in wild type [91]. Thus, miRNA-mediated translation repression probably occurs on the rER.

How AGO1 associates with the endomembrane is unknown, but it may be independent of AMP1 [91] or target mRNAs [97]. Several *ago1* mutants harboring various point mutations display compromised membrane association, and this association is further reduced by knocking down *HYDROXY METHYLGLUTARYL COA REDUCTASE 1* (*HMG1*), which encodes an isoprenoid biosynthesis enzyme [125]. Thus, aside from AGO1 itself, isoprenoid may influence the membrane association of AGO1. Loss of function in *HMG1* also leads to defective miRNA activity [125], further suggesting that the membrane association of AGO1 is essential for its role in miRNA-directed activities.

AGO1 also associates with P bodies [126]. An *Arabidopsis* P body-localized protein, VARICOSE (VCS), was found to play a role in miRNA-guided translation inhibition [89]. VCS is a component of the decapping complex, which is required for 5'-to-3' exonucleolytic degradation of mRNA. Loss of VCS results in elevated protein levels of several miRNA targets with subtle or no increases in their corresponding mRNA levels

[89]. Similar effects were observed for loss of function in *KATANIN 1* (*KTN1*), which encodes the P60 subunit of a microtubule-severing enzyme [89]. However, the mechanisms by which VCS and KTN1 influence miRNA-mediated translation repression and the connection of P bodies or microtubules with this process are still unknown.

Unlike translation repression, few reports have directly addressed the site of miRNA-guided transcript cleavage. However, the reduced cleavage efficiency observed in the *hmg1* mutant [125] and the ER association of AGO1 [91] suggest that polysomes and the rER are potential sites. Additionally, genome-wide analyses of RNA degradation products suggest that miRNA targets undergo cleavage when bound by translating ribosomes [95,96]. Furthermore, 3' cleavage fragments from a few miRNA targets were detectable in the MBP fraction [97]. Therefore, transcripts targeted by miRNAs may undergo co-translational degradation, and at least a fraction of miRNA-guided cleavage may take place on the rER.

The biogenesis of phasiRNAs probably occurs on membrane structures. SGS3 and RDR6, two essential proteins required for phasiRNA biogenesis, form cytoplasmic siRNA bodies that also contain AGO7 [127,128]. Moreover, both SGS3 and AGO7 are in the microsomal fraction, and AGO7 tends to be adjacent to vesicles decorated by a *cis*-Golgi marker [128]. All miRNAs, including 22-nt miRNAs, are enriched on MBPs and reduced membrane association of 22-nt miRNAs correlates with decreased levels of phasiRNAs [97]. *TAS* transcripts are bound by ribosomes [95] and MBPs [97]. These findings suggest that the initial miRNA-guided cleavage step of phasiRNA biogenesis occurs on MBPs and the subsequent steps occur on certain membrane structures.

Turnover of miRNAs

The levels of miRNAs must be precisely and dynamically *in vivo* and miRNA turnover is a mechanism to regulate miRNA levels. Studies of the *hen1* mutant revealed two major mechanisms underlying miRNA degradation in *Arabidopsis*: 3'-to-5' truncation and 3' uridylation [41-43] (Figure 1.3). A few genes responsible for miRNA degradation via these two mechanisms have been identified [108,129-131], but the full picture remains elusive.

miRNA stabilization by 3' methylation

Mature miRNAs are protected by 3'-end methylation catalyzed by HEN1. Loss of function in *HEN1* results in reduced abundance of almost all miRNAs, which are also heterogeneous in size due to 3' truncation and 3' tailing (predominantly uridylation) [41-43]. Similarly, loss of function in *HEN1* homologs in other eukaryotes, including rice (Abe *et al.*, 2010), *Drosophila* [46,47], *C. elegans* [51], zebra fish [50], and mouse [48], also leads to miRNA or piRNA (piwi-interacting RNA) 3' truncation and 3' uridylation. Therefore, HEN1-mediated 2'-*O*-methylation plays a general role in protecting the 3' ends of small RNAs.

Exonucleases in miRNA degradation

The *SMALL RNA DEGRADING NUCLEASE* (*SDN*) family encodes four 3'-to-5' exonucleases that function redundantly in degrading both miRNAs and siRNAs [129]. Single and double *sdn* mutants resemble wild-type plants, but knockdown of three *SDN* family members leads to severe pleiotropic developmental defects and elevated miRNA accumulation [129]. *In vitro* enzymatic assays show that SDN1 specifically acts on short single-stranded RNAs, and the exonuclease activity is partially inhibited by the methyl group at the 3' end of miRNAs [129].

SDNs are responsible for the 3' truncation of miRNAs in both *hen1* and wild-type plants [132]. Comparing miRNA profiles of *hen1* and *hen1 sdn1 sdn2* plants by small RNA-seq showed that the 3' truncation of some miRNAs is reduced when SDN1 and SDN2 are both absent [132]. Similar results were observed when comparing the miRNA profiles of wild-type and *sdn1 sdn2* plants, although 3' truncated miRNAs have very low abundance in wild type [132]. The fact that only a small number of miRNAs are affected by the absence of SDN1 and SDN2 could be due to the redundant function of other SDN members or due to non-SDN exonucleases.

SDN1 is unable to degrade U-tailed miRNAs *in vitro* [129], so it does not appear to be responsible for the degradation of uridylated miRNA species. Although it has not been reported in *Arabidopsis*, several exonucleases in other eukaryotes prefer uridylated RNAs as substrates. The 3'-to-5' exonuclease DIS3-like 2 (DIS3L2) degrades uridylated RNAs in mammals and yeast, including uridylated pre-let-7 in mammals [133,134]. In *Chlamydomonas*, depletion of the exosome subunit *Ribosomal RNA-Rrocessing Protein 6* (*RRP6*) results in elevated accumulation of small RNAs *in vivo*, and RRP6 degrades 3' uridylated miRNAs rather than nonuridylated miRNAs *in vitro* [135]. The *Arabidopsis* orthologs of *DIS3L2* and *RRP6* are *SUPPRESSOR OF VARICOSE* (*SOV*) and three *RRP6-LIKE (PPR6L)* genes, respectively, and are therefore the prime candidates for the degradation of uridylated miRNAs.

Non-templated tailing of miRNAs

3' non-templated tailing is a widespread phenomenon and a common post-transcriptional modification that regulates miRNA biogenesis, stability or activity in diverse model organisms [136]. Adenylation and uridylation are the two major types of 3' tailing

and are catalyzed by nucleotidyl transferases including non-canonical PolyA polymerases (PAPs) and terminal uridylyl transferases (TUTases), respectively [137].

In *Chlamydomonas*, uridylation of miRNAs and siRNAs is catalyzed by the nucleotidyl transferase MUT68 [135]. MUT68 promotes the *in vitro* degradation of uridylated miRNAs through the exosome subunit RRP6 [135]. MUT68 and RRP6 appear to act only on unmethylated miRNAs, as 2'-*O*-methylated miR912 oligonucleotides failed to be uridylated and degraded *in vitro* [135].

3' uridylation of miRNAs in *Arabidopsis*, rice, and maize is widely observed in *hen1* mutants in which miRNA methylation is abolished [41-43,45,122]. In *Arabidopsis*, HESO1 and URT1 uridylate unmethylated miRNAs in the *hen1* mutant, leading to miRNA degradation [130,131,138,139]. Loss of function in both *HESO1* and *URT1* rescues the developmental defects of the *hen1* mutant, accompanied by elevated miRNA accumulation and reduced 3' uridylation [130,131,138,139]. *In vitro*, both HESO1 and URT1 exhibit nucleotidyl transferase activities on unmethylated RNA oligonucleotides but not 3' methylated RNAs [108,130,131,138]. Although HESO1 and URT1 both prefer U over the other three nucleotides, they have different substrate specificities and cooperatively tail different forms of the same miRNAs *in vivo*. While HESO1 prefers U-ending miRNAs as substrates, URT1 favors A-ending miRNAs. Given the observation of substantial monouridylated miRNAs in the *hen1 heso1* double mutant [108,130,131,138], one possibility is that URT1 first uridylates unmethylated miRNAs to generate monoU-tailed forms, the preferred substrates for HESO1, to produce longer U tails.

3' uridylation may also affect miRNA activity. When AGO1-bound miR165/6 was uridylated by URT1 *in vitro*, the slicer activity was reduced [131]. The monouridylation of

miR171a by URT1 in *hen1* makes it capable of triggering the biogenesis of secondary phasiRNAs [122].

In *Populus trichocarpa* (black cottonwood), a few miRNAs undergo 3' adenylation, although the corresponding enzymes remain unknown [140]. Synthesized miRNA oligonucleotides with 3' adenylation were degraded at a slower rate in plant extracts than those without it [140], indicating that adenylation contributes to miRNA stabilization.

AGO proteins in miRNA stability

In addition to its key role in miRNA-mediated activities, AGO1 shelters its associated miRNAs from degradation, based on the reduced abundance of many miRNAs in *ago1* null mutants [141]. It is therefore counterintuitive that the weak allele *ago1-11* suppresses the 3' truncation and 3' uridylation of miRNAs in the *hen1* mutant [122]. Additionally, both truncated and tailed miRNA species associate with AGO1 *in vivo* [122,142]. This implies that during miRNA degradation SDN1 and HESO1/URT1 act on AGO1-bound miRNAs. In fact, both HESO1 and URT1 are able to tail AGO1-bound miRNAs *in vitro*, and the tailed miRNAs remain associated with AGO1 [107,108,131]. The interactions between HESO1/URT1 and AGO1 are evidenced by reciprocal co-immunoprecipitation [107,108]. Although SDN1-AGO1 interaction has not been reported, SDN1 acts on AGO1-bound miRNAs *in vitro* to generate truncated miRNAs of heterogeneous sizes that remain bound to AGO1 [132]. Given that 2'-*O*-methylation of miRNAs completely inhibits the activity of HESO1 and URT1 but not SDN1 [129-131], one possibility is that SDN1 and HESO1/URT1 cooperate in degrading AGO1-bound miRNAs that are methylated: SDN1 removes the methyl group from these miRNAs, and HESO1/URT1 cause subsequent uridylation. This would lead to miRNA degradation by an unknown exonuclease that prefers U-tailed RNAs. This hypothesis is supported by the

following observations: 3' truncated-only and 3' truncated-and-tailed miRNA species are reduced in the *hen1 sdn1 sdn2* triple mutant compared to *hen1*, while 3' tailed species are reduced in *hen1 heso1* with the concomitant increase in 3' truncated-only forms [132]. Free miRNAs, on the other hand, can be degraded solely by SDN1 or sequentially by SDN1 and HESO1/URT1.

As the closest paralog of AGO1 among the ten *Arabidopsis* AGO proteins, AGO10 is only expressed in certain cells and maintains the identity of the shoot apical meristem (SAM) and leaf polarity by repressing the activity of miR165/6 [14-16]. AGO10 has a higher binding affinity to miR165/6 than AGO1 [104], and rather than protecting this miRNA, AGO10 promotes its degradation. In *ago10* mutants, miR165/6 accumulation is sufficiently increased that it can be detected by *in situ* hybridization in *AGO10*-expressing cells, which is not the case in wild type [143]. *AGO10* overexpression results in the degradation of miR165/6 by SDN1 and SDN2 [132]. An *in vitro* assay further suggested that AGO10-bound miR165/6 is more susceptible to SDN1-mediated truncation than AGO1-bound miR165/6 [132]. Promotion of miR165/6 degradation likely contributes to AGO10-mediated maintenance of stem cells and leaf polarity.

Effect of target transcripts on miRNA stability

While the enzymes for miRNA 3' truncation or 3' uridylation act on many miRNAs, specificity in miRNA degradation may be achieved through target RNAs or noncoding RNAs. In *Arabidopsis*, miR399 is regulated by a native transcript with a miR399 binding site from the *IPS1* (*INDUCED BY PHOSPHATE STARVATION 1*) locus [144]. A 3-nt bulge at the cleavage site within the *IPS1* transcript abolishes miR399-mediated cleavage, thereby rendering the *IPS1* transcript a target mimic (TM) that sequesters miR399 from its other targets and reduces its activity [144]. Genome-wide bioinformatic analyses indicate

that many transcripts, from either noncoding genomic regions or annotated genes, can serve as potential endogenous TMs to regulate miRNA activity [145,146]. Intriguingly, in transgenic lines with artificial TMs, the levels of the corresponding miRNAs are reduced [145,146]. Similar results were observed in transgenic lines expressing Short Tandem Target Mimic (STTM) RNAs, which contain two tandem miRNA binding sites with mismatches at the cleavage positions [10,147]. STTM-triggered miRNA degradation requires the activity of SDN1 and SDN2 *in vivo* [10].

Target-induced miRNA turnover is conserved across flies and mammals. In animals, miRNAs recognize their targets through pairing at the seed region (miRNA nucleotides 2-7) [148]. Extensive pairing between miRNAs and artificial target transcripts leads to 3' trimming and tailing of miRNAs in *Drosophila* and humans [149-151]. Based on crystal structure analysis in *Thermus thermophilus* [152], the conformation of AGO is altered after a highly complementary target is in RISC such that the 3' end of the guide is released from the binding pocket in AGO. Thus, it is deduced that the 3' end of an AGO1-bound miRNA would be exposed to SDNs, HESO1, or URT1 upon recognition of highly complementary targets in *Arabidopsis*.

Subcellular sites of miRNA turnover

The subcellular localization of SDNs, HESO1, and URT1 may offer clues for the subcellular sites of miRNA turnover. In addition, because AGO1-bound miRNAs can be truncated and uridylated, AGO1 localization is another important indicator for the sites of miRNA turnover. While the localization patterns of SDNs are unknown, HESO1 and URT1 colocalize in cytoplasmic foci, where AGO1 is also localized [108]. In addition, both enzymes interact with AGO1, and uridylated miRNAs remain bound by AGO1 [107,108]. Based on these findings, the cytoplasmic foci are potential sites of miRNA degradation.

Besides uridylating unmethylated miRNAs, HESO1 and URT1 also catalyze the uridylation of the 5’ cleavage fragments from miRNA target transcripts, leading to their degradation [107]. Given that a fraction of AGO1-mediated cleavage takes place on MBPs [97], the undefined cytoplasmic foci may contain MBPs.

The post-translational regulation of AGO1 protein may also provide a clue about the sites of miRNA turnover. In pathogenic and viral contexts, AGO1 is ubiquitinylated by the polerovirus-encoded F-box protein P0 and subsequently degraded through autophagy, a process in which cytosolic proteins are delivered to lysosomes for degradation [153]. AGO1 is also regulated by another F-box protein, F-box and WD-repeat domain-containing protein 2 (FBW2), which also leads to AGO1 degradation via autophagy [154]. The colocalization of AGO1 and AUTOPHAGY 8 (ATG8), an autophagosomal membrane protein [153], further indicates that AGO1 is associated with autophagosomes. Since AGO1 degradation would indisputably impair the stability of its associated miRNAs, miRNA degradation may occur concomitantly with AGO1 autophagy.

Concluding remarks

Although many players involved in miRNA biogenesis, degradation, and activity have been discovered, much is unknown regarding the subcellular locations where these processes take place. For example, it is unknown how D-bodies containing the dicing complex are formed, how AGO1, a presumably soluble protein, associates with ER and membrane-bound polysomes, and how membrane-bound polysomes affect miRNA-guided phasiRNA biogenesis. As AGO1 associates with not only miRNAs but also siRNAs from endogenous sequences such as transposons and phasiRNA loci as well as exogenous sequences such as viruses and transgenes, the subcellular partitioning of AGO1 between the cytosol and endomembranes and between the nucleus and the

cytoplasm probably influences the activities of various types of small RNAs. The limited knowledge of the subcellular locations of miRNA biogenesis, degradation, and activity precludes a full understanding of miRNAs as well as the crosstalk between miRNAs and siRNAs.

References

1. Chen X (2005) microRNA biogenesis and function in plants. FEBS Lett 579: 5923-5931.

2. Chen X (2009) Small RNAs and their roles in plant development. Annu Rev Cell Dev Biol 25: 21-44.

3. Bologna NG, Voinnet O (2014) The diversity, biogenesis, and activities of endogenous silencing small RNAs in *Arabidopsis*. Annu Rev Plant Biol 65: 473-503.

4. Voinnet O (2009) Origin, biogenesis, and activity of plant microRNAs. Cell 136: 669-687.

5. Lee RC, Feinbaum RL, Ambros V (1993) The C. elegans heterochronic gene *lin-4* encodes small RNAs with antisense complementarity to *lin-14*. Cell 75: 843-854.

6. Jones-Rhoades MW, Bartel DP (2004) Computational identification of plant microRNAs and their targets, including a stress-induced miRNA. Mol Cell 14: 787-799.

7. Xie Z, Allen E, Fahlgren N, Calamar A, Givan SA, et al. (2005) Expression of *Arabidopsis MIRNA* genes. Plant Physiol 138: 2145-2154.

8. Griffiths-Jones S, Saini HK, van Dongen S, Enright AJ (2008) miRBase: tools for microRNA genomics. Nucleic Acids Res 36: D154-158.

9. Jones-Rhoades MW, Bartel DP, Bartel B (2006) MicroRNAS and their regulatory roles in plants. Annu Rev Plant Biol 57: 19-53.

10. Yan J, Gu Y, Jia X, Kang W, Pan S, et al. (2012) Effective small RNA destruction by the expression of a short tandem target mimic in *Arabidopsis*. Plant Cell 24(2):415-27.

11. Negrini M, Ferracin M, Sabbioni S, Croce CM (2007) MicroRNAs in human cancer: from research to therapy. J Cell Sci 120: 1833-1840.

12. Farazi TA, Hoell JI, Morozov P, Tuschl T (2013) MicroRNAs in human cancer. Adv Exp Med Biol 774: 1-20.

13. Peng Y, Croce CM (2016) The role of MicroRNAs in human cancer. Signal Transduct Target Ther 1: 15004.

14. Moussian B, Schoof H, Haecker A, Jürgens G, Laux T (1998) Role of the *ZWILLE* gene in the regulation of central shoot meristem cell fate during *Arabidopsis* embryogenesis. EMBO J 17: 1799-1809.

15. Lynn K, Fernandez A, Aida M, Sedbrook J, Tasaka M, et al. (1999) The *PINHEAD/ZWILLE* gene acts pleiotropically in *Arabidopsis* development and has overlapping functions with the *ARGONAUTE1* gene. Development 126: 469-481.

16. Mallory AC, Reinhart BJ, Jones-Rhoades MW, Tang G, Zamore PD, et al. (2004) MicroRNA control of *PHABULOSA* in leaf development: importance of pairing to the microRNA 5' region. EMBO J 23: 3356-3364.

17. Reinhart BJ, Weinstein EG, Rhoades MW, Bartel B, Bartel DP (2002) MicroRNAs in plants. Genes Dev 16: 1616-1626.

18. Meyers BC, Souret FF, Lu C, Green PJ (2006) Sweating the small stuff: microRNA discovery in plants. Curr Opin Biotechnol 17: 139-146.

19. Nozawa M, Miura S, Nei M (2012) Origins and evolution of *MicroRNA* genes in plant species. Genome Biol Evol 4: 230-239.

20. Lee Y, Kim M, Han J, Yeom KH, Lee S, et al. (2004) *MicroRNA* genes are transcribed by RNA polymerase II. EMBO J 23: 4051-4060.

21. Denli AM, Tops BB, Plasterk RH, Ketting RF, Hannon GJ (2004) Processing of primary microRNAs by the Microprocessor complex. Nature 432: 231-235.

22. Gregory RI, Yan KP, Amuthan G, Chendrimada T, Doratotaj B, et al. (2004) The Microprocessor complex mediates the genesis of microRNAs. Nature 432: 235-240.

23. Chendrimada TP, Gregory RI, Kumaraswamy E, Norman J, Cooch N, et al. (2005) TRBP recruits the Dicer complex to Ago2 for microRNA processing and gene silencing. Nature 436: 740-744.

24. Park W, Li J, Song R, Messing J, Chen X (2002) CARPEL FACTORY, a Dicer homolog, and HEN1, a novel protein, act in microRNA metabolism in *Arabidopsis thaliana*. Curr Biol 12: 1484-1495.

25. Kurihara Y, Watanabe Y (2004) *Arabidopsis* micro-RNA biogenesis through Dicer-like 1 protein functions. Proc Natl Acad Sci U S A 101: 12753-12758.

26. Kim VN, Han J, Siomi MC (2009) Biogenesis of small RNAs in animals. Nat Rev Mol Cell Biol 10: 126-139.

27. Rajagopalan R, Vaucheret H, Trejo J, Bartel DP (2006) A diverse and evolutionarily fluid set of microRNAs in *Arabidopsis thaliana*. Genes Dev 20: 3407-3425.

28. Schauer SE, Jacobsen SE, Meinke DW, Ray A (2002) DICER-LIKE1: blind men and elephants in *Arabidopsis* development. Trends Plant Sci 7: 487-491.

29. Song L, Han MH, Lesicka J, Fedoroff N (2007) *Arabidopsis* primary microRNA processing proteins HYL1 and DCL1 define a nuclear body distinct from the Cajal body. Proc Natl Acad Sci U S A 104: 5437-5442.

30. Fang Y, Spector DL (2007) Identification of nuclear dicing bodies containing proteins for microRNA biogenesis in living *Arabidopsis* plants. Curr Biol 17: 818-823.

31. Dong Z, Han MH, Fedoroff N (2008) The RNA-binding proteins HYL1 and SE promote accurate in vitro processing of pri-miRNA by DCL1. Proc Natl Acad Sci U S A 105: 9970-9975.

32. Yu B, Bi L, Zheng B, Ji L, Chevalier D, et al. (2008) The FHA domain proteins DAWDLE in *Arabidopsis* and SNIP1 in humans act in small RNA biogenesis. Proc Natl Acad Sci U S A 105: 10073-10078.

33. Morris ER, Chevalier D, Walker JC (2006) *DAWDLE*, a forkhead-associated domain gene, regulates multiple aspects of plant development. Plant Physiol 141: 932-941.

34. Han MH, Goud S, Song L, Fedoroff N (2004) The *Arabidopsis* double-stranded RNA-binding protein HYL1 plays a role in microRNA-mediated gene regulation. Proc Natl Acad Sci U S A 101: 1093-1098.

35. Vazquez F, Gasciolli V, Crete P, Vaucheret H (2004) The nuclear dsRNA binding protein HYL1 is required for microRNA accumulation and plant development, but not posttranscriptional transgene silencing. Curr Biol 14: 346-351.

36. Hiraguri A, Itoh R, Kondo N, Nomura Y, Aizawa D, et al. (2005) Specific interactions between Dicer-like proteins and HYL1/DRB-family dsRNA-binding proteins in *Arabidopsis thaliana*. Plant Mol Biol 57: 173-188.

37. Wu F, Yu L, Cao W, Mao Y, Liu Z, et al. (2007) The N-terminal double-stranded RNA binding domains of *Arabidopsis* HYPONASTIC LEAVES1 are sufficient for pre-microRNA processing. Plant Cell 19: 914-925.

38. Grigg SP, Canales C, Hay A, Tsiantis M (2005) SERRATE coordinates shoot meristem function and leaf axial patterning in *Arabidopsis*. Nature 437: 1022-1026.

39. Lobbes D, Rallapalli G, Schmidt DD, Martin C, Clarke J (2006) SERRATE: a new player on the plant microRNA scene. EMBO Rep 7: 1052-1058.

40. Yang L, Liu ZQ, Lu F, Dong AW, Huang H (2006) SERRATE is a novel nuclear regulator in primary microRNA processing in *Arabidopsis*. Plant J 47: 841-850.

41. Li J, Yang Z, Yu B, Liu J, Chen X (2005) Methylation protects miRNAs and siRNAs from a 3'-end uridylation activity in *Arabidopsis*. Curr Biol 15: 1501-1507.

42. Yu B, Yang Z, Li J, Minakhina S, Yang M, et al. (2005) Methylation as a crucial step in plant microRNA biogenesis. Science 307: 932-935.

43. Yang Z, Ebright YW, Yu B, Chen X (2006) HEN1 recognizes 21-24 nt small RNA duplexes and deposits a methyl group onto the 2' OH of the 3' terminal nucleotide. Nucleic Acids Res 34: 667-675.

44. Chen X, Liu J, Cheng Y, Jia D (2002) HEN1 functions pleiotropically in *Arabidopsis* development and acts in C function in the flower. Development 129: 1085-1094.

45. Abe M, Yoshikawa T, Nosaka M, Sakakibara H, Sato Y, et al. (2010) WAVY LEAF1, an ortholog of *Arabidopsis* HEN1, regulates shoot development by maintaining microRNA and trans-acting small interfering RNA accumulation in rice. Plant Physiol 154: 1335-1346.

46. Saito K, Sakaguchi Y, Suzuki T, Suzuki T, Siomi H, et al. (2007) Pimet, the Drosophila homolog of HEN1, mediates 2'-O-methylation of Piwi- interacting RNAs at their 3' ends. Genes Dev 21: 1603-1608.

47. Horwich MD, Li C, Matranga C, Vagin V, Farley G, et al. (2007) The Drosophila RNA methyltransferase, DmHen1, modifies germline piRNAs and single-stranded siRNAs in RISC. Curr Biol 17: 1265-1272.

48. Kirino Y, Mourelatos Z (2007) The mouse homolog of HEN1 is a potential methylase for Piwi-interacting RNAs. RNA 13: 1397-1401.

49. Kurth HM, Mochizuki K (2009) 2′-O-methylation stabilizes Piwi-associated small RNAs and ensures DNA elimination in *Tetrahymena*. RNA 15: 675-685.

50. Kamminga LM, Luteijn MJ, den Broeder MJ, Redl S, Kaaij LJT, et al. (2010) Hen1 is required for oocyte development and piRNA stability in zebrafish. EMBO J 29: 3688-3700.

51. Billi AC, Alessi AF, Khivansara V, Han T, Freeberg M, et al. (2012) The *Caenorhabditis elegans* HEN1 ortholog, HENN-1, methylates and stabilizes select subclasses of germline small RNAs. PLoS Genet 8: e1002617.

52. Huang Y, Ji L, Huang Q, Vassylyev DG, Chen X, et al. (2009) Structural insights into mechanisms of the small RNA methyltransferase HEN1. Nature 461: 823-827.

53. Xie Z, Johansen LK, Gustafson AM, Kasschau KD, Lellis AD, et al. (2004) Genetic and functional diversification of small RNA pathways in plants. PLoS Biol 2: e104.

54. Czech B, Hannon GJ (2011) Small RNA sorting: matchmaking for Argonautes. Nat Rev Genet 12: 19-31.

55. Xie Z, Khanna K, Ruan S (2010) Expression of microRNAs and its regulation in plants. Semin Cell Dev Biol 21: 790-797.

56. Mi S, Cai T, Hu Y, Chen Y, Hodges E, et al. (2008) Sorting of small RNAs into *Arabidopsis* Argonaute complexes is directed by the 5′ terminal nucleotide. Cell 133: 116-127.

57. Eamens AL, Smith NA, Curtin SJ, Wang MB, Waterhouse PM (2009) The *Arabidopsis thaliana* double-stranded RNA binding protein DRB1 directs guide strand selection from microRNA duplexes. RNA 15: 2219-2235.

58. Manavella PA, Hagmann J, Ott F, Laubinger S, Franz M, et al. (2012) Fast-forward genetics identifies plant CPL phosphatases as regulators of miRNA processing factor HYL1. Cell 151: 859-870.

59. Yi R, Qin Y, Macara IG, Cullen BR (2003) Exportin-5 mediates the nuclear export of pre-microRNAs and short hairpin RNAs. Genes Dev 17: 3011-3016.

60. Bohnsack MT, Czaplinski K, Gorlich D (2004) Exportin 5 is a RanGTP-dependent dsRNA-binding protein that mediates nuclear export of pre-miRNAs. RNA 10: 185-191.

61. Park MY, Wu G, Gonzalez-Sulser A, Vaucheret H, Poethig RS (2005) Nuclear processing and export of microRNAs in *Arabidopsis*. Proc Natl Acad Sci U S A 102: 3691-3696.

62. Smith MR, Willmann MR, Wu G, Berardini TZ, Möller B, et al. (2009) Cyclophilin 40 is required for microRNA activity in *Arabidopsis*. Proc Natl Acad Sci U S A 106: 5424-5429.

63. Kim YJ, Zheng B, Yu Y, Won SY, Mo B, et al. (2011) The role of Mediator in small and long noncoding RNA production in *Arabidopsis thaliana*. EMBO J 30: 814-822.

64. Zhang S, Xie M, Ren G, Yu B (2013) CDC5, a DNA binding protein, positively regulates posttranscriptional processing and/or transcription of primary microRNA transcripts. Proc Natl Acad Sci U S A 110: 17588-17593.

65. Zhang S, Liu Y, Yu B (2014) PRL1, an RNA-binding protein, positively regulates the accumulation of miRNAs and siRNAs in *Arabidopsis*. PLoS Genet 10: e1004841.

66. Fang X, Cui Y, Li Y, Qi Y (2015) Transcription and processing of primary microRNAs are coupled by Elongator complex in *Arabidopsis*. Nat Plants 1: 15075.

67. Jung JH, Park CM (2007) *MIR166/165* genes exhibit dynamic expression patterns in regulating shoot apical meristem and floral development in *Arabidopsis*. Planta 225: 1327-1338.

68. Zhou Y, Honda M, Zhu H, Zhang Z, Guo X, et al. (2015) Spatiotemporal sequestration of miR165/166 by *Arabidopsis* Argonaute10 Promotes shoot apical meristem maintenance. Cell Rep 10: 1819-1827.

69. Yant L, Mathieu J, Dinh TT, Ott F, Lanz C, et al. (2010) Orchestration of the floral transition and floral development in *Arabidopsis* by the bifunctional transcription factor APETALA2. Plant Cell 22: 2156-2170.

70. Yumul RE, Kim YJ, Liu X, Wang R, Ding J, et al. (2013) *POWERDRESS* and diversified expression of the *MIR172* gene family bolster the floral stem cell network. PLoS Genet 9: e1003218.

71. Wang F, Perry SE (2013) Identification of direct targets of FUSCA3, a key regulator of *Arabidopsis* seed development. Plant Physiol 161: 1251-1264.

72. Yamasaki H, Abdel-Ghany SE, Cohu CM, Kobayashi Y, Shikanai T, et al. (2007) Regulation of copper homeostasis by Micro-RNA in *Arabidopsis*. J Biol Chem 282: 16369-16378.

73. Guan Q, Lu X, Zeng H, Zhang Y, Zhu J (2013) Heat stress induction of miR398 triggers a regulatory loop that is critical for thermotolerance in *Arabidopsis*. Plant J 74: 840-851.

74. Fujii H, Chiou TJ, Lin SI, Aung K, Zhu JK (2005) A miRNA involved in phosphate-starvation response in *Arabidopsis*. Curr Biol 15: 2038-2043.

75. Bari R, Datt Pant B, Stitt M, Scheible WR (2006) PHO2, microRNA399, and PHR1 define a phosphate-signaling pathway in plants. Plant Physiol 141: 988-999.

76. Kim S, Yang JY, Xu J, Jang IC, Prigge MJ, et al. (2008) Two cap-binding proteins CBP20 and CBP80 are involved in processing primary MicroRNAs. Plant Cell Physiol 49: 1634-1644.

77. Laubinger S, Sachsenberg T, Zeller G, Busch W, Lohmann JU, et al. (2008) Dual roles of the nuclear cap-binding complex and SERRATE in pre-mRNA splicing and microRNA processing in *Arabidopsis thaliana*. Proc Natl Acad Sci U S A 105: 8795-8800.

78. Ren G, Xie M, Dou Y, Zhang S, Zhang C, et al. (2012) Regulation of miRNA abundance by RNA binding protein TOUGH in *Arabidopsis*. Proc Natl Acad Sci U S A 109: 12817-12821.

79. Lee BH, Kapoor A, Zhu J, Zhu JK (2006) STABILIZED1, a stress-upregulated nuclear protein, is required for pre-mRNA splicing, mRNA turnover, and stress tolerance in *Arabidopsis*. Plant Cell 18: 1736-1749.

80. Ben Chaabane S, Liu R, Chinnusamy V, Kwon Y, Park JH, et al. (2013) STA1, an *Arabidopsis* pre-mRNA processing factor 6 homolog, is a new player involved in miRNA biogenesis. Nucleic Acids Res 41: 1984-1997.

81. Copeland C, Xu S, Qi Y, Li X (2013) MOS2 has redundant function with its homolog MOS2H and is required for proper splicing of SNC1. Plant Signal Behav 8(9).

82. Wu X, Shi Y, Li J, Xu L, Fang Y, et al. (2013) A role for the RNA-binding protein MOS2 in microRNA maturation in *Arabidopsis*. Cell Res 23: 645-657.

83. Cho SK, Ben Chaabane S, Shah P, Poulsen CP, Yang SW (2014) COP1 E3 ligase protects HYL1 to retain microRNA biogenesis. Nat Commun 5: 5867.

84. Xie Z, Kasschau KD, Carrington JC (2003) Negative feedback regulation of Dicer-Like1 in *Arabidopsis* by microRNA-guided mRNA degradation. Curr Biol 13: 784-789.

85. Niu D, Lii YE, Chellappan P, Lei L, Peralta K, et al. (2016) miRNA863-3p sequentially targets negative immune regulator ARLPKs and positive regulator SERRATE upon bacterial infection. Nat Commun 7: 11324.

86. Vaucheret H (2009) AGO1 homeostasis involves differential production of 21-nt and 22-nt miR168 Species by *MIR168a* and *MIR168b*. PLoS ONE 4: e6442.

87. Rogers K, Chen X (2013) Biogenesis, turnover, and mode of action of plant microRNAs. Plant Cell 25: 2383-2399.

88. Hutvágner G, Zamore PD (2002) A microRNA in a multiple-turnover RNAi enzyme complex. Science 297: 2056-2060.

89. Brodersen P, Sakvarelidze-Achard L, Bruun-Rasmussen M, Dunoyer P, Yamamoto YY, et al. (2008) Widespread translational inhibition by plant miRNAs and siRNAs. Science 320: 1185-1190.

90. Yang L, Wu G, Poethig RS (2012) Mutations in the GW-repeat protein SUO reveal a developmental function for microRNA-mediated translational repression in *Arabidopsis*. Proc Natl Acad Sci U S A 109: 315-320.

91. Li S, Liu L, Zhuang X, Yu Y, Liu X, et al. (2013) MicroRNAs inhibit the translation of target mRNAs on the endoplasmic reticulum in *Arabidopsis*. Cell 153: 562-574.

92. Aukerman MJ, Sakai H (2003) Regulation of flowering time and floral organ identity by a microRNA and its APETALA2-like target genes. Plant Cell 15: 2730-2741.

93. Chen X (2004) A microRNA as a translational repressor of APETALA2 in *Arabidopsis* flower development. Science 303: 2022-2025.

94. Gandikota M, Birkenbihl RP, Höhmann S, Cardon GH, Saedler H, et al. (2007) The miRNA156/157 recognition element in the 3′ UTR of the *Arabidopsis* SBP box gene *SPL3* prevents early flowering by translational inhibition in seedlings. Plant J 49: 683-693.

95. Hou CY, Lee WC, Chou HC, Chen AP, Chou SJ, et al. (2016) Global analysis of truncated RNA ends reveals new insights into ribosome stalling in plants. Plant Cell 28:2398-2416.

96. Yu X, Willmann MR, Anderson SJ, Gregory BD (2016) Genome-wide mapping of uncapped and cleaved transcripts reveals a role for the nuclear mRNA cap-binding complex in cotranslational RNA decay in *Arabidopsis*. Plant Cell 28: 2385-2397.

97. Li S, Le B, Ma X, Li S, You C, et al. (2016) Biogenesis of phased siRNAs on membrane-bound polysomes in *Arabidopsis*. eLife 5: e22750.

98. Llave C, Xie Z, Kasschau KD, Carrington JC (2002) Cleavage of *Scarecrow-like* mRNA targets directed by a class of *Arabidopsis* miRNA. Science 297: 2053-2056.

99. German MA, Pillay M, Jeong DH, Hetawal A, Luo S, et al. (2008) Global identification of microRNA-target RNA pairs by parallel analysis of RNA ends. Nat Biotech 26: 941-946.

100. Takeda A, Iwasaki S, Watanabe T, Utsumi M, Watanabe Y (2008) The mechanism selecting the guide strand from small RNA duplexes is different among Argonaute proteins. Plant Cell Physiol 49: 493-500.

101. Montgomery TA, Howell MD, Cuperus JT, Li D, Hansen JE, et al. (2008) Specificity of ARGONAUTE7-miR390 interaction and dual functionality in *TAS3* trans-acting siRNA formation. Cell 133: 128-141.

102. Maunoury N, Vaucheret H (2011) AGO1 and AGO2 act redundantly in miR408-mediated plantacyanin regulation. PLoS ONE 6: e28729.

103. Jia X, Yan J, Tang G (2011) MicroRNA-mediated DNA methylation in plants. Front in Biol 6: 133-139.

104. Zhu H, Hu F, Wang R, Zhou X, Sze SH, et al. (2011) *Arabidopsis* Argonaute10 specifically sequesters miR166/165 to regulate shoot apical meristem development. Cell 145: 242-256.

105. Souret FF, Kastenmayer JP, Green PJ (2004) AtXRN4 degrades mRNA in *Arabidopsis* and its substrates include selected miRNA targets. Mol Cell 15: 173-183.

106. Ibrahim F, Rohr J, Jeong WJ, Hesson J, Cerutti H (2006) Untemplated oligoadenylation promotes degradation of RISC-cleaved transcripts. Science 314: 1893.

107. Ren G, Xie M, Zhang S, Vinovskis C, Chen X, et al. (2014) Methylation protects microRNAs from an AGO1-associated activity that uridylates 5′ RNA fragments generated by AGO1 cleavage. Proc Natl Acad Sci U S A 111: 6365-6370.

108. Wang X, Zhang S, Dou Y, Zhang C, Chen X, et al. (2015) Synergistic and independent actions of multiple terminal nucleotidyl transferases in the 3' tailing of small RNAs in *Arabidopsis*. PLoS Genet 11: e1005091.

109. Branscheid A, Marchais A, Schott G, Lange H, Gagliardi D, et al. (2015) SKI2 mediates degradation of RISC 5′-cleavage fragments and prevents secondary siRNA production from miRNA targets in *Arabidopsis*. Nucleic Acids Res 43: 10975-10988.

110. Alonso-Peral MM, Li J, Li Y, Allen RS, Schnippenkoetter W, et al. (2010) The microRNA159-regulated *GAMYB-like* genes inhibit growth and promote programmed cell death in *Arabidopsis*. Plant Physiol 154: 757-771.

111. Lanet E, Delannoy E, Sormani R, Floris M, Brodersen P, et al. (2009) Biochemical evidence for translational repression by *Arabidopsis* microRNAs. Plant Cell 21: 1762-1768.

112. Yoshikawa M, Peragine A, Park MY, Poethig RS (2005) A pathway for the biogenesis of trans-acting siRNAs in *Arabidopsis*. Genes Dev 19: 2164-2175.

113. Yoshikawa M, Iki T, Tsutsui Y, Miyashita K, Poethig RS, et al. (2013) 3′ fragment of miR173-programmed RISC-cleaved RNA is protected from degradation in a complex with RISC and SGS3. Proc Natl Acad Sci U S A 110: 4117-4122.

114. Arribas-Hernández L, Marchais A, Poulsen C, Haase B, Hauptmann J, et al. (2016) The slicer activity of ARGONAUTE1 is required specifically for the phasing, not production, of trans-acting short interfering RNAs in *Arabidopsis*. Plant Cell 28: 1563-1580.

115. Allen E, Xie Z, Gustafson AM, Carrington JC (2005) microRNA-directed phasing during trans-acting siRNA biogenesis in plants. Cell 121: 207-221.

116. Chen HM, Chen LT, Patel K, Li YH, Baulcombe DC, et al. (2010) 22-nucleotide RNAs trigger secondary siRNA biogenesis in plants. Proc Natl Acad Sci U S A 107: 15269-15274.

117. Cuperus JT, Carbonell A, Fahlgren N, Garcia-Ruiz H, Burke RT, et al. (2010) Unique functionality of 22-nt miRNAs in triggering RDR6-dependent siRNA biogenesis from target transcripts in *Arabidopsis*. Nat Struct Mol Biol 17: 997-1003.

118. Axtell MJ, Jan C, Rajagopalan R, Bartel DP (2006) A two-hit trigger for siRNA biogenesis in plants. Cell 127: 565-577.

119. Zhang C, Ng DW, Lu J, Chen ZJ (2012) Roles of target site location and sequence complementarity in trans-acting siRNA formation in *Arabidopsis*. Plant J 69: 217-226.

120. Yoshikawa M, Iki T, Numa H, Miyashita K, Meshi T, et al. (2016) A short open reading frame encompassing the microRNA173 target site plays a role in trans-acting small interfering RNA biogenesis. Plant Physiol 171: 359-368.

121. Fei Q, Xia R, Meyers BC (2013) Phased, secondary, small interfering RNAs in posttranscriptional regulatory networks. Plant Cell 25: 2400-15.

122. Zhai J, Zhao Y, Simon SA, Huang S, Petsch K, et al. (2013) Plant microRNAs display differential 3′ truncation and tailing modifications that are ARGONAUTE1 dependent and conserved across species. Plant Cell 25: 2417-2428.

123. Zhai J, Zhang H, Arikit S, Huang K, Nan GL, et al. (2015) Spatiotemporally dynamic, cell-type–dependent premeiotic and meiotic phasiRNAs in maize anthers. Proc Natl Acad Sci U S A 112: 3146-3151.

124. Fan Y, Yang J, Mathioni SM, Yu J, Shen J, et al. (2016) PMS1T, producing phased small-interfering RNAs, regulates photoperiod-sensitive male sterility in rice. Proc Natl Acad Sci U S A 113: 15144-15149.

125. Brodersen P, Sakvarelidze-Achard L, Schaller H, Khafif M, Schott G, et al. (2012) Isoprenoid biosynthesis is required for miRNA function and affects membrane association of ARGONAUTE 1 in *Arabidopsis*. Proc Natl Acad Sci U S A 109: 1778-1783.

126. Xu J, Chua NH (2011) Processing bodies and plant development. Curr Opin Plant Biol 14: 88-93.

127. Kumakura N, Takeda A, Fujioka Y, Motose H, Takano R, et al. (2009) SGS3 and RDR6 interact and colocalize in cytoplasmic SGS3/RDR6-bodies. FEBS Lett 583: 1261-1266.

128. Jouannet V, Moreno AB, Elmayan T, Vaucheret H, Crespi MD, et al. (2012) Cytoplasmic *Arabidopsis* AGO7 accumulates in membrane-associated siRNA bodies and is required for ta-siRNA biogenesis. EMBO J 31: 1704-1713.

129. Ramachandran V, Chen X (2008) Degradation of microRNAs by a Family of Exoribonucleases in *Arabidopsis*. Science 321: 1490-1492.

130. Zhao Y, Yu Y, Zhai J, Ramachandran V, Dinh TT, et al. (2012) The *Arabidopsis* nucleotidyl transferase HESO1 uridylates unmethylated small RNAs to trigger their degradation. Curr Biol 22: 689-694.

131. Tu B, Liu L, Xu C, Zhai J, Li S, et al. (2015) Distinct and cooperative activities of HESO1 and URT1 nucleotidyl transferases in microRNA turnover in *Arabidopsis*. PLoS Genet 11: e1005119.

132. Yu Y, Ji L, Le BH, Zhai J, Chen J, et al. (2017) ARGONAUTE10 promotes the degradation of miR165/6 through the SDN1 and SDN2 exonucleases in *Arabidopsis*. PLoS Biol 15: e2001272.

133. Chang H-M, Triboulet R, Thornton JE, Gregory RI (2013) A role for the Perlman syndrome exonuclease Dis3l2 in the Lin28-let-7 pathway. Nature 497: 244-248.

134. Ustianenko D, Hrossova D, Potesil D, Chalupnikova K, Hrazdilova K, et al. (2013) Mammalian DIS3L2 exoribonuclease targets the uridylated precursors of let-7 miRNAs. RNA 19: 1632-1638.

135. Ibrahim F, Rymarquis LA, Kim E-J, Becker J, Balassa E, et al. (2010) Uridylation of mature miRNAs and siRNAs by the MUT68 nucleotidyltransferase promotes their degradation in Chlamydomonas. Proc Natl Acad Sci U S A 107: 3906-3911.

136. Wyman SK, Knouf EC, Parkin RK, Fritz BR, Lin DW, et al. (2011) Post-transcriptional generation of miRNA variants by multiple nucleotidyl transferases contributes to miRNA transcriptome complexity. Genome Res 21: 1450-1461.

137. Martin G, Keller W (2007) RNA-specific ribonucleotidyl transferases. RNA 13: 1834-1849.

138. Ren G, Chen X, Yu B (2012) Uridylation of miRNAs by hen1 suppressor1 in *Arabidopsis*. Curr Biol 22: 695-700.

139. Karlsson P, Christie MD, Seymour DK, Wang H, Wang X, et al. (2015) KH domain protein RCF3 is a tissue-biased regulator of the plant miRNA biogenesis cofactor HYL1. Proc Natl Acad Sci U S A 112: 14096-14101.

140. Lu S, Sun Y-H, Chiang VL (2009) Adenylation of plant miRNAs. Nucleic Acids Research 37: 1878-1885.

141. Vaucheret H, Vazquez F, Crété P, Bartel DP (2004) The action of ARGONAUTE1 in the miRNA pathway and its regulation by the miRNA pathway are crucial for plant development. Genes Dev 18: 1187-1197.

142. Zhao Y, Yu Y, Zhai J, Ramachandran V, Dinh Thanh T, et al. (2012) The *Arabidopsis* nucleotidyl transferase HESO1 uridylates unmethylated small RNAs to trigger their degradation. Curr Biol 22: 689-694.

143. Liu Q, Yao X, Pi L, Wang H, Cui X, et al. (2009) The ARGONAUTE10 gene modulates shoot apical meristem maintenance and establishment of leaf polarity by repressing miR165/166 in *Arabidopsis*. Plant J 58: 27-40.

144. Franco-Zorrilla JM, Valli A, Todesco M, Mateos I, Puga MI, et al. (2007) Target mimicry provides a new mechanism for regulation of microRNA activity. Nat Genet 39: 1033-1037.

145. Ivashuta S, Banks IR, Wiggins BE, Zhang Y, Ziegler TE, et al. (2011) Regulation of gene expression in plants through miRNA inactivation. PLoS ONE 6: e21330.

146. Wu HJ, Wang ZM, Wang M, Wang XJ (2013) Widespread long noncoding RNAs as endogenous target mimics for microRNAs in plants. Plant Physiol 161: 1875-1884.

147. Tang G, Yan J, Gu Y, Qiao M, Fan R, et al. (2012) Construction of short tandem target mimic (STTM) to block the functions of plant and animal microRNAs. Methods 58: 118-125.

148. Bartel DP (2009) MicroRNAs: target recognition and regulatory functions. Cell 136: 215-233.

149. Ameres SL, Horwich MD, Hung JH, Xu J, Ghildiyal M, et al. (2010) Target RNA–directed trimming and tailing of small silencing RNAs. Science 328: 1534-1539.

150. Marcinowski L, Tanguy M, Krmpotic A, Rädle B, Lisnić VJ, et al. (2012) Degradation of cellular miR-27 by a novel, highly abundant viral transcript is important for efficient virus replication in vivo. PLoS Pathog 8: e1002510.

151. Cazalla D, Yario T, Steitz JA (2010) Down-regulation of a host microRNA by a *Herpesvirus saimiri* noncoding RNA. Science 328: 1563-1566.

152. Sheng G, Zhao H, Wang J, Rao Y, Tian W, et al. (2014) Structure-based cleavage mechanism of *Thermus thermophilus* Argonaute DNA guide strand-mediated DNA target cleavage. Proc Natl Acad Sci U S A 111: 652-657.

153. Derrien B, Baumberger N, Schepetilnikov M, Viotti C, De Cillia J, et al. (2012) Degradation of the antiviral component ARGONAUTE1 by the autophagy pathway. Proc Natl Acad Sci U S A 109: 15942-15946.

154. Earley K, Smith M, Weber R, Gregory B, Poethig R (2010) An endogenous F-box protein regulates ARGONAUTE1 in *Arabidopsis thaliana*. Silence 1: 15.

Figures

Figure 1.1 Illustrations of major steps in miRNA biogenesis in plants.

MIR genes are transcribed by Pol II, which gives rise to single-stranded pri-miRNAs under the facilitate of mediator and CDC5. DCL1 processes pri-miRNAs into mature miRNA duplexes via two steps in the dicing-bodies, together with HYL1, SE and other cofactors. HEN1 mediates the 3' end 2-*O'*-methylation of both strands in the duplexes which are later transported from nucleus to cytoplasm by HST. MiRNA strands are then loaded onto AGO1 to carry out their activities.

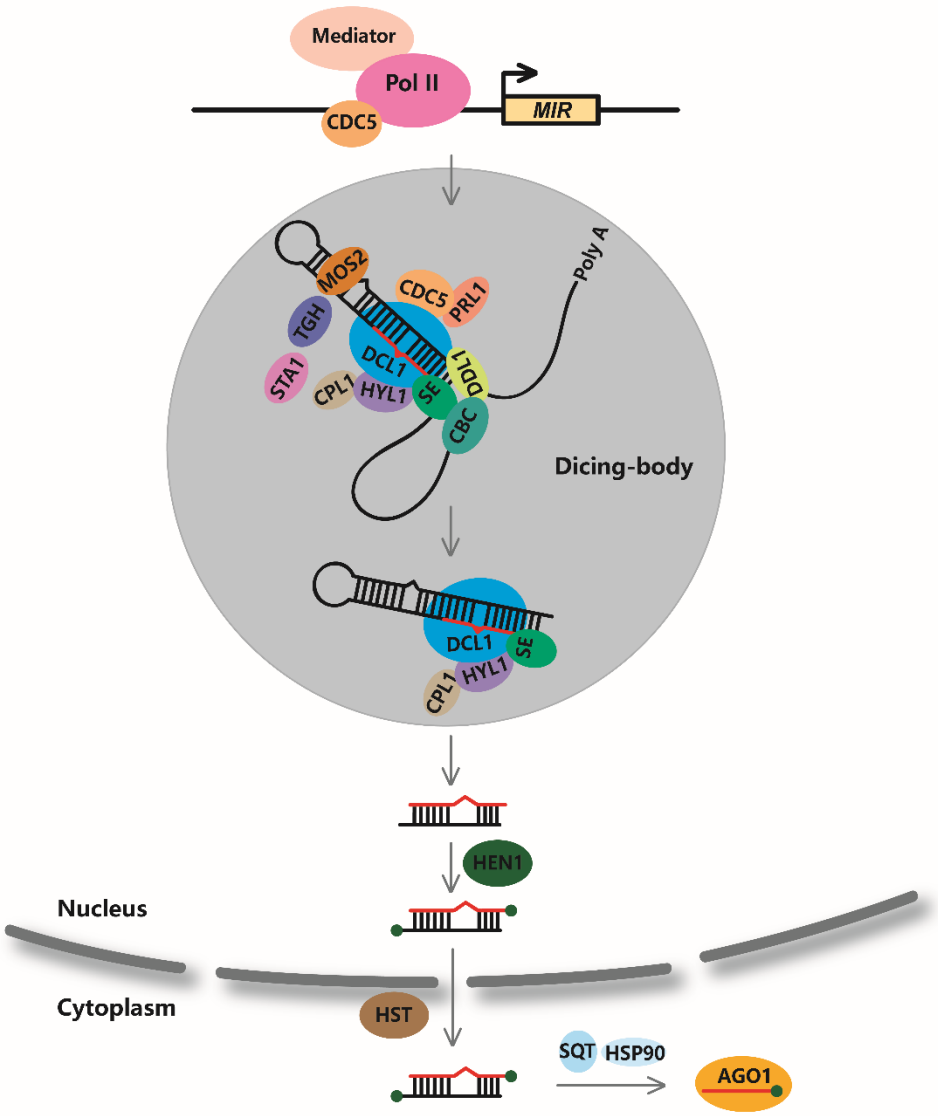
Mediator
Pol II
CDC5
MIR
MOS2
CDC5
PRL1
TGH
DCL1
DDL1
STA1
CPL1
HYL1
SE
CBC
Poly A
Dicing-body
DCL1
SE
CPL1
HYL1
HEN1
Nucleus
Cytoplasm
HST
SQT
HSP90
AGO1

Figure 1.2 Overview of miRNA modes of action in plants.

Mature miRNAs are incorporated into AGO proteins to direct PTGS via transcript cleavage and translation repression or trigger the biogenesis of secondary siRNAs. AGO1 mediates miRNA target cleavage followed by degradation of the cleavage fragments. The cytoplasmic location of this event is unclear, but the uridylation and turnover of 5' cleavage fragments occurs on AGO1. Translation repression takes place on MBPs, and requires ER-localized AMP1. Components of P-body are also involved in this process, although the function of these factors and their connection to ER remain mysterious. AGO7 cleaves miR390 targets that are associated with MBPs, and forms siRNA bodies together with SGS3 and RDR6 that are adjacent to cis-Golgi. Other *TAS* transcripts that generate phasiRNAs in response to AGO1-mediated cleavage also associate with MBPs. Events are classified with colored lines according to miRNA-mediated actions (dark lines) and subsequent processing (light purple) of their targets.

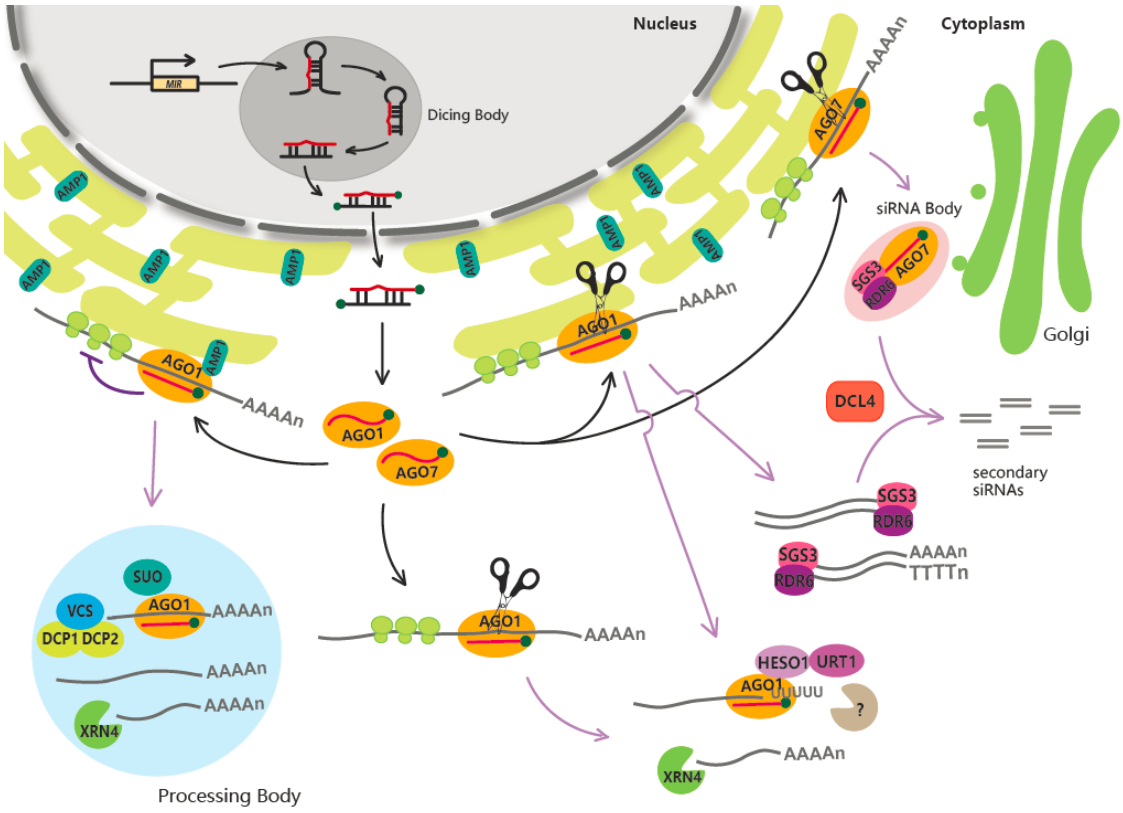
Nucleus
Cytoplasm
MIR
Dicing Body
AMP
AGO1
AGO7
AAAAn
siRNA Body
SGS3
RDR6
Golgi
DCL4
secondary
siRNAs
TTTTn
SUO
VCS
DCP1 DCP2
XRN4
Processing Body
HESO1
URT1
UUUU
?

Figure 1.3 Mechanisms of plant miRNA turnover.

MiRNA degradation starts with the removal of the methyl group at the 3' end by SDN1, which is followed by 3' uridylation through HESO1 and/or URT1. The tailed miRNAs are subsequently degraded by an unknown exonuclease. SDN1 and nucleotidyl transferases (HESO1 and URT1) can act on both AGO-bound miRNAs and free miRNAs in the cytoplasm. Free miRNAs are also degraded by SDN1 directly. The degradation of AGO1 via autophagy may also contribute to miRNA turnover.

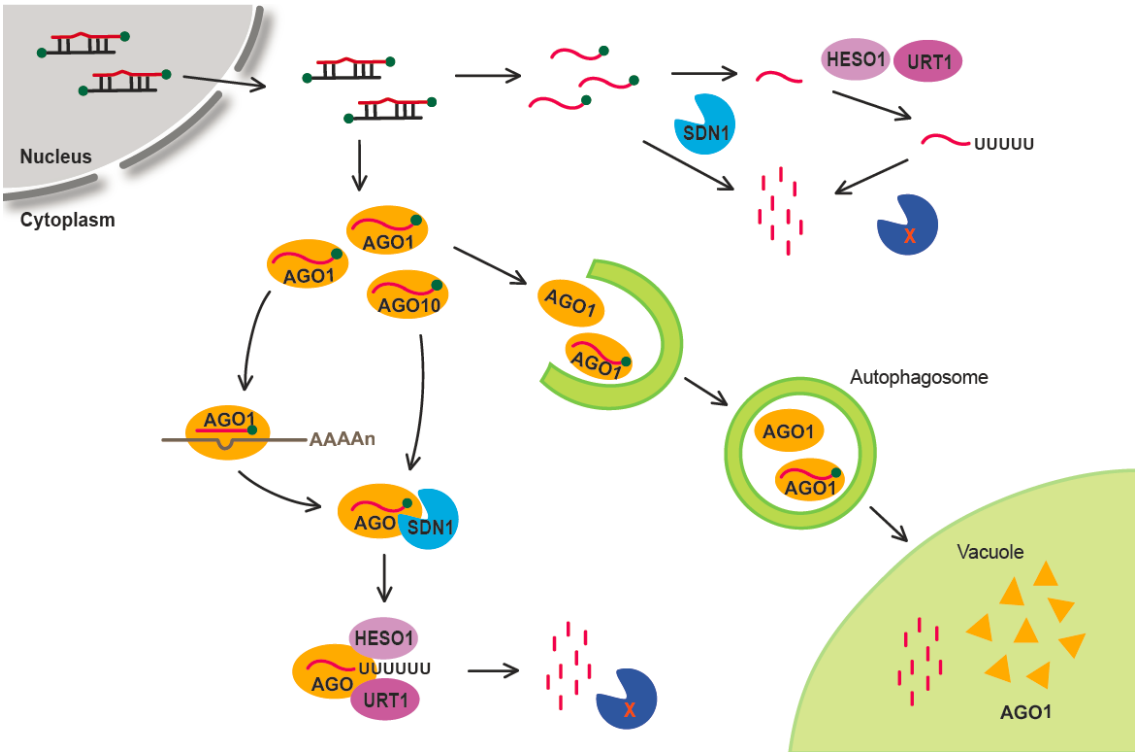
Nucleus
Cytoplasm
HESO1
URT1
SDN1
UUUUU
X
AGO1
AGO1
AGO10
AGO1
AGO1
AGO1
AAAAn
AGO
SDN1
Autophagosome
AGO1
AGO1
Vacuole
AGO1
HESO1
AGO
UUUUUU
URT1
X

Chapter 2

Argonaute 10 promotes degradation of miR165/6 through exonucleases SDN1 and SDN2 in *Arabidopsis*

Abstract

The degradation of small RNAs in plants and animals is associated with small RNA 3' truncation and 3' uridylation and thus relies on exonucleases and nucleotidyl transferases. ARGONAUTE (AGO) proteins associate with small RNAs *in vivo* and are essential for not only the activities but also the stability of small RNAs. AGO1 is the miRNA effector in *Arabidopsis* and its closest homolog, AGO10, maintains stem cell homeostasis in meristems by sequestration of miR165/6, a conserved miRNA acting through AGO1. Here, we show that SMALL RNA DEGRADING NUCLEASES (SDNs) initiate miRNA degradation by acting on AGO1-bound miRNAs to cause their 3' truncation, and the truncated species are uridylated and degraded. We report that *AGO10* reduces miR165/6 accumulation by enhancing its degradation by SDN1 and SDN2 *in vivo*. *In vitro*, AGO10-bound miR165/6 is more susceptible to SDN1-mediated 3' truncation than AGO1-bound miR165/6. Thus, AGO10 promotes the degradation of its associated miRNAs, which is contrary to the stabilizing effect of all known AGO proteins on their associated small RNAs. Our work identifies a class of exonucleases responsible for miRNA 3' truncation *in vivo* and uncovers a mechanism of specificity determination in miRNA turnover. This work, together with previous studies on AGO10, suggests that spatially regulated miRNA degradation underlies stem cell maintenance in plants.

Introduction

Arabidopsis ARGONAUTE10 (*AGO10*), also known as *ZWILLE* (*ZLL*) or *PINHEAD* (*PNH*), maintains stem cell homeostasis in the shoot apical meristem (SAM) and floral meristems through repression of miR165/6 activity [1-5]. The conserved miR165/6 family acts through *AGO1* to down-regulate the type III homeodomain-leucine zipper (HD-Zip III) genes that are critical for stem cell maintenance, leaf polarity, and vasculature development [6-10]. *AGO10* is expressed in the adaxial side of organ primordia and in the provasculature underneath the SAM to maintain stem cells in the SAM in a non-cell autonomous manner [3,4,11], whereas miR165/6 is restricted to the abaxial side of organ primordia and excluded from the SAM [2,7]. As AGO10 binds miR165/6 with higher affinity than AGO1, it was hypothesized that AGO10, which accumulates in a highly restricted manner in the plant [3,4,11], sequesters miR165/6 to prevent it from repressing its target genes through the ubiquitously present AGO1 protein [5,12].

AGO10 has also been implicated in repressing the accumulation of miR165/6. In multiple *ago10* loss-of-function mutants, the levels of miR165/6 are moderately increased (to 1.5-2 fold of wild-type levels) as determined by northern blotting with whole seedlings or inflorescences [1,2,5]. Given that *AGO10*-expressing cells constitute only a tiny portion of the tissues used in these studies, the small increase is likely an underestimate for the ability of *AGO10* to repress miR165/6 accumulation. In fact, *in situ* hybridization revealed that miR165/6, which is normally excluded from the SAM, accumulates in the SAM in *ago10* mutants [2], suggesting that AGO10 not only sequesters miR165/6 but also represses its accumulation. The impact of AGO10 on miR165/6 contrasts the positive effects of *Arabidopsis* AGO1 on the accumulation of miRNAs, including miR165/6 [1,13]. The mechanism by which AGO10 reduces the levels of miR165/166 is currently unknown.

The steady-state levels of miRNAs are determined by the balance between biogenesis and degradation. miRNA biogenesis is a multistep process. After the transcription of *MIR* genes into pri-miRNAs, DICER-LIKE1 (DCL1) processes pri-miRNAs into pre-miRNAs and pre-miRNAs into the miRNA/miRNA* duplexes. The duplexes are methylated by HEN1, and the miRNA strand is loaded into AGO1, the major miRNA effector, to form the RNA-induced silencing complex (RISC) (reviewed in [14]).

The mechanisms of miRNA degradation are not well understood. Degradation intermediates are hard to detect in the wild-type background, but they are readily detectable in *hen1* mutants, in which miRNAs and small interfering RNAs (siRNAs) in plants and Piwi-interacting RNAs (piRNAs) in animals lose 2'-*O*-methylation on the 3' terminal ribose and are more susceptible to degradation [15-25]. Studies of the consequences of loss of methylation in both plant and animal *hen1* mutants revealed two molecular processes associated with small RNA degradation, namely 3' truncation and 3' uridylation [15,18,19,21,22]. The enzyme that causes miRNA 3' truncation is presumably an exonuclease, but its nature is as yet unknown in *Arabidopsis*. Two nucleotidyl transferases, HESO1 and URT1, play a major and minor role, respectively, in miRNA uridylation [26-29]. Both enzymes are able to uridylate AGO1-bound, unmethylated miRNAs *in vitro* and they act in a partially redundant and synergistic manner to uridylate unmethylated miRNAs *in vivo* [26-29]. The sequence of events in miRNA degradation (truncation followed by tailing or tailing followed by truncation) is unknown.

In *Arabidopsis*, the SDN family of 3' to 5' exonucleases consisting of five family members degrades short RNAs *in vitro* and limits the accumulation of miRNAs *in vivo* [30]. Prior *in vitro* enzymatic assays with SDN1 were performed with free RNA oligonucleotides as substrates, and in these assays, SDN1 was able to reduce the size of its substrate

RNA to a uniform and very small size [30]. This is apparently inconsistent with SDN1 being responsible for the observed miRNA 3' truncation activity *in vivo*, as the truncated species lack a small and varying number of nucleotides from the 3' end. However, *in vivo*, miRNAs are associated with, and protected by, AGO1; it is possible that the observed varying degree of 3' truncation is due to the balance between protection by AGO1 and exonucleolytic degradation by SDN1. It is unknown whether SDN1 is able to act on AGO1-bound miRNAs, and if so, whether the interplay between AGO1 and SDN1 leads to the truncation of a varying number of nucleotides. The answer to this question is critical in understanding how miRNAs are degraded *in vivo*, as SDN1 can act on methylated miRNAs [30] whereas HESO1 and URT1 cannot [26-29], which makes SDN proteins the prime candidates in initiating the degradation of methylated miRNAs *in vivo*.

In this study, we show that SDN1 and SND2 are responsible for the 3' truncation of a subset of miRNAs in the *hen1* background and miR165/6 species in the wild-type background, thereby revealing an enzyme associated with the 3' truncation process *in vivo*. We show that 3' truncated miRNAs are further tailed by HESO1 to lead to their degradation, thus clarifying the relationship between the two miRNA degradation processes. Furthermore, we show that, *in vitro*, SDN1 acts on AGO1-bound, methylated miRNAs to produce 3' truncated miRNAs of varying sizes, similar to those observed *in vivo*. These findings provide a molecular framework of miRNA degradation that acts on many miRNAs. Furthermore, we show that AGO10 promotes the degradation of its associated miR165/6 *in vivo*, and this effect requires SDNs. AGO10-bound miR165/6 is more susceptible to SDN1-mediated 3' truncation than AGO1-bound miR165/6 *in vitro*. This study reveals an unexpected activity of an AGO protein causing the degradation of its associated miRNA, uncovers a mechanism of specificity determination in miRNA

turnover, and implicates the importance of regulated miRNA degradation in stem cell maintenance.

Results

SDN1 and SDN2 are responsible for the 3' truncation of some miRNAs *in vivo*

In wild type, 3' truncated miRNA species are rare, presumably because the truncated species are rapidly degraded. Thus, to determine whether SDNs are responsible for miRNA 3' truncation, we resorted to a *hen1* mutant, in which the lack of 3' terminal 2'-*O*-methylation of miRNAs is associated with rampant miRNA 3' truncation and 3' uridylation. Truncated and/or tailed species of miRNAs are readily detectable by northern blotting [22,25] and quantifiable by small RNA high throughput sequencing (sRNA-seq) [26-29]. To ascertain whether SDNs are responsible for the production of 3' truncated miRNA species *in vivo*, we generated the *hen1-8 sdn1-1 sdn2-1* triple mutant (hereafter referred to as *hen1 sdn1 sdn2*) and compared its miRNA profiles with those of the *hen1-8* single mutant by sRNA-seq. To determine the sequence of events (3' truncation vs. 3' tailing), we also examined published sRNA-seq data from *hen1-8* and *hen1-8 heso1-1* [29]. Reads corresponding to each miRNA were classified into the full-length (FL), 3' truncated-only (TR-only), 3' tailed-only (TA-only), and 3' truncated-and-tailed (TR+TA) categories and quantified [29]. For both pairs of genotypes, two biological replicates were performed or analyzed. To be consistent, we present the 23 most abundant miRNAs (RPM>10) across all eight libraries.

We compared the levels of TR-only and TR+TA species in *hen1 sdn1 sdn2* and *hen1* as these species represented the miRNA 3' truncation activity. Nine out of the 23 miRNAs showed a significant reduction in the levels of either TR+TA or TR-only species in *hen1 sdn1 sdn2* (Figure 2.1A and Figure 2.2). In addition, one miRNA (miR167ab)

showed a significant reduction in TR+TA+TR-only species, although the reduction in either TR+TA or TR-only species was not statistically significant (Figure 2.1A). Thus, ten of the 23 miRNAs showed reduced 3' truncation. Many miRNAs also showed reduced 3' truncation in both biological replicates but did not pass the p-value cutoff (<0.05) while few miRNAs showed increased 3' truncation. This indicates that *SDN1* and *SDN2* are responsible for the production of 3' truncated species *in vivo* from at least some miRNAs. Functional redundancy with the remaining family members could be responsible for the lack of an observable effect on the 3' truncation of other miRNAs. Alternatively, non-SDN exonucleases also cause miRNA 3' truncation.

Having shown that SDN1 and SDN2 cause the 3' truncation of some miRNAs, we next sought to determine which occurred first, truncation by SDN1/2 or tailing by HESO1. Either is theoretically possible – SDN1 truncates miRNAs and HESO1 uridylates truncated miRNAs, or HESO1 uridylates miRNAs and SDN1 acts on uridylated miRNAs to cause their 3' truncation. In the hen1 heso1 double mutant, the levels of TR+TA species for many of the 23 miRNAs were reduced, and those of TR-only species were increased (Figure 2.1B). Therefore, HESO1 tailed the TR-only species to generate the TR+TA species. In particular, for the ten miRNAs with a significant reduction in 3' truncation in hen1 sdn1 sdn2 (Figure 2.1A), nine showed a significant increase in TR-only species in hen1 heso1 (Figure 2.1B). These data indicate that 3' truncated species generated by SDNs are further uridylated by HESO1 for degradation.

miR165/6 species were drastically affected in *hen1 sdn1 sdn2* relative to *hen1*. The proportion of full-length species of miR165 and miR166 was much higher in *hen1 sdn1 sdn2* than in *hen1* while those of TR-only or TR+TA species were much reduced (Figure 2.1C and Figure 2.2). The proportion of TA-only species was either unaffected

(miR166) or affected to a smaller extent (miR165) (Figure 2.1C and Figure 2.2). This demonstrated a role of SDN1 and SDN2 in the production of 3' truncated species of miR165/6 in the *hen1* background. In the wild-type background, the proportions of TR-only, TR+TA, and TA-only miR165/6 species were much lower than those in the *hen1* background (Figure 2.1C, D). Nevertheless, a reduction in the proportions of TR+TA species was observed in *sdn1 sdn2* relative to wild type (Figure 2.1D). Therefore, SDN1 and SDN2 are responsible for the 3' truncation of miR165/6 *in vivo* in both *hen1* and wild-type backgrounds. In *hen1 heso1*, the reduction in TR+TA miR165 or miR166 species is accompanied by an increase in TR-only species (Figure 2.1E), indicating that HESO1 tails 3' truncated miR165/6 species generated by SDN1/2.

SDN1 acts on AGO1-bound, methylated miRNAs *in vitro*

Given the results above, an appealing model (Figure 2.3, right panel) of miRNA degradation is that methylated, full-length miRNAs are first truncated by SDN1/2, which results in 3' truncated miRNAs that lack 3' terminal methylation. These 3' truncated species are then tailed by HESO1 and URT1 to cause their complete degradation. One important question related to this model is whether SDN1/2 can act on AGO1-bound miRNAs (Figure 2.3, left panel), as mature miRNAs are associated with AGO1 *in vivo*. HESO1 and URT1 are able to uridylate AGO1-bound, unmethylated miRNAs *in vitro* [26-29], but previous biochemical assays with SDN1 were only conducted with free RNA oligonucleotides as substrates [30]. Intriguingly, although SDN1 degrades RNA substrates to a uniform and very small size *in vitro* [30], the 3' truncated species that depended on SDN1/2 for accumulation *in vivo* had a small and varying number of nucleotides truncated from the 3' ends (Figure 2.2). One possibility is that SDN1 cannot completely degrade AGO1-bound miRNAs but instead only cause their 3' truncation.

To test this, we conducted SDN1 assays with AGO1 immunoprecipate (IP) (Figure 2.4A) as the substrate under enzyme excess conditions. miR165/6 was detected by northern blotting before and after the reactions. While SDN1 was able to nearly completely degrade a free RNA oligonucleotide, it was largely ineffective in degrading miR165/6 in AGO1 IP (Figure 2.4B). Thus, AGO1 protects miR165/6 from being degraded by SDN1 *in vitro*. However, we noticed that upon extended incubation (>2hr), weak signals representing shorter miR165/6 species were detectable in the AGO1 IP (Figure 2.4B), suggesting that SDN1 caused miR165/6 3' truncation at a low level. As northern blotting was not a sensitive method to detect such 3' truncated species, we performed sRNA-seq to determine whether SDN1 caused 3' truncation of AGO1-bound miR165/6 and other miRNAs. AGO1 IP was used as the substrate in assays with a mock (no enzyme) control, SDN1, and a catalytic mutant ($SDN1^{D283A}$) control for one hour. After the reactions, AGO1 was precipitated again and the associated small RNAs were subjected to high throughput sequencing. Two biological replicates yielded highly similar results (Figure 2.5). For the quantification of miRNA 3' truncation, the 3' truncated species present in the mock reactions were subtracted from those in the SDN1 or $SDN1^{D283A}$ reactions. We analyzed the 3' truncation status of all abundant miRNAs (RPM>10 in all six samples). 15 of 43 abundant miRNAs exhibited higher levels of 3' truncation in the SDN1 reactions as compared to the $SDN1^{D283A}$ reactions (Figure 2.6A). Several conclusions can be drawn from this *in vitro* study. First, SDN1 can act on AGO1-bound miRNAs, and unlike its activities on free RNAs, it generates heterogeneous, 3' truncated species from AGO1-bound miRNAs (Figure 2.6D), consistent with the 3' truncation observed in *hen1* mutants *in vivo*. Second, miRNAs in AGO1 IP should be methylated. Thus, SDN1 can act on methylated, AGO1-bound miRNAs, consistent with its ability to degrade methylated RNA

oligonucleotides [30]. Third, SDN1 was ineffective against many AGO1-bound miRNAs *in vitro* (Figure 2.6A), suggesting that other factors assist SDN1 in miRNA 3' truncation in *vivo* or other exonucleases also cause miRNA 3' truncation *in vivo*.

AGO10 represses miR165/6 accumulation

Loss-of-function *ago10* mutants, such as *pnh-2* and *ago10-13*, show increased levels of miR165/6 [1,2]. In northern blots with young seedlings of wild type, *pnh-2* and *ago10-13*, we consistently observed an increase in miR165/6 levels in six biological replicates (Figure 2.7A). We examined whether the increase in miR165/6 accumulation in these mutants could be attributed to enhanced miR165/6 biogenesis. miR165/6 is encoded by two *MIR165* and seven *MIR166* loci. We designed primers that allowed the detection of the sum of pri- and pre-miRNA species from each of the nine loci. RT-PCR was performed to determine whether pri/pre-miR165/6 species from all nine loci were present in young seedlings in wild type. While PCR using genomic DNA as the template produced a specific band at each locus, RT-PCR produced a band at all nine loci except for miR166g (Figure 2.7B). The finding that eight *MIR165/6* genes were expressed in young, wild-type seedlings was in agreement with findings from analyses of promoter activities of *MIR165/6* genes [31]. We performed real-time RT-PCR in wild-type, *pnh-2*, and *ago10-13* seedlings for these eight loci. The levels of the eight pri/pre-miR165/6 species were not increased in the two *ago10* mutants (Figure 2.7C). Consistent with this analysis, northern blotting showed that the levels of pre-miR166a were similar in wild-type and *pnh-2* seedlings (Figure 2.7D). Therefore, loss of function in *AGO10* resulted in an increase in the levels of mature miR165/6 but did not affect the transcription of *MIR165/6* genes or the processing of pri-miR165/6, suggesting that *AGO10* represses miR165/6 accumulation at a step after precursor processing.

AGO10 has been shown to recognize features of the miR165/miR165* or miR166/miR166* duplex during the loading of miR165/6 into AGO10 [5]. As miRNA/miRNA* duplexes are the substrates of HEN1, we asked whether AGO10's association with the duplex of miR165/6 and miR165/6* could compete with HEN1-mediated methylation. We immunoprecipitated AGO1 and AGO10 from a *zll-1 ZLLp::YFP-ZLL* line in which the *YFP-ZLL* (*AGO10*) transgene driven by the *ZLL* (*AGO10*) promoter fully rescues the morphological defects of *zll-1* [11].

β-elimination assays that interrogated the methylation status of miR165/6 showed that both AGO1- and AGO10-bound miR165/6 was fully methylated *in vivo* (Figure 2.7E), suggesting that *AGO10* does not affect the methylation status of this miRNA. Therefore, we conclude that *AGO10* must repress the accumulation of miR165/6 at a step after its biogenesis.

AGO10 over expression causes a reduction in miR165/6 levels

AGO10 is expressed in a highly restricted manner in meristems and developing organ primordia, and the expression domains of *AGO10* and miR165/6 are largely exclusive [2-4,7,11]. We reasoned that, if AGO10's association with miR165/6 leads to the degradation of the miRNA, *AGO10* over and ectopic expression should lead to further sequestration of miR165/6 from AGO1 and consequently a reduction in miR165/6 levels. To test this hypothesis, we introduced *YFP-AGO10* driven by the strong and constitutive *Cauliflower Mosaic Virus* 35S promoter into wild-type plants. Among independent T1 transgenic lines, most exhibited phenotypic alterations similar to what was previously observed to be associated with *AGO10* over expression [32]. The phenotypes were classified into the Weak (W), Moderate (M), and Strong (S) categories (Table 2.1). Plants in the different categories were largely similar in size to wild-type plants, but they differed

from wild type and from each other in the degrees of leaf hyponasty (upward curling) and serration as shown in Figure 2.8A. We focused on an *AGO10* over expression (*AGO10 OE*) line in the Strong category (referred to as *AGO10 OE S1*) for subsequent analyses. *AGO10* mRNA levels were much higher in this line than in wild type (Figure 2.9A). A large reduction in miR165/6 levels was observed in *AGO10 OE S1* (Figure 2.8B). Levels of pri/pre-miR165/6 from the eight genes with detectable expression in seedlings were unaffected (Figure 2.9B). The levels of pre-miR166a were also unaffected by *AGO10* over expression in two independent transgenic lines (one in the wild-type background (*AGO10 OE S1*) and the other in *pnh-2*) (Figure 2.9C). These data indicated that *AGO10* over expression did not affect the biogenesis of miR165/6.

Developmental phenotypes of the primary *AGO10 OE* transformants were classified into 4 categories: wild type (WT)-like, Weak, Moderate, and Strong, based on the degree of deviation from the wild-type leaf phenotype. 35 primary *AGO10 OE* transformants in wild-type background and 57 *AGO10 OE* transformants in the *sdn1 sdn2* background were analyzed.

Among the six miRNAs examined by northern blotting in *AGO10 OE S1*, miR173 was found to also accumulate at a lower level (Figure 2.8B). This raised the possibility that the reduced abundance of miR165/6 and miR173 in *AGO10 OE S1* was due to reduced *AGO1* expression, as previous studies demonstrated the association between miR168 and AGO10 and implicated *AGO10* in the repression of *AGO1* expression at the posttranscriptional level through miR168 [1,33]. Real time RT-PCR showed that the levels of *AGO1* mRNA were reduced by about 20% in *AGO10 OE S1* (Figure 2.9A). AGO1 protein levels were reduced by about 50% (Figure 2.9D). To evaluate whether *AGO10* over expression indirectly repressed the accumulation of miR165/6 and miR173 through

inhibition of *AGO1* expression, we introduced *4mAGO1,* which renders *AGO1* resistant to miR168 [13], into *AGO10 OE S1*. Transgenic lines were screened by RT-PCR to obtain one in which *AGO10* mRNA levels were comparable to those of *AGO10 OE S1* but *AGO1* expression was elevated (Figure 2.9E). AGO1 protein levels were also elevated in *AGO10 OE 4mAGO1* (Figure 2.9F). Elevated *AGO1* expression in *AGO10 OE 4mAGO1* failed to rescue the levels of miR165/6 or miR173 (Figure 2.8C). Note that miR168 levels were comparable in wild type and *AGO10 OE S1* and elevated in *AGO10 OE 4mAGO1* (Figure 2.8B, C), consistent with the previous observation that miR168 accumulation is tightly buffered by AGO1 [34]. In conclusion, although *AGO10* overexpression led to reduced *AGO1* expression, the reduced accumulation of miR165/6 and miR173 was not attributable to lower *AGO1* expression.

We evaluated whether there was any dosage effects of *AGO10* over expression on miR165/6 levels. We chose another four independent lines of *AGO10 OE* based on the severity of the morphological phenotypes (Figure 2.8A). Lines S2, M1 and M2, and W1 were from the Strong (S), Moderate (M), and Weak (W) categories. The levels of *AGO10* mRNA in these lines were concordant with the severity of morphological defects (Figure 2.8D). We conducted sRNA-seq for wild type and the four *AGO10 OE* lines. The abundance of miR165 and miR166 was reduced in all four lines and was largely anti-correlated with the levels of *AGO10* expression (Figure 2.8E).

AGO10 over expression results in increased 3' truncation of miR165/6

As *AGO10* loss-of-function and over expression led to higher and lower levels of miR165/6, respectively, without affecting miR165/6 biogenesis, we hypothesized that *AGO10* promotes miR165/6 degradation. As miRNA degradation is manifested by the presence of 3' truncated and/or 3' tailed intermediates, we examined the status of miRNA

3’ truncation and tailing in wild type and *AGO10 OE S1* with sRNA-seq (three biological replicates). The proportion of full-length miR165/6 reads was significantly reduced in *AGO10 OE S1* (Figure 2.10A and Figure 2.11). Species of miR165/166 showing 3’ truncation, including both TR-only and TR+TA forms, were increased in *AGO10 OE* relative to wild type, suggesting that *AGO10* over expression enhanced the 3’-to-5’ truncation of miR165/6 (Figure 2.10A and Figure 2.11). Of the TA-only species, only miR165 was modestly increased in abundance (Figure 2.10A). This suggested that 3’ truncation, but not 3’ tailing, was the primary event in miR165/6 degradation induced by *AGO10 OE*. To examine whether the enhanced degradation of miR165/6 in *AGO10 OE* was due to reduced *AGO1* expression, we also sequenced small RNAs from *AGO10 OE 4mAGO1* plants. The 3’ truncation of miR165/6 induced by *AGO10* over expression was not rescued by *4mAGO1* (Figure 2.10B and Figure 2.11). Therefore, the degradation of miR165/6 induced by *AGO10* over expression was not attributable to reduced *AGO1* expression.

We examined whether *AGO10* over expression affected the status of 3’ truncation of other miRNAs. For the top 20 most abundant miRNAs in the sRNA-seq datasets (Col and *AGO10 OE S1*), miR165/6 were the only species with significant changes in 3’ truncation (Figure 2.10C). No miRNAs showed reduced 3’ truncation.

***AGO10* over expression causes further sequestration of miR165/6 from AGO1**

To elucidate how *AGO10* over expression repressed miR165/6 accumulation, we first tested whether *AGO10* over expression caused sequestration of miR165/6 from AGO1. AGO1 was immunoprecipitated from wild type and *AGO10 OE S1* seedlings, and four associated miRNAs were examined by northern blotting. Note that AGO1 levels in *AGO10 OE S1* were about 50% of those in wild type (Figure 2.9D), but for northern blotting

to detect AGO1-associated miRNAs, the amounts of AGO1 IP were adjusted such that AGO1 levels were similar in the two genotypes (Figure 2.12A). Relative to a similar amount of AGO1, miR165/6 was the only miRNA with reduced levels in AGO1 IP from *AGO10 OE S1* (Figure 2.12A). Thus, *AGO10* over expression caused further sequestration of miR165/6 from AGO1.

To obtain a global picture of the miRNAs associated with AGO1 and AGO10 in *AGO10 OE S1*, we performed sRNA-seq from AGO1 and AGO10 immunoprecipitates. Three biological replicates were performed for AGO1 and AGO10 IP from *AGO10 OE S1*. The binding of AGO1 (or AGO10) to a miRNA was quantified by the percentage of reads corresponding to this miRNA in total reads for all annotated miRNAs identified within the small RNA library from the AGO1 (or AGO10) immunoprecipitates. Results showed that the overall profiles of miRNAs associated with AGO1 or AGO10 in *AGO10 OE* resembled those in wild type [5]. AGO1 associated with most miRNAs while AGO10 preferentially associated with miR165/6 (Figure 2.12B).

To determine whether *AGO10* over expression caused a further sequestration of miR165/6 from AGO1, AGO1 IP was performed with wild type and *AGO10 OE S1* with one biological replicate. Consistent with the northern blot results (Figure 2.12A), reads for AGO1-associated miR165/6 were substantially reduced in *AGO10 OE S1* as compared to wild type (Figure 2.12C). The northern blotting and sRNA-seq results demonstrated that elevated AGO10 levels allowed AGO10 to compete more effectively with AGO1 for binding to miR165/6. The only other miRNA that showed a similar effect was miR173 (Figure 2.12D).

We next examined whether there was any dosage effect of *AGO10* over expression on the sequestration of miRNAs from AGO1. We conducted AGO1 IP from

AGO10 OE S2, *M1*, *M2*, and *W1* lines and sequenced AGO1-associated small RNAs (one biological replicate). Indeed, there was an AGO10 dosage-dependent reduction of miR165/6 levels in AGO1 IP (Figure 2.12E). A similar dosage effect was found for miR173 but not other miRNAs (Figure 2.12F).

AGO10 RISCs contain higher levels of 3' truncated miRNAs than AGO1 RISCs

Mechanistically the enhanced degradation of miR165/6 by AGO10 could happen under several scenarios. First, 3' truncation may happen more easily when miR165/6 is bound by AGO10 than when it is bound by AGO1. Second, miR165/6 is dislodged faster from the AGO10 RISC than from the AGO1 RISC and the degradation happens after miR165/6 is released from RISC. A third (and hybrid) model is that the initial 3' truncation occurs on AGO10 RISC and triggers the dissociation of miR165/6 from AGO10. In the first and the third model, we would expect the AGO10 RISC to contain more 3' truncated miR165/6 than the AGO1 RISC. Under the second scenario, AGO1 and AGO10 RISCs are not expected to differ in terms of their association with 3' truncated species. We examined the status of 3' tailing and 3' truncation of miRNAs that were present in AGO1 and AGO10 immunoprecipitates from *AGO10 OE S1* (sRNA-seq in three biological replicates). We found that the most abundant species of miR165/6 in both AGO1 and AGO10 RISCs were the full-length miRNA (Figure 2.13A). However, the AGO10 IP showed a statistically significant increase in the TR-only miR166 species (Figure 2.13A). An increase in the TR-only miR165 species was also found in AGO10 IP, although the increase did not pass the p-value cutoff (Figure 2.13A). These data were consistent with the first or the hybrid model and suggested that 3' truncation occurred, at least initially, on AGO10-associated miR165/6.

Interestingly, we observed a statistically significant increase in the levels of 3' TR-only species in AGO10 IP for 16 out of 48 miRNAs at >1RPM in any of the six libraries (Figure 2.13B). Only one miRNA (miR403) showed a significant reduction in 3' TR-only species in AGO10 IP (Figure 2.13B). This implies that AGO10 RISCs with many different resident miRNAs are more susceptible to miRNA 3' truncation *in vivo*. The lack of an effect of *AGO10* over expression on the levels of most miRNAs is probably because these miRNAs are still mostly bound by AGO1 in *AGO10 OE*.

AGO10-bound miR165/6 species are more susceptible to SDN1-mediated 3' truncation *in vitro*

To biochemically test whether AGO10 renders miR165/6 more susceptible to 3' truncation, we conducted SDN1 assays *in vitro*. A *His-Flag-AGO10 ago10* line [5] was used to immunoprecipitate AGO10 with anti-Flag antibodies and AGO1 with anti-AGO1 antibodies. Both IPs were successful as shown by western blotting to detect AGO1 and AGO10, as well as northern blotting to detect miR165/6 (Figure 2.4A, C). Like for AGO1 IP, SDN1 was unable to degrade miR165/6 in AGO10 IP, as shown by northern blotting to detect miR165/6 before and after incubation with SDN1 under enzyme excess conditions (Figure 2.4B). The lack of a large amount of AGO10 IP precluded the detection of miR165/6 3' truncation by northern blotting (Figure 2.4B). We resorted to sRNA-seq to compare the degree of SDN1-mediated truncation of miR165/6 in AGO1 IP and AGO10 IP. The AGO1 IP and AGO10 IP were incubated with buffer alone (mock), SDN1 or $SDN1^{D283A}$. After the reactions, the AGOs were precipitated, and small RNAs were isolated and subjected to high throughput sequencing. Two biological replicates gave reproducible results (Figure 2.5). Among 13 miRNAs present at >10RPM in AGO10 IP (in all six samples of mock, SDN1, and $SDN1^{D283A}$), five including miR165/6 species showed 3'

truncation by SDN1 (Figure 2.6B). The AGO10 IP showed more pronounced miR165/6 3' truncation than AGO1 IP (Figure 2.6C, D), indicating that AGO10 rendered miR165/6 more susceptible to 3' truncation by SDN1 than AGO1.

AGO10-induced 3' truncation of miR165/6 *in vivo* requires *SDN1* and *SDN2*

SDN1 and SDN2 mediate the 3' truncation of some miRNAs including miR165/6 in the *hen1* background and the 3' truncation of miR165/6 in *HEN1* backgrounds. This, together with the finding that SDN1 trimmed AGO10-bound miR165/6 *in vitro*, prompted us to test whether the increase in miR165/6 3' truncation in *AGO10 OE* was mediated by SDNs. We generated a large population of primary transformants of *35S::YFP-AGO10* in *sdn1-1 sdn2-1* (hereafter referred to as *sdn1 sdn2*) and Col (wild type) backgrounds, identified lines that had comparable levels of *AGO10* expression in the two genotypes (Figure 2.14A) and performed sRNA-seq. Sequencing small RNAs from seedlings of one pair of lines (*AGO10 OE* and *sdn1 sdn2 AGO10 OE*) or inflorescences of another independent pair showed that increased 3' truncation of miR165/6 in *AGO10 OE* was largely suppressed by *sdn1 sdn2* (Figure 2.14B and Figure 2.15). Therefore, *AGO10* overexpression triggered SDN-dependent 3' truncation of miR165/6. The incomplete suppression of 3' truncation of miR165/6 by *sdn1 sdn2* was either due to the activities of other *SDN* family members or yet unknown nucleases that turnover miR165/6.

We also evaluated the effects of the *sdn* mutations on the severity of the developmental phenotypes caused by *AGO10* over expression. The percentage of primary transformants in each of the four phenotypic categories was documented and compared between wild type and *sdn1 sdn2* (Table 2.1). The *sdn1 sdn2* background had higher ratios of plants with WT-like and weak phenotypes (36.8% and 43.9%), in contrast to the low ratios in the Col background (25.7% and 11.4%) (Table 2.1). The Col

background had a higher ratio of plants with strong phenotypes as compared to that in the *sdn1 sdn2* background (48.6% vs. 8.8%) (Table 2.1). In conclusion, the degradation of miR165/6 triggered by *AGO10* over expression and the associated developmental consequences require *SDN1* and *SDN2*.

Discussion

A model of miRNA degradation *in vivo*

Universal small RNA decay processes in plants and metazoans appear to include 3'-to-5' truncation and 3' uridylation. In *Arabidopsis*, the nucleotidyl transferases HESO1 and URT1 are responsible for miRNA uridylation when miRNAs lack 2'-*O*-methylation, but the enzymes responsible for miRNA 3' truncation were unknown, and the relationship between 3' truncation and 3' tailing was also unknown. In this study, we provided genetic evidence documenting a role of SDN1 and SDN2 in miRNA 3' truncation *in vivo*. In a *hen1* background, loss of function in *SDN1* and *SDN2* resulted in a reduction in miRNA 3' truncation for some miRNAs. The lack of an effect on other miRNAs could be due to the presence of other *SDN* paralogs or other exonucleases. In addition, we observed that, in the *hen1 heso1* background, 3' truncated miRNAs accumulate at much higher levels than in the *hen1* background. This supports the model (Figure 2.3) that miRNA degradation is initiated by SDN-mediated 3' truncation and followed by the uridylation of truncated species, which are further degraded by as yet unknown nucleases. Therefore, these genetic studies not only establish SDNs as one class of enzymes that causes miRNA 3' truncation but also elucidate the relationship between miRNA 3' truncation and 3' tailing in miRNA turnover.

While the observations discussed above were made in the *hen1* background, genetic evidence also supports a role of SDN1 and SDN2 in miRNA 3' truncation in the

wild-type background. In the wild-type background, loss of function in *SDN1* and *SDN2* resulted in a reduction in the levels of truncated-only and truncated-and-tailed miR165/6. In *AGO10 OE* plants, loss of function in *SDN1* and *SDN2* reduced the levels of 3' truncated miR165/6 and partially rescued the developmental abnormalities. These observations were especially important as they suggest that SDN1 and SDN2 cause the 3' trimming of miR165/6 when it is methylated (as miRNAs are nearly completely methylated in *HEN1* backgrounds).

Furthermore, we provided biochemical evidence showing that SDN1 acts on AGO1-bound and methylated miRNAs *in vitro*. In fact, SDN1 had different effects on free and AGO1-bound miRNAs – it nearly completely degrades free miRNAs [30] but causes the truncation of a small and varying number of nucleotides from AGO1-bound miRNAs (this study). The 3' truncated, AGO1-bound miRNAs caused by SDN1 *in vitro* mimic the 3' truncated species in *hen1* mutants *in vivo*. This indicates that the 3' trimmed miRNA species that accumulate *in vivo* result from the balancing act between AGO1-mediated protection and SDN1-mediated truncation.

In summary, these genetic and biochemical observations support the following model of miRNA degradation. SDNs initiate miRNA degradation in wild type by 3' truncation of AGO1-bound and methylated miRNAs to result in AGO1-bound, 3' truncated-and-unmethylated miRNAs, which are uridylated by HESO1 and/or URT1. The AGO1-bound, truncated-and-uridylated miRNAs are further degraded by an as yet unknown enzyme. However, we acknowledge that SDNs may not be the only exonucleases causing miRNA 3' truncation. In addition, miRNA degradation may also entail mechanisms other than 3' truncation and 3' tailing.

AGO10 destabilizes its associated miR165/6

In addition to establishing a model of miRNA degradation, the study also uncovered an unexpected function of an AGO protein in destabilizing miR165/6. *In vivo*, *AGO10* over expression caused further sequestration of miR165/6 from AGO1, enhanced its 3' truncation through SDN1/2, and reduced its accumulation. *In vitro*, AGO10-bound miR165/6 species were more susceptible to SDN1-mediated 3' truncation than AGO1-bound miR165/6. The 3' truncation of an AGO-bound miRNA should entail the displacement of the miRNA 3' end from the binding pocket in the PAZ domain [35]. Perhaps the 3' end of miR165/6 is more accessible in an AGO10 RISC than in an AGO1 RISC. It is not known whether AGO10 confers 3' end accessibility to its resident miRNAs in general. One observation consistent with this notion is that many miRNAs have higher levels of 3' truncation in AGO10 IP than in AGO1 IP (Figure 2.13B). However, *AGO10* over expression did not affect the abundance of most miRNAs. This is probably because most miRNAs are still bound by AGO1 despite *AGO10* over expression (Figure 2.12B).

Another miRNA that is reduced in abundance by *AGO10* over expression is miR173 (Figure 2.8B). *AGO10* over expression caused a depletion of miR173 from AGO1 RISC relative to other miRNAs (Figure 2.12D) but not relative to AGO1 levels (Figure 2.12A). Thus, the reduced abundance of miR173 by *AGO10* over expression was perhaps attributable to the lower levels of AGO1. However, increasing AGO1 levels in *AGO10 OE S1* could not restore miR173 accumulation (Figure 2.8C). Intriguingly, miR173 happens to be the second most preferred miRNA by AGO10 for binding in a previous study [5]. Therefore, it is likely that *AGO10* over expression allowed AGO10 to better compete with AGO1 for binding to miR173 and lead to its degradation.

This study, together with previous studies demonstrating the importance of *AGO10*-mediated repression of miR165/6 in meristem homeostasis [1,2,5], provides an example of active miRNA degradation being employed as a mechanism to regulate stem cells in development. In developing seedlings, the spatial pattern of AGO10 protein accumulation is complementary to that of miR165/6. We propose that *AGO10* enhances the degradation of miR165/6 to help restrict this miRNA to cells not expressing *AGO10*. The clearance of miR165/6 from the SAM by *AGO10* is crucial for stem cell maintenance as *ago10* mutants accumulate ectopic miR165/6 in the SAM and fail to maintain the stem cell population [2]. But why is such a mechanism employed to clear miR165/6 from the SAM in addition to restricting the transcription of *MIR165/6* from the stem cells? This may have to do with the potential movement of this miRNA between cells. miR165/6 probably moves across a few cell layers from its site of synthesis in the root and in leaf primordia [36-41]. The non-cell autonomy means that cell-type specific transcription alone is not sufficient to restrict the miRNA from the SAM.

Materials and Methods

Plant materials and growth conditions

The *pnh-2* and *ago10-13* alleles [1,3] are in the Landsberg *erecta* (L*er*) background. The *hen1-8* allele and the *sdn1-1 sdn2-1* double mutant are both in the Col background and were previously described [30,42]. The *hen1-8 sdn1-1 sdn2-1* triple mutant was generated through a cross between *hen1-8* and *sdn1-1 sdn2-1*. *zll-1 ZLLp::YFP-ZLL* is a transgenic line in which the *YFP-ZLL* (*AGO10*) transgene driven by the *ZLL* (*AGO10*) promoter fully rescues the morphological defects of *zll-1* [11]. The *His-Flag-AGO10* line is in the Col background and is described [5]. Wild-type Columbia (Col) or *sdn1-1 sdn2-1* plants were transformed with the *35S::YFP-AGO10* plasmid via the floral

dipping method [43] to obtain *AGO10 OE*. The *4mAGO1* plasmid was obtained from Dr. Herve Vaucheret (INRA, Versailles, France) and introduced into *AGO10 OE* plants via the floral dipping method.

When not specified, the plant materials used in this study were 12- to 13-day-old seedlings grown at 22°C under long day (16 h light/ 8 h darkness) conditions. In only one instance (mentioned in the text), inflorescences were used for small RNA sequencing in one pair of *AGO10 OE* and *sdn1 sdn2 AGO10 OE* lines.

Plasmid construction

To generate the *AGO10* over expression construct, full-length *AGO10* coding region was amplified from cDNA using gene-specific primers containing sequences for TOPO reaction (Table 2.2). The *AGO10* clone in the Gateway Entry vector was moved into pEarleyGate104 using LR reaction to produce *35S::YFP-AGO10*. The clone was sequenced to ensure the absence of mutations.

For the expression of recombinant SDN1 protein, the full-length *SDN1* cDNA was amplified using primers SDN1 F and SDN1 R (Table 2.2) and cloned into pET28-SMT3 (pSUMO). The D283A mutation was introduced into *SDN1* using the Stratagene QuikChange Site-Directed Mutagenesis Kit with a pair of primers, SDN1D283A F and SDN1D283A R (Table 2.2). The pSUMO-SDN1 ^{D283A} clone was validated by sequencing.

Protein expression and enzymatic assay

The pSUMO-SDN1 and pSUMO-SDN1 ^{D283A} plasmids were transformed into the *E. coli* strain BL21 Star (DE3) for protein expression. The *E. coli* cells were cultured at 37°C until the OD600 reached 0.6. Isopropyl β-D-1-thiogalactopyranoside (IPTG) was added to a final concentration of 0.1 mM and the cultures were incubated at 16°C for 16 hrs. Cells were collected via centrifugation, resuspended in Lysis Buffer (20 mM Tris, pH

8.0, 500 mM NaCl, 25 mM Imidazole, pH 8.0) and sonicated on ice. The lysate was centrifuged again, and the supernatant was applied to a column containing pre-loaded nickel beads for purification. After washes with Lysis Buffer for 2 times, the homemade 6xHis-ULP in Dilution Buffer (20 mM Tris, pH 8.0, 50 mM NaCl, 25 mM Imidazole, pH 8.0) was loaded to the column to remove the His-SUMO tag on the recombinant proteins. The free SDN1 and SDN1^{D283A} proteins were then eluted with Elution Buffer (20 mM Tris, pH 8.0, 100 mM NaCl, 25 mM Imidazole, pH 8.0).

For SDN1 enzymatic assay, AGO1 and AGO10 complexes were immunoprecipitated from *His-Flag-AGO10* transgenic plants using anti-AGO1 (Agrisera) and anti-Flag (Sigma-Aldrich) antibodies, respectively. 1/12 of the IP was used for western blotting to detect AGO1 and AGO10, another 1/12 was used for northern blotting to detect miR165/6, and the remainder was resuspended in reaction buffer (50 mM Tris, pH 8.0, 150 mM NaCl, 1mM DTT, 2.5 mM MnCl2, 1 mM ATP). The beads in reaction buffer were evenly split into two parts for incubation with SDN1 and SDN1^{D283A}. The reactions were carried out with 2.7 µM SDN1 or SDN1^{D283A} and approximately 5.3 nM and 0.6 nM of small RNAs present in AGO1 IP and AGO10 IP, respectively (see below for the estimation of sRNA concentrations). After incubation at room temperature for 1 hr, the beads were collected again for RNA extraction followed by small RNA library construction.

For the estimation of the amount of small RNAs in AGO1 or AGO10 IP, northern blotting was performed with the IPs and a miR165 oligonucleotide standard. The amount of miR165/6 in AGO1 and AGO10 IPs was deduced by comparing the signal intensities of miR165/6 in the IPs to those of the standard. Next, the amount of all sRNAs in the AGO1 and AGO10 IPs was estimated based on the proportions of miR165/6 reads in total small RNA reads from the AGO1 and AGO10 IPs (as determined by sRNA-seq).

RNA extraction, realtime RT-PCR, and northern blotting

Total RNA was extracted using TRI-reagent (Molecular Research Center, Inc. TR 118). For the detection of pri- and pre-miR165/6 species together, reverse transcription was performed with random primers, and real-time PCR was then performed as described [1] with gene-specific primers located within the pre-miRNAs from each locus. Values were obtained by normalizing to *UBIQUITIN5*. Northern blotting to detect miRNAs or pre-miR166a was performed as described [43,44]. Antisense DNA oligonucleotides (Table 2.2) were 5'-end labeled with γ^{32}P-ATP to detect miRNAs. A DNA fragment amplified from genomic DNA using primers pre-miR166a-Nb F and pre-miR166a-Nb R (Table 2.2) was randomly labeled with α^{32}P-dCTP for the northern blotting to detect pre-miR166a.

β-elimination assay

β-elimination followed by northern blotting to examine the methylation status of miR165/6 was performed as described [25].

Immunoprecipitation and western blotting

Immunoprecipitation of AGO1 and AGO10 was performed as described [28]. In brief, 1g of 12-day-old seedlings was ground in liquid nitrogen and dissolved in 1.5 ml IP buffer. The extract from *AGO10 OE* or *zll-1 ZLLp::YFP-ZLL* was incubated with anti-AGO1 antibodies (Agrisera) and anti-GFP antibodies (Clontech), respectively. Then protein-antibody complexes were captured by Dynabeads-Protein-A (Life Technologies). After washes, the beads containing AGO1 or AGO10 immunoprecipitates were collected for small RNA analysis.

Western blotting to determine AGO1 protein levels was performed with anti-AGO1 antibodies, and HSC70 (Enzo Life Sciences) was used as an internal control. The His-Flag-AGO10 protein was detected using anti-AGO10 antibodies (Agrisera).

Small RNA library construction and bioinformatics analysis

Small RNA libraries were prepared using the Illumina Tru-Seq kit [29] and the NEBNext Multiplex Small RNA Library Prep Set for Illumina kit (NEB) and sequenced with Illumina's HiSeq2000 or Illumina NextSeq500 platform at the UCR Institute for Integrative Genome Biology (IIGB) genomic core facility. Bioinformatics analyses to categorize miRNA reads into the “full-length”, “3’ truncated-only”, “3’ tailed-only”, and “3’ truncated-and-tailed” categories were performed as described [29].

References

1. Ji L, Liu X, Yan J, Wang W, Yumul RE, et al. (2011) ARGONAUTE10 and ARGONAUTE1 regulate the termination of floral stem cells through two microRNAs in *Arabidopsis*. PLoS Genet 7: e1001358.

2. Liu Q, Yao X, Pi L, Wang H, Cui X, et al. (2009) The *ARGONAUTE10* gene modulates shoot apical meristem maintenance and establishment of leaf polarity by repressing miR165/166 in *Arabidopsis*. Plant J 58: 27-40.

3. Lynn K, Fernandez A, Aida M, Sedbrook J, Tasaka M, et al. (1999) The *PINHEAD/ZWILLE* gene acts pleiotropically in *Arabidopsis* development and has overlapping functions with the ARGONAUTE1 gene. Development 126: 469-481.

4. Moussian B, Schoof H, Haecker A, Jurgens G, Laux T (1998) Role of the *ZWILLE* gene in the regulation of central shoot meristem cell fate during *Arabidopsis* embryogenesis. EMBO J 17: 1799-1809.

5. Zhu H, Hu F, Wang R, Zhou X, Sze SH, et al. (2011) *Arabidopsis* Argonaute10 specifically sequesters miR166/165 to regulate shoot apical meristem development. Cell 145: 242-256.

6. Emery JF, Floyd SK, Alvarez J, Eshed Y, Hawker NP, et al. (2003) Radial patterning of *Arabidopsis* shoots by class III *HD-ZIP* and *KANADI* genes. Curr Biol 13: 1768-1774.

7. Kidner CA, Martienssen RA (2005) The role of ARGONAUTE1 (AGO1) in meristem formation and identity. Dev Biol 280: 504-517.

8. Kim J, Jung JH, Reyes JL, Kim YS, Kim SY, et al. (2005) microRNA-directed cleavage of *ATHB15* mRNA regulates vascular development in *Arabidopsis* inflorescence stems. Plant J 42: 84-94.

9. Mallory AC, Reinhart BJ, Jones-Rhoades MW, Tang G, Zamore PD, et al. (2004) MicroRNA control of *PHABULOSA* in leaf development: importance of pairing to the microRNA 5′ region. EMBO J 23: 3356-3364.

10. Tang G, Reinhart BJ, Bartel DP, Zamore PD (2003) A biochemical framework for RNA silencing in plants. Genes Dev 17: 49-63.

11. Tucker MR, Hinze A, Tucker EJ, Takada S, Jurgens G, et al. (2008) Vascular signalling mediated by ZWILLE potentiates WUSCHEL function during shoot meristem stem cell development in the *Arabidopsis* embryo. Development 135: 2839-2843.

12. Bohmert K, Camus I, Bellini C, Bouchez D, Caboche M, et al. (1998) AGO1 defines a novel locus of *Arabidopsis* controlling leaf development. EMBO J 17: 170-180.

13. Vaucheret H, Vazquez F, Crete P, Bartel DP (2004) The action of ARGONAUTE1 in the miRNA pathway and its regulation by the miRNA pathway are crucial for plant development. Genes Dev 18: 1187-1197.

14. Rogers K, Chen X (2013) Biogenesis, turnover, and mode of action of plant microRNAs. Plant Cell 25: 2383-2399.

15. Ameres SL, Horwich MD, Hung JH, Xu J, Ghildiyal M, et al. (2010) Target RNA-directed trimming and tailing of small silencing RNAs. Science 328: 1534-1539.

16. Billi AC, Alessi AF, Khivansara V, Han T, Freeberg M, et al. (2012) The Caenorhabditis elegans HEN1 ortholog, HENN-1, methylates and stabilizes select subclasses of germline small RNAs. PLoS Genet 8: e1002617.

17. Horwich MD, Li C, Matranga C, Vagin V, Farley G, et al. (2007) The Drosophila RNA methyltransferase, DmHen1, modifies germline piRNAs and single-stranded siRNAs in RISC. Curr Biol 17: 1265-1272.

18. Kamminga LM, Luteijn MJ, den Broeder MJ, Redl S, Kaaij LJ, et al. (2010) Hen1 is required for oocyte development and piRNA stability in zebrafish. EMBO J 29: 3688-3700.

19. Kamminga LM, van Wolfswinkel JC, Luteijn MJ, Kaaij LJ, Bagijn MP, et al. (2012) Differential impact of the HEN1 homolog HENN-1 on 21U and 26G RNAs in the germline of Caenorhabditis elegans. PLoS Genet 8: e1002702.

20. Kirino Y, Mourelatos Z (2007) Mouse Piwi-interacting RNAs are 2'-O-methylated at their 3' termini. Nat Struct Mol Biol 14: 347-348.

21. Kurth HM, Mochizuki K (2009) 2'-O-methylation stabilizes Piwi-associated small RNAs and ensures DNA elimination in Tetrahymena. RNA 15: 675-685.

22. Li J, Yang Z, Yu B, Liu J, Chen X (2005) Methylation protects miRNAs and siRNAs from a 3'-end uridylation activity in *Arabidopsis*. Curr Biol 15: 1501-1507.

23. Montgomery TA, Rim YS, Zhang C, Dowen RH, Phillips CM, et al. (2012) PIWI associated siRNAs and piRNAs specifically require the Caenorhabditis elegans HEN1 ortholog henn-1. PLoS Genet 8: e1002616.

24. Saito K, Sakaguchi Y, Suzuki T, Suzuki T, Siomi H, et al. (2007) Pimet, the Drosophila homolog of HEN1, mediates 2'-O-methylation of Piwi- interacting RNAs at their 3' ends. Genes Dev 21: 1603-1608.

25. Yu B, Yang Z, Li J, Minakhina S, Yang M, et al. (2005) Methylation as a crucial step in plant microRNA biogenesis. Science 307: 932-935.

26. Ren G, Chen X, Yu B (2012) Uridylation of miRNAs by hen1 suppressor1 in *Arabidopsis*. Curr Biol 22: 695-700.

27. Tu B, Liu L, Xu C, Zhai J, Li S, et al. (2015) Distinct and cooperative activities of HESO1 and URT1 nucleotidyl transferases in microRNA turnover in *Arabidopsis*. PLoS Genet 11: e1005119.

28. Wang X, Zhang S, Dou Y, Zhang C, Chen X, et al. (2015) Synergistic and independent actions of multiple terminal nucleotidyl transferases in the 3' tailing of small RNAs in *Arabidopsis*. PLoS Genet 11: e1005091.

29. Zhao Y, Yu Y, Zhai J, Ramachandran V, Dinh TT, et al. (2012) The *Arabidopsis* nucleotidyl transferase HESO1 uridylates unmethylated small RNAs to trigger their degradation. Curr Biol 22: 689-694.

30. Ramachandran V, Chen X (2008) Degradation of microRNAs by a family of exoribonucleases in *Arabidopsis*. Science 321: 1490-1492.

31. Jung JH, Park CM (2007) *MIR166/165* genes exhibit dynamic expression patterns in regulating shoot apical meristem and floral development in *Arabidopsis*. Planta 225: 1327-1338.

32. Newman KL, Fernandez AG, Barton MK (2002) Regulation of axis determinacy by the *Arabidopsis PINHEAD* gene. Plant Cell 14: 3029-3042.

33. Mallory AC, Hinze A, Tucker MR, Bouche N, Gasciolli V, et al. (2009) Redundant and specific roles of the ARGONAUTE proteins AGO1 and ZLL in development and small RNA-directed gene silencing. PLoS Genet 5: e1000646.

34. Vaucheret H, Mallory AC, Bartel DP (2006) AGO1 homeostasis entails coexpression of *MIR168* and *AGO1* and preferential stabilization of miR168 by AGO1. Mol Cell 22: 129-136.

35. Ma JB, Ye K, Patel DJ (2004) Structural basis for overhang-specific small interfering RNA recognition by the PAZ domain. Nature 429: 318-322.

36. Carlsbecker A, Lee JY, Roberts CJ, Dettmer J, Lehesranta S, et al. (2010) Cell signalling by microRNA165/6 directs gene dose-dependent root cell fate. Nature 465: 316-321.

37. Juarez MT, Kui JS, Thomas J, Heller BA, Timmermans MC (2004) microRNA-mediated repression of rolled leaf1 specifies maize leaf polarity. Nature 428: 84-88.

38. Miyashima S, Honda M, Hashimoto K, Tatematsu K, Hashimoto T, et al. (2013) A comprehensive expression analysis of the *Arabidopsis MICRORNA165/6* gene family during embryogenesis reveals a conserved role in meristem specification and a non-cell-autonomous function. Plant Cell Physiol 54: 375-384.

39. Miyashima S, Koi S, Hashimoto T, Nakajima K (2011) Non-cell-autonomous microRNA165 acts in a dose-dependent manner to regulate multiple differentiation status in the *Arabidopsis* root. Development 138: 2303-2313.

40. Nogueira FT, Chitwood DH, Madi S, Ohtsu K, Schnable PS, et al. (2009) Regulation of small RNA accumulation in the maize shoot apex. PLoS Genet 5: e1000320.

41. Yao X, Wang H, Li H, Yuan Z, Li F, et al. (2009) Two types of cis-acting elements control the abaxial epidermis-specific transcription of the *MIR165a* and *MIR166a* genes. FEBS Lett 583: 3711-3717.

42. Yu B, Bi L, Zhai J, Agarwal M, Li S, et al. (2010) siRNAs compete with miRNAs for methylation by HEN1 in *Arabidopsis*. Nucleic Acids Res 38: 5844-5850.

43. Kurihara Y, Takashi Y, Watanabe Y (2006) The interaction between DCL1 and HYL1 is important for efficient and precise processing of pri-miRNA in plant microRNA biogenesis. RNA 12: 206-212.

44. Yu B, Bi L, Zheng B, Ji L, Chevalier D, et al. (2008) The FHA domain proteins DAWDLE in *Arabidopsis* and SNIP1 in humans act in small RNA biogenesis. Proc Natl Acad Sci U S A 105: 10073-10078.

Figures and Tables

Figure 2.1 SDN1 and 2 are responsible for miRNA 3' truncation *in vivo.*

High-throughput sequencing was conducted to profile miRNAs in wild type (Col), *sdn1 sdn2*, *hen1*, and *hen1 sdn1 sdn2*. Published sRNA-seq from *hen1* and *hen1 heso1* [29] was also analyzed. Two biological replicates were performed for each genotype and the error bars represent standard deviations. * p-value < 0.05, ** p-value < 0.01, *** p-value < 0.001. (A-B) Heatmaps showing the levels of truncated-and-tailed (TR+TA) and truncated-only (TR-only) species of 23 miRNAs in *hen1 sdn1 sdn2* (A) or *hen1 heso1* (B) as compared to *hen1*. For each miRNA, the ratio of TR+TA (or TR-only) species to all reads corresponding to this miRNA is shown. The red asterisks indicate statistically significant reduction in the sum of TR+TA and TR-only species for the indicated miRNAs (no miRNAs showed a statistically significant increase). (C-D) The composition of miR165 and miR166 reads corresponding to full-length (FL), TR-only, TR+TA, and tailed-only (TA-only) species in *hen1*, *hen1 sdn1 sdn2*, Col, and *sdn1 sdn2* as indicated. (E) The composition of miR165 and miR166 reads in *hen1* and *hen1 heso1*. The reduction in the levels of TR+TA species in *hen1 heso1* is accompanied by the increase in the levels of TR-only species.

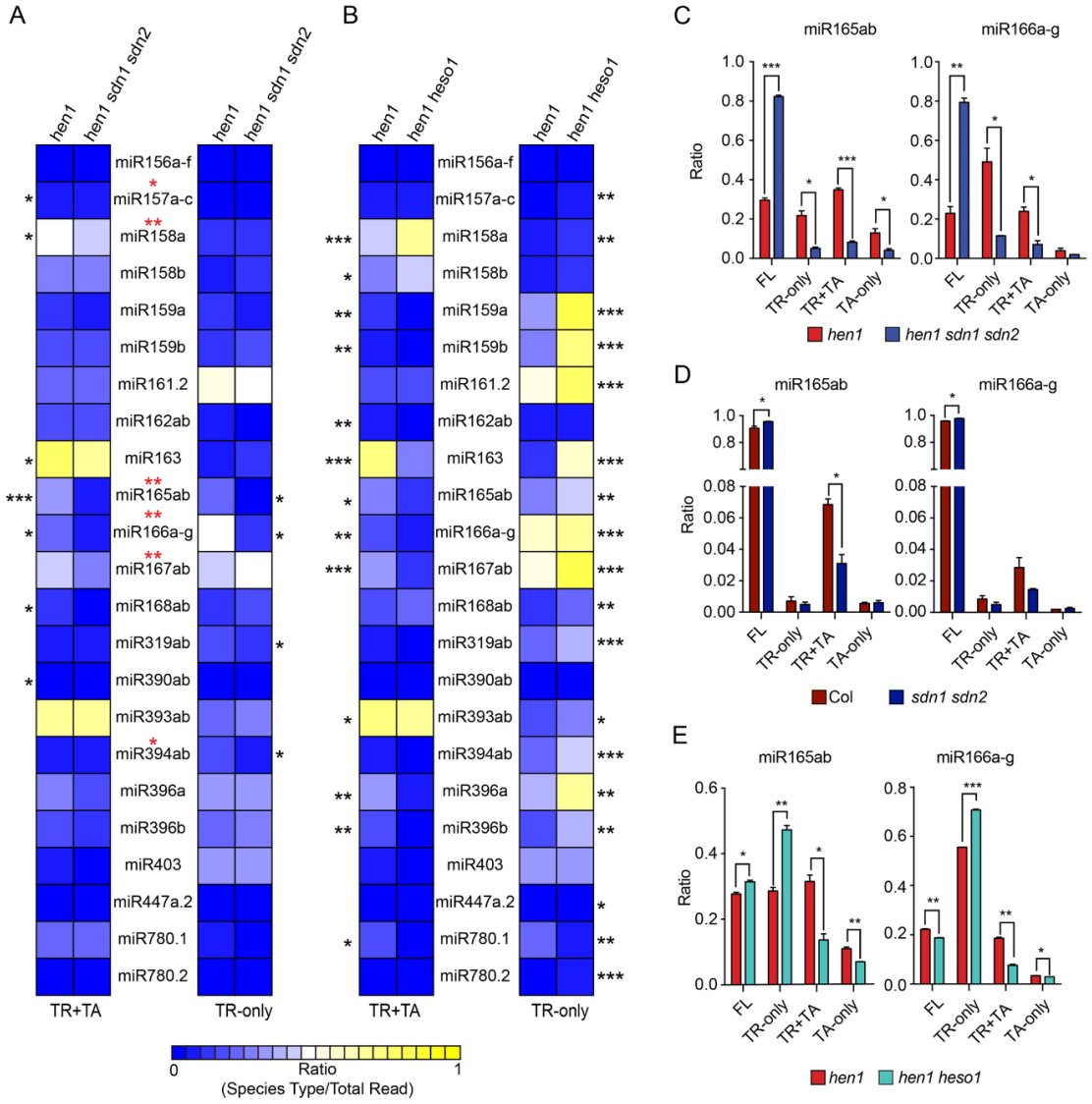
A
hen1
hen1 sdn1 sdn2
hen1
hen1 sdn1 sdn2
miR156a-f
miR157a-c
miR158a
miR158b
miR159a
miR159b
miR161.2
miR162ab
miR163
miR165ab
miR166a-g
miR167ab
miR168ab
miR319ab
miR390ab
miR393ab
miR394ab
miR396a
miR396b
miR403
miR447a.2
miR780.1
miR780.2
TR+TA
TR-only
B
hen1
hen1 heso1
hen1
hen1 heso1
TR+TA
TR-only
0
Ratio
1
(Species Type/Total Read)
C
miR165ab
miR166a-g
Ratio
FL
TR-only
TR+TA
TA-only
hen1
hen1 sdn1 sdn2
D
miR165ab
miR166a-g
Ratio
Col
sdn1 sdn2
E
miR165ab
miR166a-g
Ratio
hen1
hen1 heso1

Figure 2.2 Matrices representing the composition of reads for various miRNAs in *hen1* and *hen1 sdn1 sdn2* libraries.

The X axis represents the number of nucleotides truncated from the 3′ end. The Y axis represents the number of nucleotides added to the 3′ end. The relative proportions of the species are indicated by the sizes of the circles. Two biological replicates (br1 and br2) are shown separately. Selected miRNAs with or without a reduction in 3′ truncation in *hen1 sdn1 sdn2* from Figure 2.1A are shown.

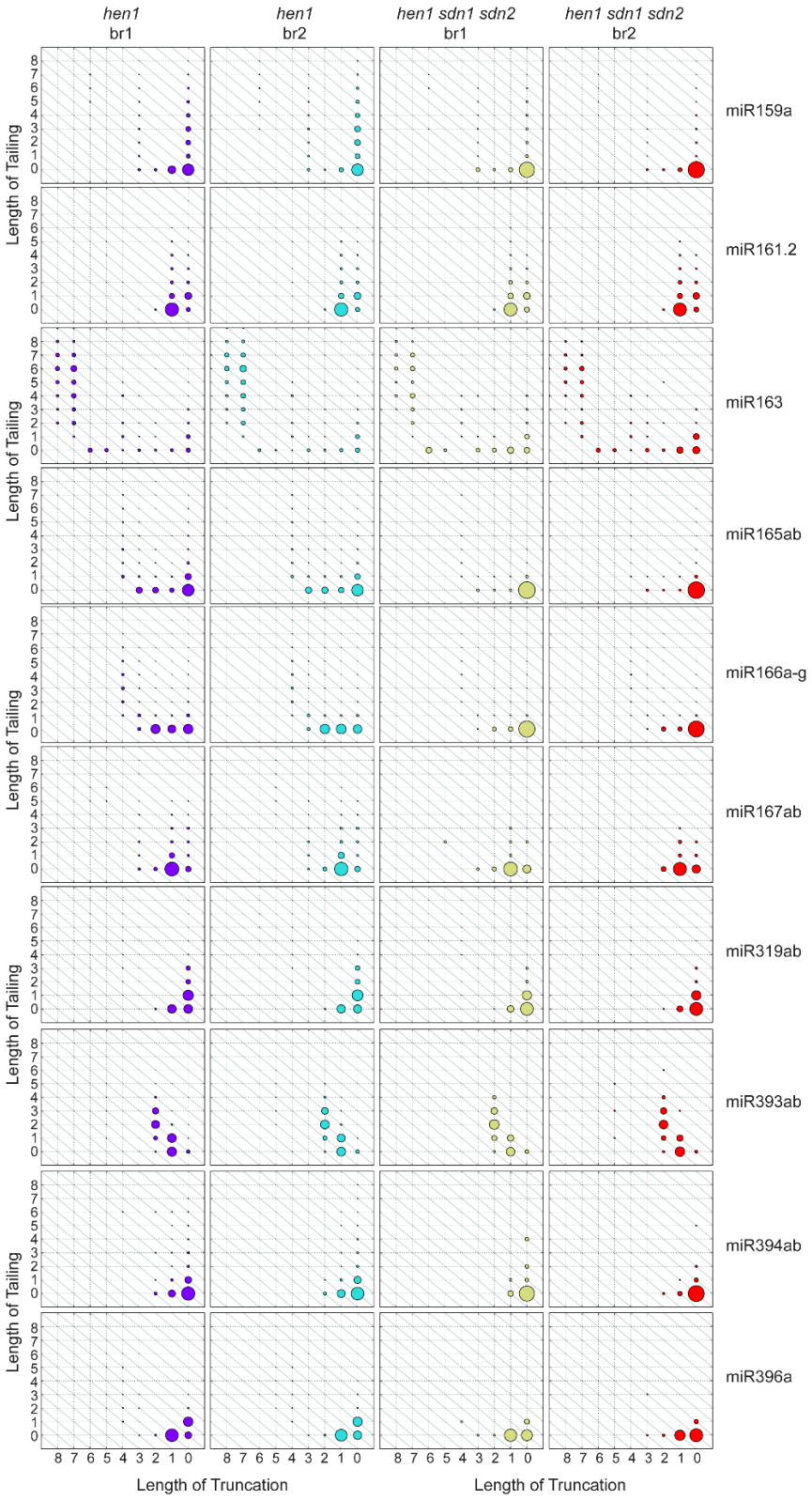
hen1
br1
hen1
br2
hen1 sdn1 sdn2
br1
hen1 sdn1 sdn2
br2
Length of Tailing
Length of Truncation
miR159a
miR161.2
miR163
miR165ab
miR166a-g
miR167ab
miR319ab
miR393ab
miR394ab
miR396a

Figure 2.3 A model of miRNA degradation.

SDNs initiate degradation by trimming the miRNA to result in a 3′ truncated and unmethylated miRNA, which is uridylated by HESO1 or URT1. The tailed species are further degraded by an as yet unknown enzyme. SDN1 (this study) and the nucleotidyl transferases (HESO1 and URT1) can act on AGO1-bound miRNAs as well as free miRNAs.

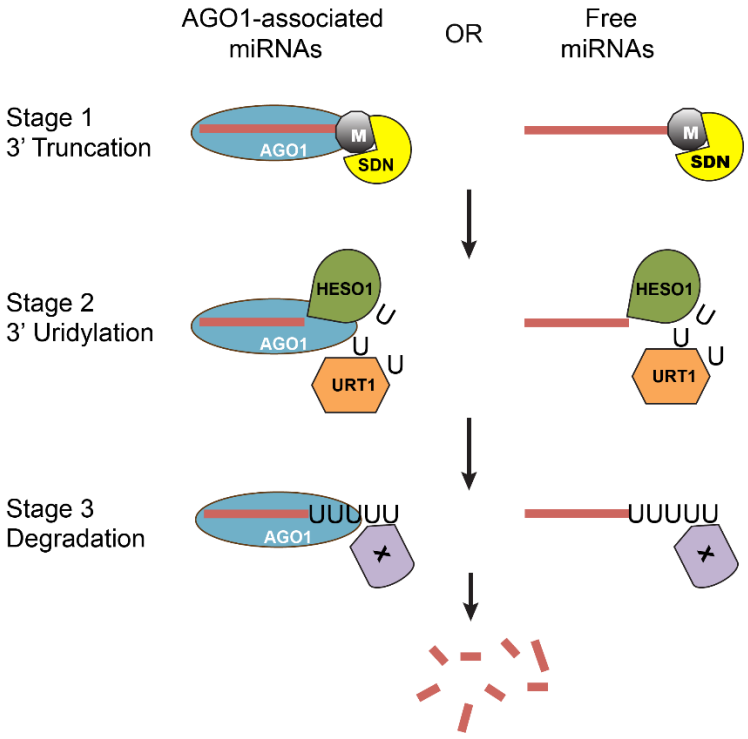
AGO1-associated miRNAs
OR
Free miRNAs
Stage 1
3' Truncation
AGO1
M
SDN
M
SDN
Stage 2
3' Uridylation
HESO1
AGO1
U
U
U
URT1
HESO1
U
U
U
URT1
Stage 3
Degradation
UUUUU
AGO1
UUUUU

Figure 2.4 SDN1 enzymatic assays with AGO1 and AGO10 IP as substrates.

Immunoprecipitation (IP) was performed with wild type (Col) or a line with the *His-Flag-AGO10* transgene in an *ago10* mutant background [5]. AGO1 and AGO10 IP was performed with anti-AGO1 and anti-Flag antibodies, respectively. (A) The AGO1 IP was subjected to western blotting to detect AGO1 and northern blotting to detect miR165/6. (B) SDN1 enzymatic assays with AGO1 IP, AGO10 IP, and an RNA oligonucleotide as substrates under enzyme excess conditions. Northern blotting was performed to detect miR165/6 in the reactions with AGO1 and AGO10 IPs as substrates. The RNA oligonucleotide was 5′ labeled with 32P to aid detection. The bands below the full-length form were shorter species present in the RNA oligonucleotide preparation. These shorter versions as well as the full-length form were degraded by SDN1. (C) AGO10 IP was subjected to western blotting with anti-AGO10 antibodies to detect AGO10 and northern blotting to detect miR165/6. The band present in the transgenic line but not in Col is His-Flag-AGO10. The other bands in the input samples are likely non-specific signals.

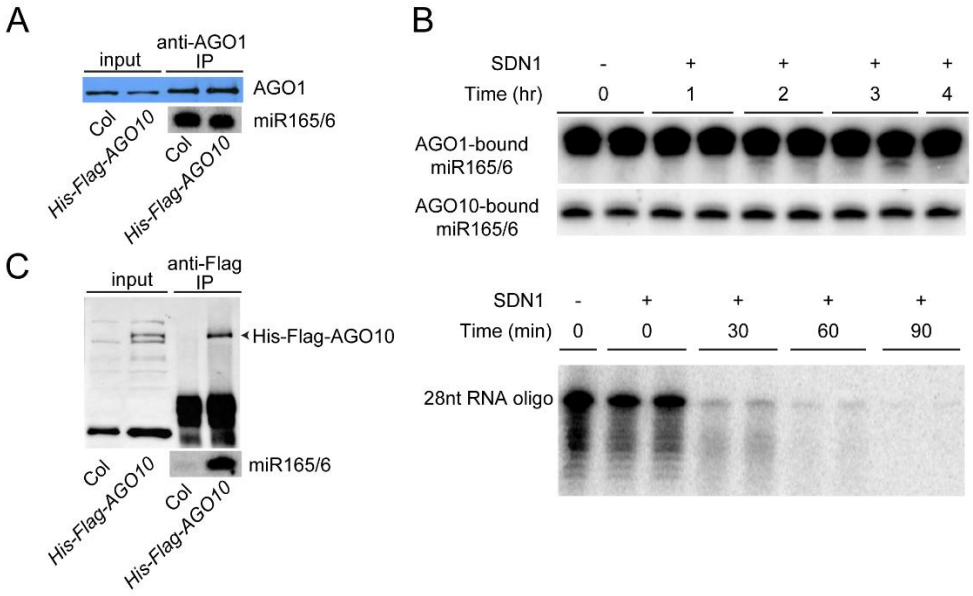
A
anti-AGO1
input
IP
AGO1
miR165/6
Col
His-Flag-AGO10
Col
His-Flag-AGO10
B
SDN1
-
+
+
+
+
Time (hr)
0
1
2
3
4
AGO1-bound miR165/6
AGO10-bound miR165/6
SDN1
-
+
+
+
+
Time (min)
0
0
30
60
90
28nt RNA oligo
C
anti-Flag
input
IP
His-Flag-AGO10
miR165/6
Col
His-Flag-AGO10
Col
His-Flag-AGO10

Figure 2.5 Hierarchical clustering analysis showing the degree of similarity among the sRNA-seq libraries.

Sample-to-sample distances were calculated based on log-transformed normalized read counts. The biological replicates of each sample type were highly reproducible.

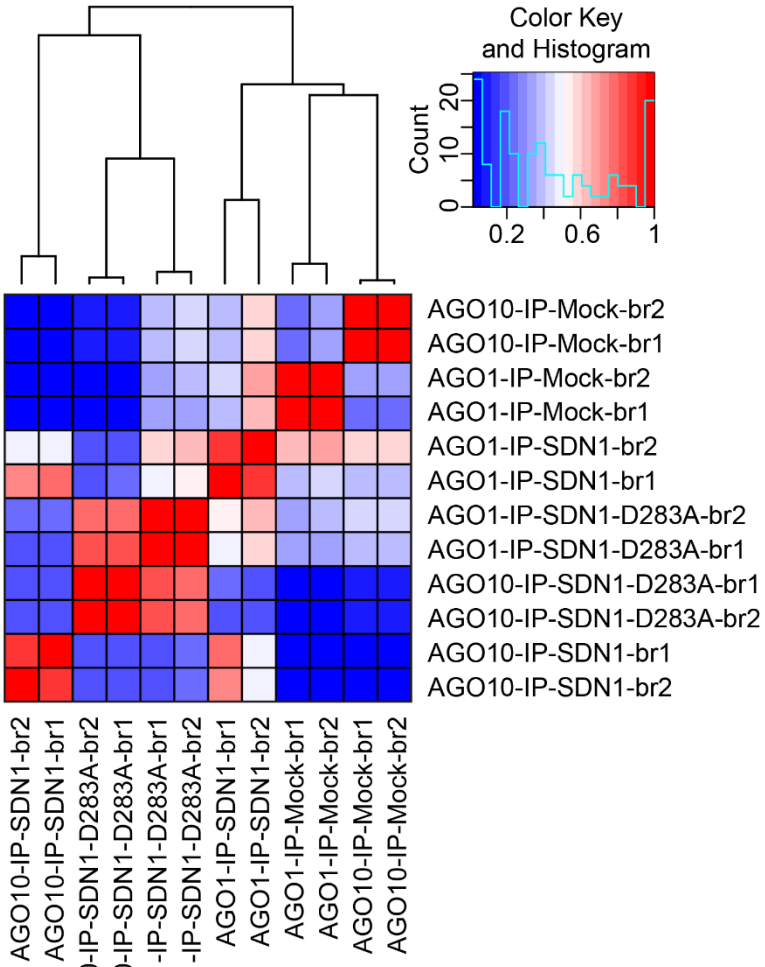
Color Key
and Histogram
Count
0
10
20
0.2
0.6
1
AGO10-IP-Mock-br2
AGO10-IP-Mock-br1
AGO1-IP-Mock-br2
AGO1-IP-Mock-br1
AGO1-IP-SDN1-br2
AGO1-IP-SDN1-br1
AGO1-IP-SDN1-D283A-br2
AGO1-IP-SDN1-D283A-br1
AGO10-IP-SDN1-D283A-br1
AGO10-IP-SDN1-D283A-br2
AGO10-IP-SDN1-br1
AGO10-IP-SDN1-br2
AGO10-IP-SDN1-br2
AGO10-IP-SDN1-br1
AGO10-IP-SDN1-D283A-br2
AGO10-IP-SDN1-D283A-br1
AGO1-IP-SDN1-D283A-br1
AGO1-IP-SDN1-D283A-br2
AGO1-IP-SDN1-br1
AGO1-IP-SDN1-br2
AGO1-IP-Mock-br1
AGO1-IP-Mock-br2
AGO10-IP-Mock-br1
AGO10-IP-Mock-br2

Figure 2.6 SDN1 is able to trim AGO1- and AGO10-bound miRNAs *in vitro*.

AGO1 IP or AGO10 IP was used as the substrate in enzymatic reactions with mock (no enzyme), SDN1 or a catalytic mutant ($SDN1^{D283A}$) in two biological replicates. sRNA-seq was conducted to examine the 3' trimming of miRNAs. (A-B) Plots showing the ratio of 3' truncated-only (TR-only) species to full-length (FL) species for various miRNAs after the enzymatic reactions. TR-only species present in the mock control were subtracted from the SDN1 or $SDN1^{D283A}$ reactions. The diagonal lines represent equal levels of 3' truncated species in the SDN1 and $SDN1^{D283A}$ reactions, indicating that the truncated species were not generated by SDN1. The miRNAs marked in red showed SDN1-mediated 3' truncation. As the levels of 3' truncation were low, the two biological replicates were combined to derive the values. Only abundant miRNAs (RPM>10) were examined. (C) Bar plot showing higher levels of 3' truncation by SDN1 of miR165/6 in AGO10 IP than in AGO1 IP. The Y axis represents SDN1-mediated 3' truncation; any truncated species present in the $SDN1^{D283A}$ reactions were subtracted from those in the SDN1 reactions. (D) Diagrams showing the status of 3' truncation and tailing of miR165/6. The X axis represents the number of nucleotides truncated from the 3' end. The Y axis represents the number of nucleotides added to the 3' end. The relative proportions of the species are indicated by the sizes of the circles. Two biological replicates (br1 and br2) are shown separately. The 3' truncated species accumulating at higher levels in the SDN1 reactions relative to the mock and $SDN1^{D283A}$ reactions are marked.

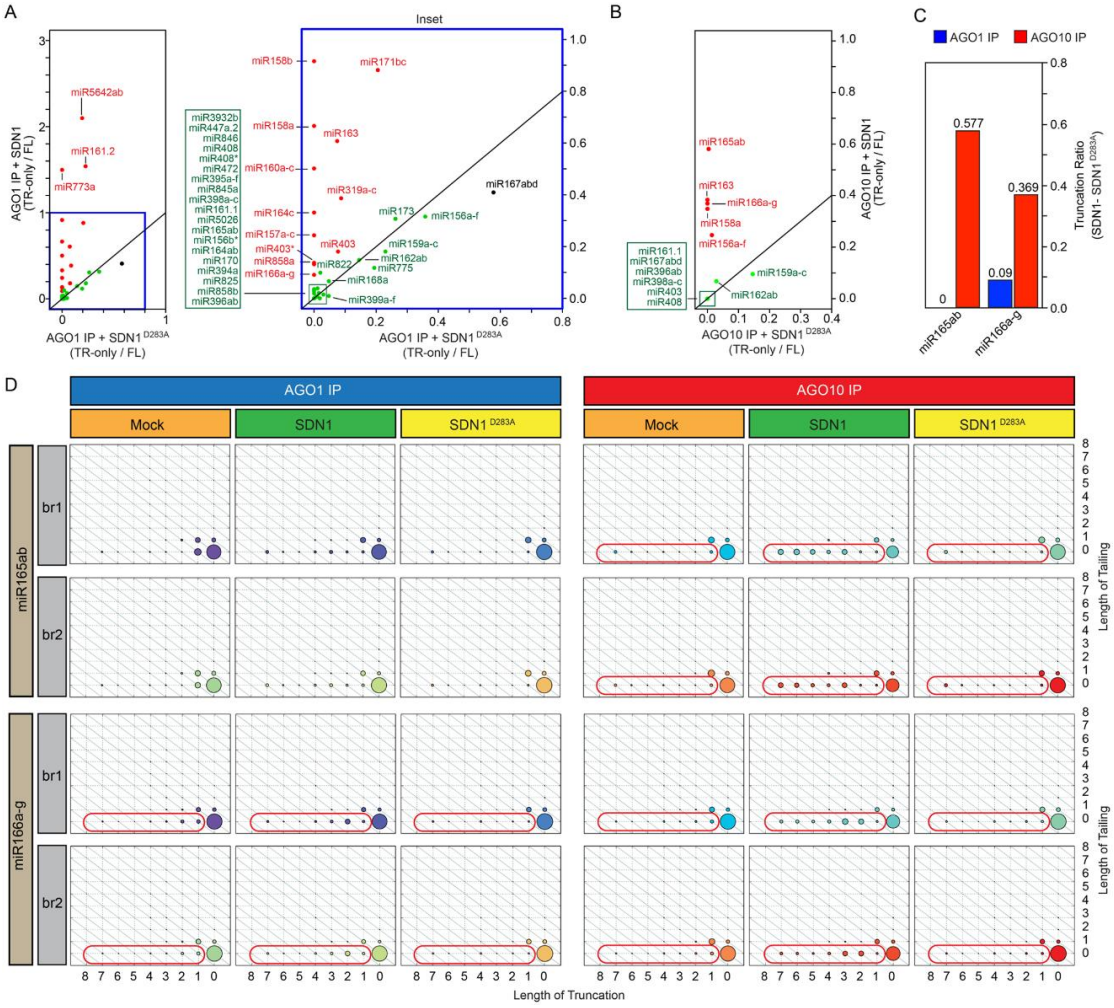
A
Inset
miR5642ab
miR161.2
miR773a
miR158b
miR171bc
miR158a
miR163
miR160a-c
miR319a-c
miR167abd
miR164c
miR173
miR156a-f
miR157a-c
miR403
miR159a-c
miR403*
miR162ab
miR858a
miR822
miR775
miR166a-g
miR168a
miR399a-f
miR3932b
miR447a.2
miR846
miR408
miR408*
miR472
miR395a-f
miR845a
miR398a-c
miR161.1
miR5026
miR165ab
miR156b*
miR164ab
miR170
miR394a
miR825
miR858b
miR396ab
AGO1 IP + SDN1 (TR-only / FL)
AGO1 IP + SDN1 D283A (TR-only / FL)
B
miR165ab
miR163
miR166a-g
miR158a
miR158a-f
miR159a-c
miR162ab
miR161.1
miR167abd
miR396ab
miR398a-c
miR403
miR408
AGO10 IP + SDN1 (TR-only / FL)
AGO10 IP + SDN1 D283A (TR-only / FL)
C
AGO1 IP
AGO10 IP
0.577
0.09
0.369
0
Truncation Ratio (SDN1- SDN1 D283A)
miR165ab
miR166a-g
D
AGO1 IP
AGO10 IP
Mock
SDN1
SDN1 D283A
miR165ab
miR166a-g
br1
br2
Length of Tailing
Length of Truncation

Figure 2.7 *ago10* mutations do not affect miR165/6 biogenesis.

(A) Mature miR165/6 levels were increased in the seedlings of *pnh-2* and *ago10-13* as compared to wild type (L*er*) in 6 biological replicates. The numbers represent mean ± standard deviations. (B) PCR to test the specificity of primers from each *MIR165/6* locus using genomic DNA as the template (upper panel); RT-PCR to determine whether the nine *MIR165/6* genes were expressed (lower panel). Reverse transcription was conducted with random primers followed by PCR with the same pairs of gene-specific primers as used for the PCR with genomic DNA above. The primers were designed such that the sum of pri- and pre-miR165/6 species (denoted by "pri/e-miR165/6") from a *MIR165/6* gene were detected. (C) Real-time RT-PCR to measure the relative transcript levels of pri/e-miR165/6s in wild type (L*er*) vs. *pnh-2* and *ago10-13* seedlings. * p-value < 0.05 (D) The levels of pre-miR166a in wild type (L*er*) vs. *pnh-2* as determined by northern blotting. The image on the left was the stained gel. U6 was a loading control. (E) AGO1- or AGO10-bound miR165/6 is methylated. AGO1 and AGO10 were separately immunoprecipitated from *zll-1 ZLLp::YFP-ZLL* plants, and the associated RNAs were subjected to β-elimination followed by northern blotting to examine the methylation status of miR165/6. The lack of a shift in molecular weight after β-elimination indicated that miR165/6 was fully methylated. A control (*hen1-8*) was included to show that the β-elimination treatment was effective, as the miRNA lacking methylation in this mutant showed an expected shift. Note that the *hen1-8* RNA was treated at the same time as the AGO IPs, resolved in the same gel, and transferred to the same membrane. The membrane was split into two for northern blotting to prevent the signals from the *hen1-8* sample from interfering with the signals in the AGO IPs.

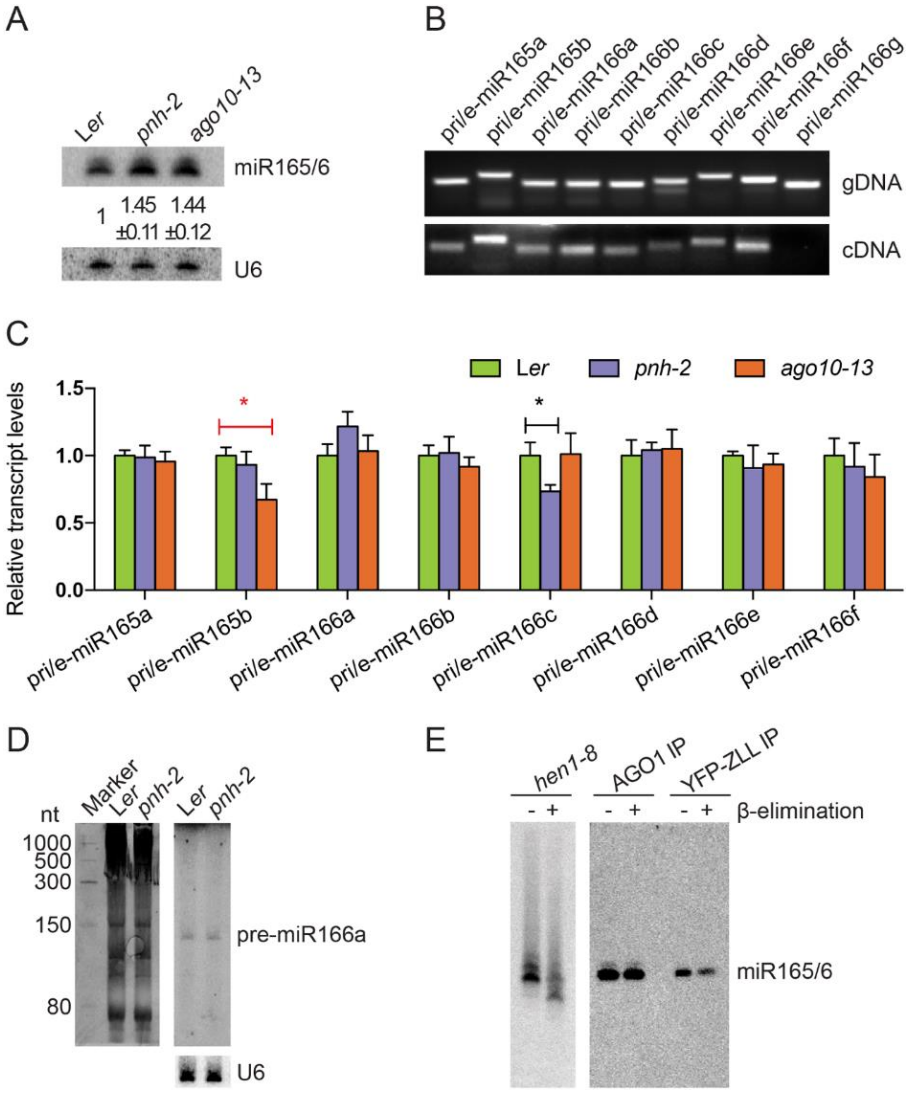
A
Ler
pnh-2
ago10-13
miR165/6
1
1.45 ±0.11
1.44 ±0.12
U6
B
pri/e-miR165a
pri/e-miR165b
pri/e-miR166a
pri/e-miR166b
pri/e-miR166c
pri/e-miR166d
pri/e-miR166e
pri/e-miR166f
pri/e-miR166g
gDNA
cDNA
C
Ler
pnh-2
ago10-13
Relative transcript levels
1.5
1.0
0.5
0.0
*
*
pri/e-miR165a
pri/e-miR165b
pri/e-miR166a
pri/e-miR166b
pri/e-miR166c
pri/e-miR166d
pri/e-miR166e
pri/e-miR166f
D
nt
Marker
Ler
pnh-2
Ler
pnh-2
1000
500
300
150
80
pre-miR166a
U6
E
hen1-8
AGO1 IP
YFP-ZLL IP
- + - + - +
β-elimination
miR165/6

Figure 2.8 *AGO10* over expression causes reduced miR165/6 accumulation.

(A) Phenotypes of wild type (WT) and *AGO10* over expression (*AGO10 OE*) lines in Weak (W), Moderate (M) and Strong (S) categories. The classification of *AGO10 OE* lines was based on the degree of deviation from the wild-type leaf phenotype. (B) The levels of six miRNAs in wild type and *AGO10 OE S1* seedlings as determined by northern blotting. U6 served as the internal control, and the numbers indicate the abundance of the miRNAs in *AGO10 OE S1* relative to wild type (Col). (C) The levels of four miRNAs in wild type, *AGO10 OE S1*, *AGO10 OE 4mAGO1* seedlings as determined by northern blotting. U6 served as the internal control, and the numbers indicate the abundance of the miRNAs relative to wild type (Col). (D) Real-time RT-PCR to determine *AGO10* transcript levels in wild type (Col) and four *AGO10 OE* lines. (E) Levels of miR165/6 in various *AGO10 OE* lines as compared to wild type (Col). The abundance of the miRNAs was determined by sRNA-seq.

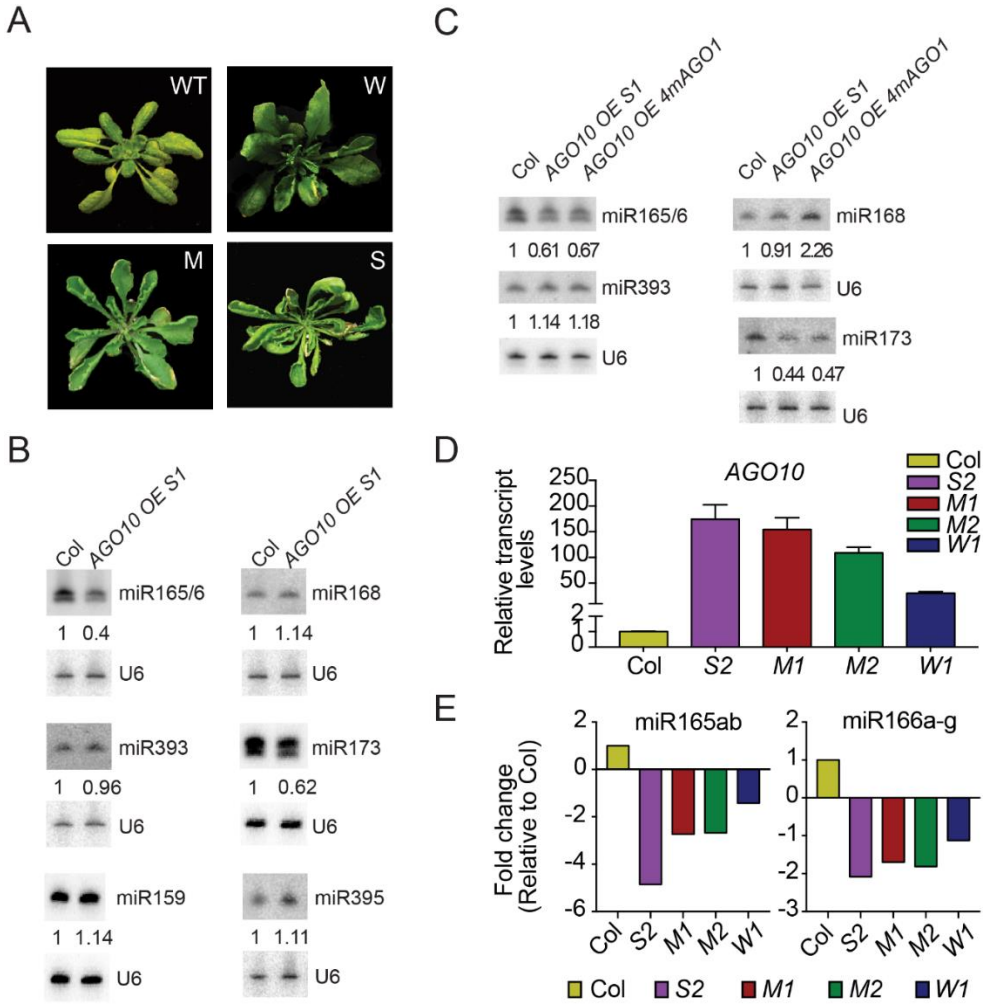
A
WT
W
M
S
B
Col
AGO10 OE S1
miR165/6
1 0.4
U6
miR168
1 1.14
U6
miR393
1 0.96
U6
miR173
1 0.62
U6
miR159
1 1.14
U6
miR395
1 1.11
U6
C
Col
AGO10 OE S1
AGO10 OE 4mAGO1
miR165/6
1 0.61 0.67
miR393
1 1.14 1.18
U6
miR168
1 0.91 2.26
U6
miR173
1 0.44 0.47
U6
D
AGO10
Relative transcript levels
250
200
150
100
50
2
1
0
Col
S2
M1
M2
W1
E
miR165ab
miR166a-g
Fold change (Relative to Col)
2
0
-2
-4
-6
1
-1
-3
Col
S2
M1
M2
W1

Figure 2.9 Characterization of *AGO10* over expression lines.

(A) Real-time RT-PCR to quantify transcript levels of *AGO1* and *AGO10* in wild type (Col) and *AGO10 OE S1*. ** p-value < 0.01, *** p-value < 0.001. (B) Real-time RT-PCR to detect pri/pre-miR165/6 from eight *MIR165*/*6* genes that were expressed in seedlings. (C) Northern blotting to detect pre-miR166a in the indicated genotypes. *pnh-2* is an *ago10* mutant in the L*er*background. *AGO10 OE S1* and *pnh-2 AGO10 OE* are two independent *AGO10 OE* lines in Col and Ler accessions, respectively. The stained gel is shown on the left. U6 was an internal control. (D) Western blotting to determine AGO1 levels in wild type (Col) and *AGO10 OE S1*. Three biological replicates were performed. The numbers represent AGO1 levels relative to wild type in each replicate. HSC70 was the loading control. (E) Real-time RT-PCR to determine *AGO1* and *AGO10* transcript levels in *AGO10 OE S1* and *AGO10 OE 4mAGO1*. (F) Western blotting to detect AGO1 in the indicated genotypes. AGO1 protein levels were increased in *AGO10 OE 4mAGO1*. HSC70 was the loading control.

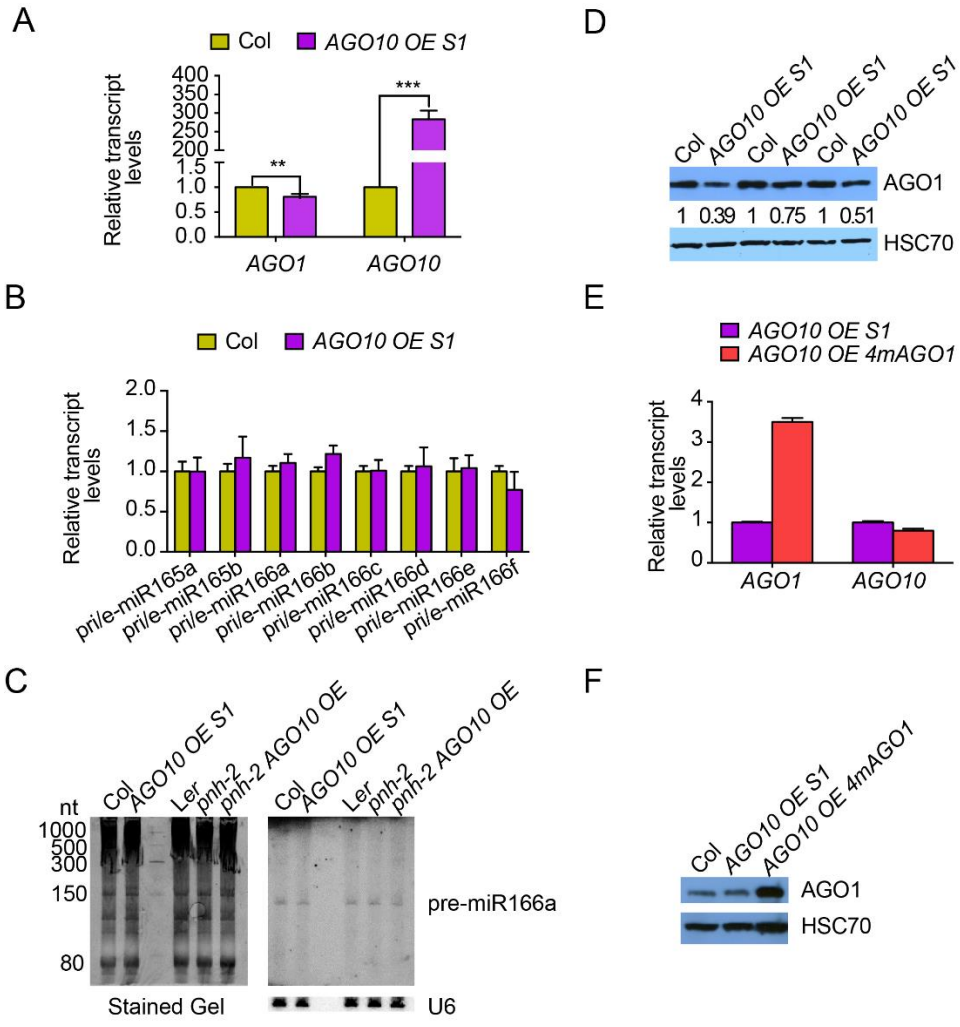
A
Col
AGO10 OE S1
Relative transcript levels
400
350
300
250
200
1.5
1.0
0.5
0.0
**
***
AGO1
AGO10
D
Col
AGO10 OE S1
Col
AGO10 OE S1
Col
AGO10 OE S1
AGO1
1 0.39 1 0.75 1 0.51
HSC70
B
Col
AGO10 OE S1
Relative transcript levels
2.0
1.5
1.0
0.5
0.0
pri/e-miR165a
pri/e-miR165b
pri/e-miR166a
pri/e-miR166b
pri/e-miR166c
pri/e-miR166d
pri/e-miR166e
pri/e-miR166f
E
AGO10 OE S1
AGO10 OE 4mAGO1
Relative transcript levels
4
3
2
1
0
AGO1
AGO10
C
nt
Col
AGO10 OE S1
Ler
pnh-2
pnh-2 AGO10 OE
Col
AGO10 OE S1
Ler
pnh-2
pnh-2 AGO10 OE
1000
500
300
150
80
pre-miR166a
Stained Gel
U6
F
Col
AGO10 OE S1
AGO10 OE 4mAGO1
AGO1
HSC70

Figure 2.10 *AGO10* over expression results in reduced levels of full-length and increased levels of 3' truncated miR165/6.

High-throughput sequencing was conducted to profile miRNAs in wild type (Col) and *AGO10 OE S1*. Three biological replicates were performed and the error bars represent standard deviations, * p-value < 0.05, ** p-value < 0.01, *** p-value < 0.001. One replicate was performed for *AGO10 OE 4mAGO1*. (A) Proportions of various types of miR165/6 species in wild type (Col) and *AGO10 OE S1*. (B) Proportions of various types of miR165/6 species in wild type (Col), *AGO10 OE S1*, and *AGO10 OE 4mAGO1. 4mAGO1* failed to suppress the elevated 3' truncation of miR165/6 in *AGO10 OE*. (C) The status of 3' truncation for the 20 most abundant miRNAs in the sRNA-seq datasets. Truncation ratio is the proportion of truncated species (TR+TA and TR-only) in total species for each miRNA.

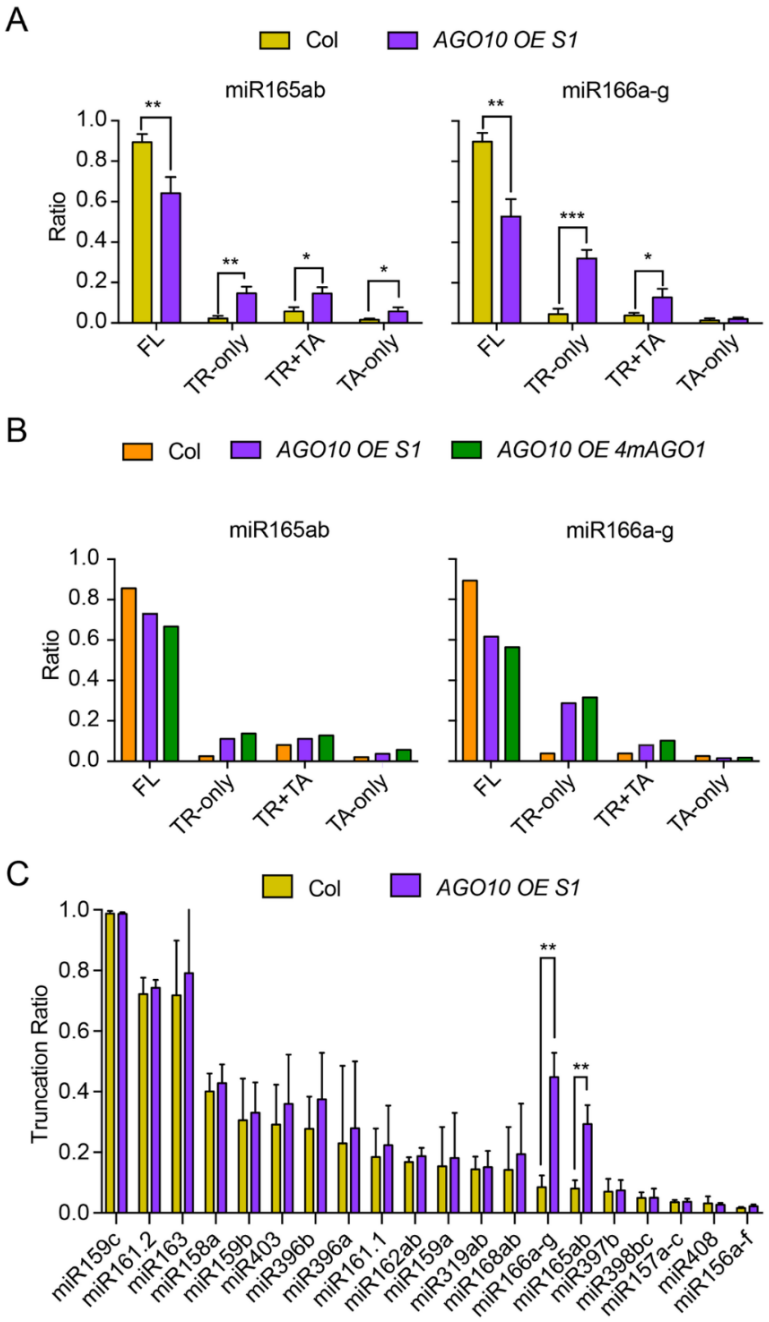
A
Col
AGO10 OE S1
miR165ab
miR166a-g
Ratio
1.0
0.8
0.6
0.4
0.2
0.0
**
**
*
*
**
***
*
FL
TR-only
TR+TA
TA-only
B
Col
AGO10 OE S1
AGO10 OE 4mAGO1
miR165ab
miR166a-g
Ratio
FL
TR-only
TR+TA
TA-only
C
Col
AGO10 OE S1
Truncation Ratio
**
**
miR159c
miR161.2
miR163
miR158a
miR159b
miR403
miR396b
miR396a
miR161.1
miR162ab
miR159a
miR319ab
miR168ab
miR166a-g
miR165ab
miR397b
miR398bc
miR157a-c
miR408
miR156a-f

Figure 2.11 Matrices representing the composition of miR165/6 reads in Col, *AGO10 OE S1* and *AGO10 OE 4mAGO1* libraries.

miR165/6 3′ truncation was increased in *AGO10 OE S1* relative to wild type. *4mAGO1* failed to rescue this increase in miR165/6 3′ truncation. The data were based on one biological replicate.

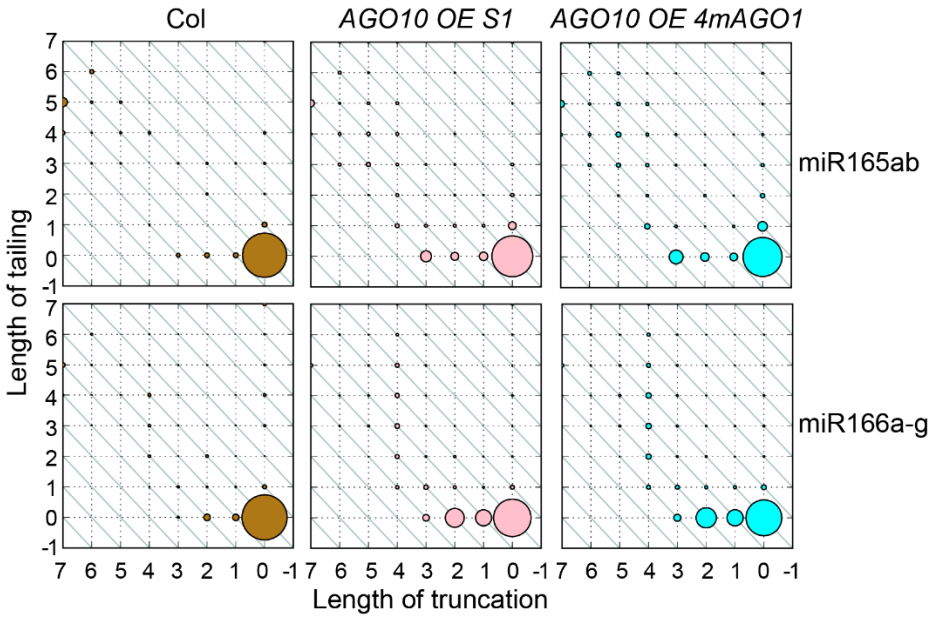
Col
AGO10 OE S1
AGO10 OE 4mAGO1
miR165ab
miR166a-g
Length of tailing
Length of truncation
7 6 5 4 3 2 1 0 -1

Figure 2.12 *AGO10* over expression results in sequestration of miR165/6 from AGO1.

(A) AGO1 was immunoprecipitated from wild type (Col) and *AGO10 OE S1*, and the associated RNAs were subjected to northern blotting to detect four miRNAs. The AGO1 immunoprecipitates (IP) were also subjected to western blotting to determine the levels of the AGO1 protein. (B) Composition of miRNAs in AGO1 and AGO10 IP from *AGO10 OE S1*. sRNA-seq was performed with three biological replicates of AGO1 and AGO10 IP from *AGO10 OE S1*. Reads corresponding to a particular miRNA were quantified against those of all annotated miRNAs and shown as percentage of total reads. (C-D) The levels of various miRNAs in AGO1 IP from wild type (Col) and *AGO10 OE S1*. The y-axis indicates the proportion of an individual miRNA in the total miRNA pool in AGO1 IP. A few miRNAs from each of four magnitudes of abundance levels in AGO1 IP (as indicated by the y-axis scales) were chosen to be shown in (D); the choices were random except for miR168, miR173, and miR393, which were chosen for comparison with (A). The data were derived from one biological replicate. (E-F) Levels of various miRNAs in AGO1 IP from various *AGO10 OE* lines with varying levels of *AGO10* expression (in decreasing order from *S2* to *W1*). The y-axis indicates the proportion of an individual miRNA in the total miRNA pool in AGO1 IP. Data were from one biological replicate.

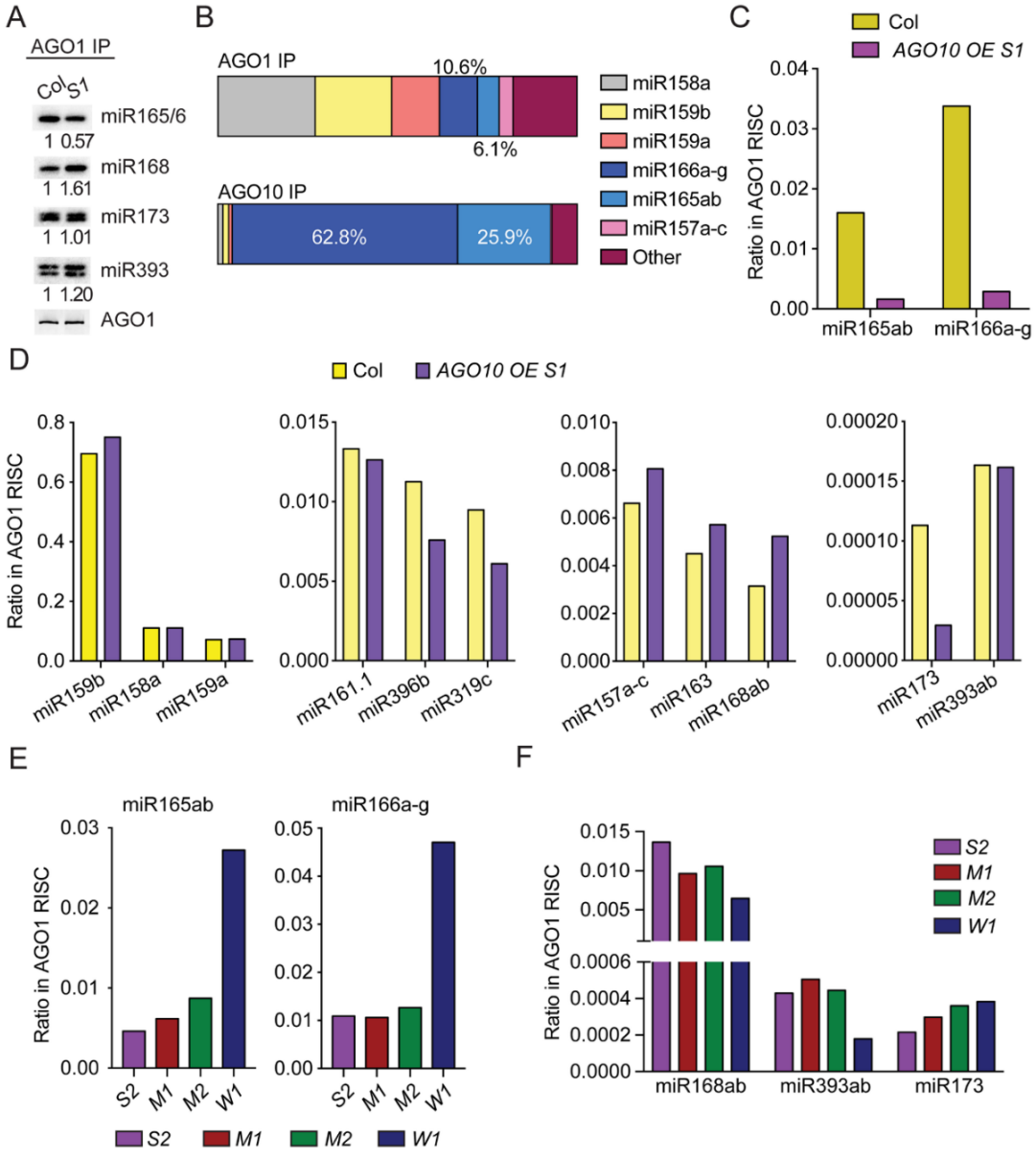
A
AGO1 IP
Col
S1
miR165/6
1 0.57
miR168
1 1.61
miR173
1 1.01
miR393
1 1.20
AGO1
B
AGO1 IP
10.6%
6.1%
AGO10 IP
62.8%
25.9%
miR158a
miR159b
miR159a
miR166a-g
miR165ab
miR157a-c
Other
C
Col
AGO10 OE S1
Ratio in AGO1 RISC
miR165ab
miR166a-g
D
Col
AGO10 OE S1
Ratio in AGO1 RISC
miR159b
miR158a
miR159a
miR161.1
miR396b
miR319c
miR157a-c
miR163
miR168ab
miR173
miR393ab
E
miR165ab
miR166a-g
Ratio in AGO1 RISC
S2
M1
M2
W1
F
Ratio in AGO1 RISC
S2
M1
M2
W1
miR168ab
miR393ab
miR173

Figure 2.13 3' truncated miRNAs in *AGO10 OE* are preferentially bound by AGO10. AGO1 and AGO10 were separately immunoprecipitated from *AGO10 OE S1*, and the associated small RNAs were subjected to high-throughput sequencing. Three biological replicates were performed and the error bars represent standard deviations. * p-value < 0.05. (A) Proportions of various types of miR165/6 species in AGO1 IP and AGO10 IP. For miR165ab, the increase in TR-only species had a p-value of 0.065. (B) The TR-only ratio of various miRNAs in AGO1 IP and AGO10 IP. The TR-only ratio is the proportion of TR-only species in total species for each miRNA. 17 of the top 48 most abundant miRNAs are shown; they were the only ones with statistically significant differences in the TR-only ratio in AGO1 IP and AGO10 IP. All showed reduced TR-only species in AGO10 IP except for miR403.

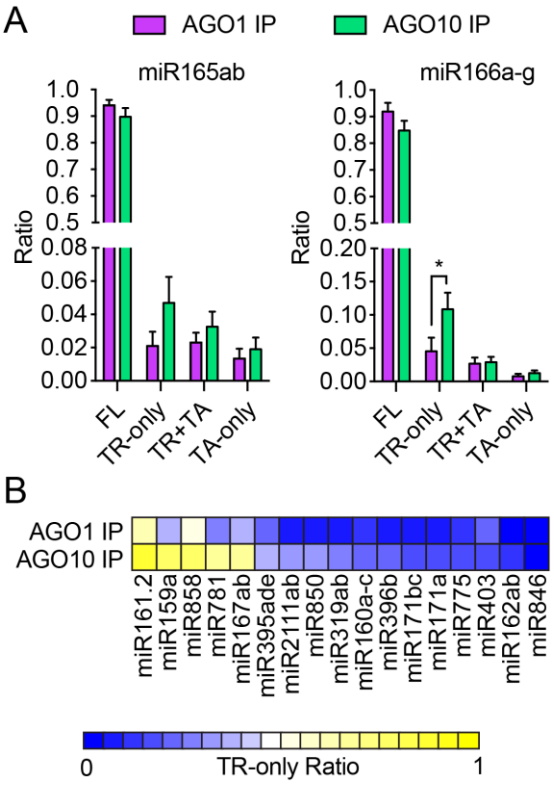
A
AGO1 IP
AGO10 IP
miR165ab
miR166a-g
Ratio
1.0
0.9
0.8
0.7
0.6
0.5
0.08
0.06
0.04
0.02
0.00
0.20
0.15
0.10
0.05
*
FL
TR-only
TR+TA
TA-only
B
AGO1 IP
AGO10 IP
miR161.2
miR159a
miR858
miR781
miR167ab
miR395ade
miR2111ab
miR850
miR319ab
miR160a-c
miR396b
miR171bc
miR171a
miR775
miR403
miR162ab
miR846
0
TR-only Ratio
1

Figure 2.14 *AGO10* over expression-induced miR165/6 3' truncation requires *SDN1* and *SDN2*.

(A) Relative transcript levels of *AGO1* and *AGO10* in Col, *AGO10 OE* and *sdn1 sdn2 AGO10 OE* plants. *35S::YFP-AGO10* was introduced into wild type and *sdn1 sdn2* by transformation. Multiple T1 transgenic lines were screened for *AGO10* expression by real time RT-PCR, and two independent pairs of lines (I and II) with similar *AGO1* and *AGO10* transcript levels were chosen for further analysis. For pair I, seedling tissues were used for the analyses (denoted by "I_s"). For pair II, inflorescence tissues were used (denoted by "II_f"). (B) The composition of the four types (full-length, 3' truncated-only, 3' tailed-only, and 3' truncated-and-tailed) of reads of miR165 and miR166 in *AGO10 OE* vs. *sdn1 sdn2 AGO10 OE*. Note that the proportion of 3' truncated-only reads was reduced and that of the full-length reads was concordantly increased in *sdn1 sdn2* background. Although the data shown here are from one biological replicate, the two pairs of samples represented two independent experiments and showed a similar trend.

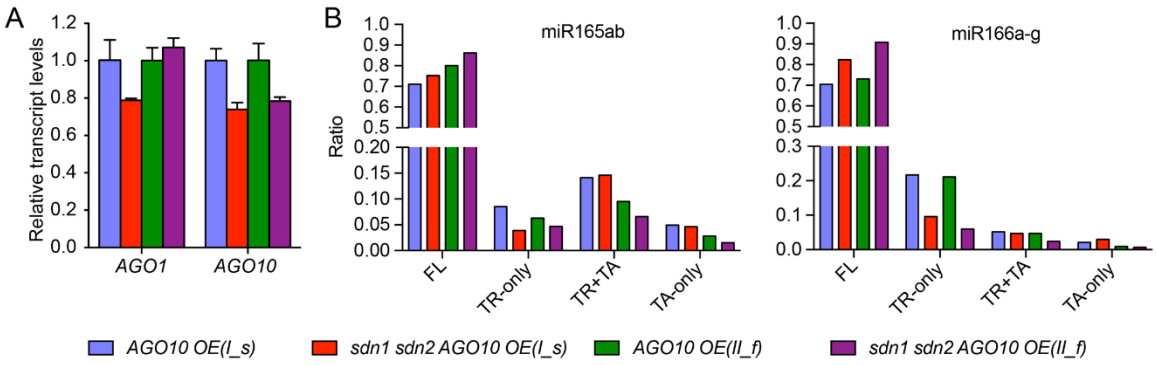
A
Relative transcript levels
AGO1
AGO10
B
miR165ab
miR166a-g
Ratio
FL
TR-only
TR+TA
TA-only
AGO10 OE(I_s)
sdn1 sdn2 AGO10 OE(I_s)
AGO10 OE(II_f)
sdn1 sdn2 AGO10 OE(II_f)

Figure 2.15 Matrices representing the compositions of miR165/6 reads in *AGO10 OE* and *sdn1 sdn2 AGO10 OE* libraries.

Total small RNAs were sequenced from seedling tissues (“s”) of one pair (I) of transgenic lines (*AGO10 OE* and *sdn1 sdn2 AGO10 OE*) and inflorescence tissues (“f”) of another independent pair (II) of transgenic lines. *AGO10* over expression in the *sdn1 sdn2* double mutant caused lower levels of miR165/6 3′ truncation. Although the data were based on a single biological replicate, the two independent pairs served as experimental repeats and gave similar trends.

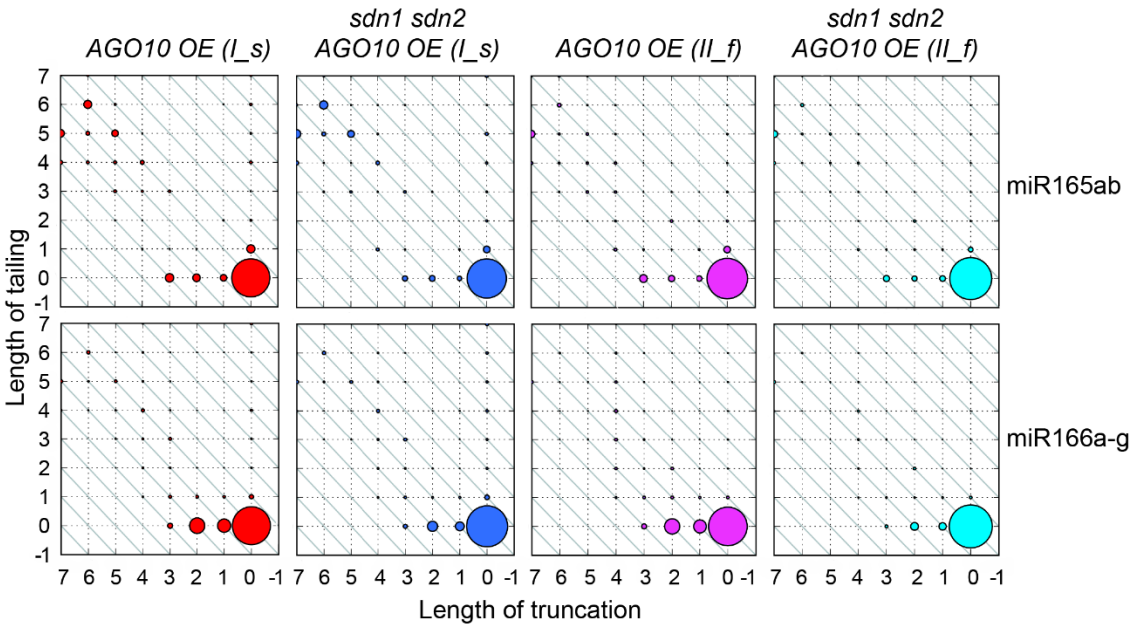
AGO10 OE (I_s)
sdn1 sdn2
AGO10 OE (I_s)
AGO10 OE (II_f)
sdn1 sdn2
AGO10 OE (II_f)
miR165ab
miR166a-g
Length of tailing
Length of truncation
7 6 5 4 3 2 1 0 -1

Table 2.1 *sdn1 sdn2* partially suppresses the developmental phenotype of *AGO10 OE*.

	AGO10 OE	*sdn1 sdn2 AGO10 OE*
WT-like	9 (25.7%)	21 (36.8%)
Weak	4 (11.4%)	25 (43.9%)
Moderate	5 (14.3%)	6 (10.5%)
Strong	17 (48.6%)	5 (8.8%)
Total	35	57

Developmental phenotypes of the primary AGO10 OE transformants were classified into 4 categories: wild type (WT)-like, Weak, Moderate, and Strong, based on the degree of deviation from the wild-type leaf phenotype. 35 primary *AGO10 OE* transformants in wild type background and 57 *AGO10 OE* transformants in *sdn1 sdn2* backgrounds were analyzed.

Table 2.2 Oligonucleotides used in this study.

Oligo Name	Sequence
caccAGO10 F	caccATGCCGATTAGGCAAATGAAAGA
AGO10 R	TTAGCAGTAGAACATTACTCTCT
SDN1 F	ACGGATCCGAGCTTAAACTAGCCACCGCCGA
SDN1 R	ACGCGTCGACTCATTCATCTTGAACCATTTTACGGACA
SDN1D283A F	CATGATTGTGTACATGCCGCATCAGCTGCGATGAAACTTG
SDN1D283A R	CAAGTTTCATCGCAGCTGATGCGGCATGTACACAATCATG
UBQ5 F	GGTGCTAAGAAGAGGAAGAA
UBQ5 R	CTCCTTCTTTCTGGTAAACGT
pre-miR165a F	TTGTCTGGATCGAGGATATTATAGATAT
pre-miR165a R	TCCGAGGATACTCTCTATGATCACT
pre-miR165b F	TGTTGTTTGGATCGAGGATATCA
pre-miR165b R	TACCATGTGGCATGTATGTATATATATGTA
pre-miR166a F	TTCATGTTGGATCTCTTTCGATCT
pre-miR166a R	CGCTAAAACCCTAATCAAATCTG
pre-miR166b F	TGGCTCGAGGACTCTTATTCTAA
pre-miR166b R	AAACCCTAATCAATCATCAGATCTG
pre-miR166c F	TTGTCTGGCTCGAGGTCATG
pre-miR166c R	GGGTTTTCTTAATTTGTTCTTCCAAA
pre-miR166d F	TTGTCTGGCTCGAGGTCATGA
pre-miR166d R	TGGTCCGAGAATCATTTAGGG
pre-miR166e F	GCACGAGGCCCTTAACTTAGATC
pre-miR166e R	TCCGACGTCATTAACCGTAAAA
pre-miR166f F	GAATGATGCCTGGCTCGAGAC
pre-miR166f R	GGAATGAAGCCTGGTCCGACA
pre-miR166g F	CGAGGTCATGGAGAGTAATTCG
pre-miR166g R	AGCCTGGTCCGAGAATCATTT
AGO1-RT F	TGGACCACCGCAGAGACAAT
AGO1-RT R	CATCATACGCTGGAAGACGAC
AGO10-RT F	GGGTATTCAGGGAACAAGCA
AGO10-RT R	TAGAAACGTGCTCGAAATGCT
miR159-AS probe	TAGAGCTCCCTTCAATCCAAA
miR166-AS probe	GGGGAATGAAGCCTGGTCCGA
miR168-AS probe	TTCCCGACCTGCACCAAGCGA
miR173-AS probe	GTGATTTCTCTCTGTAAGCGA
miR393-AS probe	GATCAATGCGATCCCTTTGGA
miR395-AS probe	GAGTTCCCCCAAACACTTCAG
U6 probe	AGGGGCCATGCTAATCTTCTC
pre-miR166a-Nb F	AGATATATATTCAGAAACCCTAG
pre-miR166a-Nb R	GGTTCATTCACTGGATCTGAAAC

Chapter 3

Characterization of *Arabidopsis* RCD1's role in small RNA metabolism

Abstract

Numerous environmental factors such as salinity, drought, oxidative stress, pathogens and viral diseases affect plant growth and development. To survive, plants optimally balance growth and stress responses via a complex gene expression regulatory network. In *Arabidopsis*, the protein RADICAL-INDUCED CELL DEATH 1 (RCD1) regulates both growth and stress responses. Its pleiotropic effects have been attributed to the diversity of its interacting partners, including many transcription factors involved in different regulatory pathways. In this study, we focused on the *rcd1* mutant *int51* to investigate the effect of RCD1 on small RNAs. Through small RNA sequencing and bioinformatic analysis of the *int51* mutant, we found that miRNA and tasiRNA accumulation was unchanged, but many 24-nt siRNAs were either up-regulated or down-regulated. Whole-genome bisulfate-sequencing revealed that DNA methylation in all sequence contexts was greatly reduced on euchromatin arms in *int51*, with no change at heterochromatic regions. The global level of H3K9me2 was also reduced in *int51*, although the affected sites remain unknown. The changes observed in *int51* resemble those of mutants defective in DNA or histone methylation, providing a novel link to further dissect the RCD1-mediated regulatory network.

Introduction

Arabidopsis RADICAL-INDUCED CELL DEATH 1 (RCD1) is an important cellular hub protein involved in diverse biological processes through its interaction with numerous transcription factors [1-5]. The mutant of this gene was first isolated based on its sensitivity to apoplastic reactive oxygen species (ROS), particularly superoxide [6]. Subsequent studies reported the functions of RCD1 in response to various stresses including salinity [7,8], UV-B [9,10], heat [11,12], freezing [8] and high light [9] in addition to oxidative stress [7,8,13]. RCD1 is also involved in the responses to several hormones including ethylene, abscisic acid (ABA) and methyl jasmonate [1,6]. In loss-of-function *rcd1* mutants, the pleiotropic defects include dwarfed stature, altered leaf and rosette morphology, increased branching, early flowering and early senescence [1,3,5,6,8,9]. Collectively, these findings suggest that RCD1 acts as an integration point for different stress responses and hormone signaling pathways and plant growth and development.

The *RCD1* gene encodes a protein with the following components: three nuclear localization signals (NLS), a WWE domain, a poly(ADP-ribose) polymerase (PARP) domain and a C-terminal RCD1-SRO1-TAF4 (RST) domain [1,2,7]. The three NLSs at the N-terminus determine its predominantly nuclear localization under unstressed conditions. Under stress conditions, however, the protein also appears in the cytoplasm [7], indicating that stresses trigger a differential RCD1 expression pattern through an unknown mechanism. The WWE domain, named after its conserved tryptophan (W) and glutamic acid (E) residues, is a predicted protein-protein interaction domain [14], but no partners have been found to interact with RCD1 through this domain. Instead, the C-terminal RST domain, which is shared by RCD1, SRO1 and TBP-ASSOCIATED FACTOR 4 (TAF4) based on sequence similarity, serves as the critical interaction domain between RCD1

and its interacting proteins, most of which are transcription factors (TFs) [2,4]. These TFs represent several families, including the AP2/ERF, NAC and basic helix–loop–helix (bHLH) families [2], whose diverse functions in organ development, stress responses, hormone pathways and defense underscore the importance of the RST domain. The PARP domain is considered a catalytic core that adds poly(ADP-ribose) to various target proteins [15,16]. However, no functional ADP-ribosylating activity has been observed for RCD1 so far.

The interaction of RCD1 with various TFs underlies its diverse functions. The AP2/EREBP TF family accounts for an essential portion of these gene regulatory networks by integrating developmental, hormonal and environmental signals under stress acclimation and retrograde signaling [17-19]. For example, the RCD1-mediated responses to drought and heat stresses, as well as leaf senescence, are attributed to its interacting partner DEHYDRATION-RESPONSIVE ELEMENT BINDING 2A (DREB2A) [11,12]. However, the interplay with DREB2A is required but not sufficient for RCD1 to induce the expression of downstream genes under stress [12]. Moreover, RCD1 may target DREB2A for degradation under heat stress, based on an opposite accumulation status observed for RCD1 and DREB2A under these conditions [12]. Given that DREB2A is a TF that can activate the expression of downstream target genes [11,12], it has been posited that RCD1 may play a negative role in gene expression by inhibiting transcription at its associated loci.

Gene expression is regulated in various ways at both the transcriptional and post-transcriptional levels. DNA methylation and histone modifications are two important epigenetic marks that usually repress gene expression at the transcriptional level, referred to as transcriptional gene silencing (TGS). The well-studied mechanisms of TGS include

DNA cytosine methylation, histone H3K9 dimethylation (H3K9me2) and H3K27 trimethylation (H3K27me3) (reviewed in [20,21]). In plants, DNA methylation is found in a small number of genes and is largely associated with transposon silencing to maintain genome integrity. DNA methylation may influence TF binding to target promoters and thereby inhibit transcription [22]. Alternatively, DNA methylation may recruit histone modifiers that establish a heterochromatic environment to repress transcription [23]. The three types of DNA methylation are based on their sequence contexts, CG, CHG and CHH (where H represents A, T or C) [24], and are maintained by different enzymes [25]. CG and CHG methylation are symmetric and primarily maintained by DNA METHYLTRANSFERASE 1 (MET1) [26,27] and CHROMOMETHYLASE 3 (CMT3) [28,29], respectively. The RNA-directed DNA methylation (RdDM) pathway also contributes to the maintenance of CHG methylation at some loci (reviewed in [20,21]). In contrast, CHH methylation is asymmetric and maintained by CHROMOMETHYLASE 2 (CMT2) at heterochromatic pericentromeric regions and by the RdDM pathway on euchromatic arms. RdDM is a plant-specific mechanism that requires 24-nucleotide (nt) small interfering RNAs (siRNAs) generated from transposons or repeats along with several essential factors that mediate DNA methylation at euchromatic regions (reviewed in [20,21]).

Histone modification is a post-translational regulation that mainly occurs on the tails of H2A, H2B and H3 and H4. H3K9me2 and H3K27me3 are two well-characterized repressive histone markers that primarily occur in heterochromatic and euchromatic regions, respectively [30]. H3K9me2 targets transposons and repeats and is highly correlated with CHG methylation [30-32]. The H3K9me2 mark is maintained by three histone methyltransferases: KYP/SUVH4, SUVH5 and SUVH6 [30,33]. In contrast,

H3K27me3 primarily targets genes and is maintained by POLYCOMB REPRESSIVE COMPLEX 2 (PRC2) (reviewed in [21]). Although gene expression regulation by DNA methylation and histone modification is well studied in terms of the underlying mechanisms and major players, the contributions of other potential factors may still be uncovered. Therefore, it is interesting to examine whether RCD1 participates in these pathways as a means of regulating gene expression.

The developmental defects of *rcd1* mutants and the broad impact of RCD1 on different processes are in some ways similar to the wide-ranging effects of microRNAs (miRNAs), which influence growth and development, responses to stress and hormones and disease defense (reviewed in [34,35]). MiRNAs post-transcriptionally regulate the expression of their target genes, including many TFs, via transcript cleavage or translation repression. Altered miRNA accumulation or defective miRNA-mediated activity often leads to pleiotropic developmental phenotypes, which is quite similar to that of *rcd1* mutants (reviewed in [34,35]). In light of these similarities, it is possible that RCD1 cooperates with miRNAs to regulate TFs involved in plant growth, development and stress responses.

In this study, we studied the *int51* mutant, which harbors a point mutation in the *RCD1* gene that results in a premature stop codon [5]. The analyses were aimed at dissecting how RCD1 regulates plant growth and development, stress and hormone responses and pathogenic disease defense as well as the connection to small RNAs. We found comparable miRNA accumulation and activity in *int51* and wild-type plants, but differences were observed for siRNAs. Hundreds of hypo- or hyper- differential small RNA regions (DSRs) of diverse lengths were detected in *int51*, with a predominance of 24-nt siRNAs mainly from TEs and intergenic regions. Both hypo- and hyper-siRNAs identified in *int51* were Pol IV-, RDR2- and DCL3-dependent. While the siRNAs at hypo-DSR loci

seemed to affect DNA methylation in all sequence contexts, DNA methylation was generally not affected at hyper-DSR loci in *int51*. We also observed a global reduction of H3K9me2 in the *int51* mutant. The observed changes in the accumulation of 24-nt siRNAs, DNA methylation and H3K9me2 in *int51* resemble those of the *suvh4 suvh5 suvh6* and *drm1 drm2 cmt2 cmt3* mutants, suggesting a potential role of RCD1 in gene expression regulation through the control of epigenetic modifications.

Results

Loss of *RCD1* induces differential expression of siRNAs without affecting miRNA abundance or activity

Because the developmental defects of the *int51* mutant are similar to those of mutants with compromised miRNA accumulation or activity, we first examined whether the miRNA pathway is affected in *int51*. Both 13-day-old seedlings and inflorescences were used for northern blotting to detect the abundance of several conserved miRNAs. All of the tested miRNAs had similar abundance in wild type and *int51* (Fig 3.1A). High-throughput small RNA sequencing was also performed to examine genome-wide miRNA levels in both seedlings and inflorescences. Consistently, no significant differences were observed between wild type and *int51*. To analyze whether miRNA-mediated cleavage of target transcripts was impaired, the transcript levels of miRNA target genes, many of which are essential for growth and development, were detected by semi-quantitative RT-PCR. Based on several biological replicates, the transcript levels of most miRNA targets were comparable in wild type and *int51*, although several genes were slightly reduced in the mutant (Fig 3.1B). Protein levels of a few miRNA targets were also detected by western blotting. Only CSD2 showed elevated protein levels (data not shown), but the increase could also have been caused by other factors. Taken together, these results suggest that

loss of *RCD1* affects neither miRNA accumulation nor miRNA-guided cleavage activity. No conclusions can presently be made regarding miRNA-mediated translational repression, and additional miRNA target proteins should be examined.

The altered leaf morphology of *int51* could also be attributable to trans-acting siRNA (tasiRNA)-directed regulation of *AUXIN RESPONSE FACTOR 2* (*ARF2*), *ARF3* and *ARF4*, which are required for proper leaf shape and leaf polarity [36]. The levels of the three tasiRNAs and the corresponding target transcripts were examined by northern blotting and semi-quantitative RT-PCR, respectively. No defect was observed in either the accumulation or activity of the tasiRNAs (Fig 3.1A, B), suggesting that the leaf phenotype of the *int51* mutant is not related to tasiRNAs.

In contrast to miRNAs and tasiRNAs, reduced siRNA abundance or function usually has no effect on plant growth and development processes. In fact, mutants of genes involved in the RdDM pathway display normal morphological phenotypes, , implying that siRNAs and the RdDM pathway are not responsible for plant morphogenesis. For this reason, the pleiotropic phenotypes of the *int51* mutant did not seem likely to be attributable to siRNAs. Surprisingly, bioinformatic analysis of the small RNA-seq data from both seedlings and inflorescences identified hundreds of differential small RNA regions (DSRs), in which the abundance of small RNAs differed between wild type and *int51*. These small RNAs, mainly siRNAs either enriched or reduced in *int51*, were designated as *int51* hyper-DSRs and hypo-DSRs, respectively. These siRNAs ranged in size from 21 to 24 nt, but 24-nt species predominated, with 237 24-nt hypo-DSR loci and 115 24-nt hyper-DSR loci in seedlings. More loci were identified in inflorescences, with 891 24-nt hypo-DSR loci and 675 24-nt hyper-DSR loci (Table 3.1). This difference is probably due to the greater concentration of stem cells in inflorescences than in seedlings and the more active

production of small RNAs in stem cells. To determine the locations from which these siRNAs derived, all of the DSR loci were mapped to the *Arabidopsis* genome. While the hyper-DSRs predominantly mapped to centromeric and pericentromeric regions corresponding to heterochromatin, the hypo-DSRs spread along the euchromatin arms. In fact, DSR loci of different sizes overlapped with each other when mapped (Fig 3.2A). In other words, the 21- to 24-nt siRNAs may have been produced from the same loci. To validate these DSRs, northern blotting was performed to detect siRNAs at both hyper- and hypo-DSR loci. Considering the extremely low abundance of these siRNAs, 30 µg small RNAs, enriched from 300 µg total RNA from inflorescences, was used for each locus. Many hyper-DSRs siRNAs were detectable, and significant increases were validated at these loci in *int51*, whereas only two hypo-DSR loci were validated due to low abundance of siRNAs at these loci (Fig 3.2B). Therefore, we mainly focused on the 24-nt hyper-DSRs to further study their features, activities and connection to RCD1 functions.

24-nt hyper-DSRs are mainly LTR-Gypsy TEs

To characterize the DSRs, we analyzed the genome-wide features associated with the hyper- and hypo-DSRs. Features associated with hyper-DSRs were quite similar, despite their size variation from 21 to 24 nt. Around 90% of the hyper-DSR loci were TEs, and less than 10% were other regions, including intergenic regions and protein-coding genes (Fig 3.3A). In contrast, the features associated with hypo-DSRs were more diverse. TEs, protein-coding genes and intergenic regions accounted for the majority of hypo-DSRs, although the percentages of each varied for the different sizes of hypo-DSRs (Fig 3.3A). Among the four groups of hypo-DSRs classified by length, 23-nt and 24-nt hypo-DSRs had a similar pattern, with 50% being intergenic regions and 40% being TEs. For 21-nt hypo-DSRs, about 35% were related to miscellaneous regions (MISC) and 30%

were intergenic regions. The largest portion of 22-nt hypo-DSRs, around 35%, were protein-coding genes, while 25% and 20% were TEs and intergenic regions, respectively. The large percentage of protein-coding genes observed for 22-nt hypo-DSRs was not similarly observed for any other hypo- or hyper-DSRs. Considering the specific length and location type, these 22-nt DSRs may correspond to secondary siRNAs, since many secondary siRNAs produced from protein-coding gene transcripts have been reported to play important roles in stress response and plant defense. However, further study is required to determine whether secondary siRNAs are indeed highly represented among the 22-nt DSRs, and if so, what triggers these 22-nt siRNAs and what roles they play in the *int51* mutant.

We next focused on the features of TEs associated with 24-nt hyper- and hypo-DSRs, as 24-nt DSRs were the most abundant length class and TEs made up the largest proportion of all DSRs. We were also interested in the similarity and differences between the features of TEs related to hyper- and hypo-DSRs. Briefly, the percentage of each type of TE was calculated for 24-nt hyper- and hypo-DSRs, and the genome-wide TE distribution was used as a reference. The analysis showed that hypo-DSRs resembled the pattern of the control, but the hyper-DSRs had a distinct pattern: 89% of the TEs associated with 24-nt hyper-DSRs belonged to the LTR-Gypsy TE family, which accounted for only 10% of 24-nt hypo-DSRs (Fig 3.3B). The predominant overlap of 24-nt hyper-DSRs with Gypsy TEs is reasonable, given that LTR-Gypsy TEs are mainly located at heterochromatic regions close to the centromere (Fig 3.3C). However, the function of LTR-Gypsy TEs is still unclear, and it will be interesting to know how these 24-nt siRNAs are specifically produced from this TE family, how these siRNAs function, and whether LTR-Gypsy TEs contribute to the function of RCD1.

We also analyzed several specific genome-wide features associated with the 24-nt DSRs. First, we focused on protein-coding genes that gave rise to 24-nt siRNAs in *int51*. For this analysis, the same relative length from the transcription start site (TSS) to the transcription termination site (TTS) was assigned to the whole gene body of each locus. An overall reduction of 24-nt siRNA abundance was observed along the gene bodies in *int51*, although the levels were still higher than in intergenic regions (Fig 3.4A), and this should correspond to the hypo-DSRs mainly in the 24-nt length class. Next, we analyzed repeat loci, including tandem repeats (TRs), inverted repeats (IRs) and dispersed repeats (DRs). Similarly, the repeat loci were normalized to the same relative length. At all three types of repeat loci, 24-nt siRNAs were reduced in *int51* (Fig 3.4B), and these probably corresponded to the hypo-DSRs from the euchromatic arms as well. Interestingly, the siRNAs associated with IRs were more enriched at the 5' end than the 3' end of the IRs, which was not observed for either TRs or DRs, suggesting that these siRNAs were specifically derived from one strand even IRs are supposed to form hairpin structures and give rise to siRNAs from both strands. Lastly, we focused on each DSR locus to determine if there were any common or distinct patterns among them. The siRNAs at hypo-DSR loci were generally present at a higher level in wild type than in *int51* throughout a given DSR locus, whereas only some specific regions within hyper-DSR loci generated more siRNAs than other regions (Fig 3.4C). This pattern may suggest that some special regions or sequences at hyper-DSR loci are preferentially selected for siRNA biogenesis by an unknown mechanism.

The biogenesis of 24-nt hyper-DSRs requires components of the RdDM pathway

siRNAs are derived from double-stranded RNAs (dsRNAs), and their biogenesis and activity distinguish them from other small RNAs. One canonical and well-studied

pathway of 24-nt siRNA biogenesis is the Pol IV-dependent RdDM pathway, in which siRNA precursors are transcribed by the plant-specific RNA POLYMERASE IV (Pol IV) and converted into dsRNAs by RNA-DIRECTED RNA POLYMERASE 2 (RDR2). DICER-LIKE 3 (DCL3) processes the dsRNAs into 24-nt mature siRNA duplexes, from which one strand is loaded onto AGO4 and directed to the target loci by POL V transcripts to mediate DNA methylation through DNA REARRANGED METHYLASE 2 (DRM2) (reviewed in [20,35]). As mentioned above, siRNA-directed DNA methylation mainly takes place on euchromatic arms because one essential protein, DEFECTIVE IN RNA-DIRECTED DNA METHYLATION 1 (DRD1) [37], required for RdDM is not functionally effective at heterochromatic regions. DNA methylation at heterochromatic regions close to the centromere is mediated by CMT2 and is siRNA-independent. Nevertheless, CMT2 loci also give rise to 24-nt siRNAs that are Pol IV- and RDR2-dependent and whose functions are still unknown [20]. To address what factors are required for the biogenesis of the 24-nt siRNAs at hyper-DSR loci identified in *int51*, we first analyzed the available published small RNA-seq (sRNA-seq) datasets from various mutants, particularly those from RdDM mutants. By comparing different biological replicates of sRNA-seq data, we found that the abundance of 24-nt siRNAs from the hyper-DSR loci was reduced in *pol4*, *rdr2* and *dcl3* mutants but was not altered in *pol5* and *ago4* mutants (Fig 3.5A). These results were validated by northern blotting of the 24-nt siRNAs at several hyper-DSR loci in these RdDM mutants, using 30 µg enriched small RNAs from inflorescences. Consistent with the bioinformatic analysis, the tested 24-nt siRNAs from hyper-DSR loci completely disappeared in the *pol4* mutant, and only a very weak band could be detected in *rdr2* and *dcl3* mutants (Fig 3.6A). For *pol5* and *ago4* mutants, no changes were observed (Fig 3.6A). However, this analysis only addressed the biogenesis requirements of 24-nt

siRNAs at *int51* hyper-DSR loci in wild-type plants. To examine whether RdDM pathway components are required for enrichment of the siRNAs in the *int51* mutant as well, we made a series of double mutants by crossing *int51* into RdDM pathway mutants. All the double mutants, including *int51 pol4*, *int51 rdr2*, *int51 dcl3*, *int51 pol5* and *int51 ago4*, displayed similar morphological phenotypes to the *int51* single mutant, indicating that the defective developmental phenotypes observed in *int51* are not attributable to the RdDM pathway or DNA methylation in the CHH context. Northern blotting was also performed for the 24-nt hyper-DSRs in the double mutants. Similar to the single mutant analysis, the accumulation of the 24-nt siRNAs decreased in *int51 pol4*, *int51 rdr2* and *int51 dcl3* but was comparable to wild type in *int51 pol5* and *int51 ago4* (Fig 3.6B). Thus, the biogenesis of 24-nt siRNAs at *int51* hyper-DSR loci requires some RdDM pathway components, including Pol IV, RDR2 and DCL3, but not Pol V and AGO4.

We also analyzed sRNA-seq datasets of mutants defective in DNA methylation and histone methylation, mainly focusing on the 24-nt hyper- and hypo-DSR loci discovered in *int51*. Intriguingly, we found that the accumulation of 24-nt siRNAs was also elevated at *int51* hyper-DSR loci in several of these mutants, including a *decreased dna methylation 1* (*ddm1*) mutant, the *drm1 drm2 cmt3* triple mutant and the *suvh4 suvh5 suvh6* triple mutant (Fig 3.5B). Thus, 24-nt siRNAs at *int51* hyper-DSR loci may have some connection to DNA methylation and H3K9me2 methylation, and RCD1 may play a role together with DDM1, DRM1, DRM2, CMT3 or SUVH in the regulatory network affecting 24-nt siRNAs, DNA methylation and H3K9me2 methylation.

***int51* hypo-DSRs have reduced DNA methylation in all sequence contexts**

The well-known function of 24-nt siRNAs is to mediate DNA methylation, specifically CHH methylation, primarily on euchromatic arms. With so many 24-nt hyper-

and hypo-DSRs identified, we speculated that CHH methylation would be altered in *int51*. In addition, 24-nt siRNAs were elevated at *int51* hyper-DSR loci in the DNA methylation defective mutants *ddm1* and *drm1 drm2 cmt3*, indicating that CG and CHG methylation may also be affected in the *int51* mutant. To examine whether loss of RCD1 influences DNA methylation status, we treated genomic DNA extracted from wild-type and *int51* seedlings with McrBC, followed by chop-PCR at several hyper-DSR loci, which were selected based on the northern blotting results. The McrBC endonuclease specifically cleaves DNA containing methylated cytosine on one or both strands, while leaving unmethylated DNA intact. Although PCR analysis of McrBC-treated DNA can detect overall changes in DNA methylation level between samples, it cannot distinguish DNA methylation in the CG, CHG and CHH sequence contexts. We tested several hyper-DSR loci and did not find any changes in DNA methylation levels between *int51* and wild type (Fig 3.7), indicating that DNA methylation at these hyper-DSR loci was not affected by loss of RCD1. This is not surprising because DNA methylation at heterochromatic centromeric and pericentromeric regions is siRNA-independent.

Next, we performed bisulfate-sequencing of genomic DNA extracted from wild-type and *int51* seedlings to determine whether genome-wide DNA methylation was impaired in the mutant. DNA methylation levels at all hyper-DSR loci were compared between wild type and *int51*, and no changes in DNA methylation were detected for any sequence contexts (Fig 3.8A), consistent with the McrBC result. Since 24-nt hyper-DSRs were mainly associated with LTR-Gypsy TEs, we analyzed DNA methylation in all contexts at LTR-Gypsy loci in wild type and *int51*. Slightly decreased CHH methylation, increased CHG methylation and unaltered CG methylation were detected in *int51* at these loci (Fig 3.8B). DNA methylation at all hypo-DSR loci located on euchromatic arms was also

analyzed. As expected, the level of CHH methylation at hypo-DSR loci was slightly decreased in *int51* (Fig 3.8C), indicating that RCD1 may promote the production of 24-nt siRNAs to facilitate CHH methylation on euchromatin arms. Strikingly, more significant reductions in both CG and CHG methylation were observed at these hypo-DSR loci in *int51*, resembling the DNA methylation changes in the *ddm1* and *drm1 drm2 cmt3* mutants (ref). This further supports our hypothesis that RCD1 may be part of the regulatory network between DNA methylation and small RNAs. Regarding DNA methylation at gene bodies and LTR-copia TE loci, there were no obvious differences between wild type and *int51* (Fig 3.8D). Although the underlying mechanism by which these hyper- or hypo-DSRs influence DNA methylation is still unknown, it appears that DNA methylation in different contexts is specifically regulated in *int51* at certain loci.

Histone modification status is altered in *int51*

The connection between DNA methylation and the hyper- or hypo-DSRs of *int51*, together with the common features observed among the *int51*, *ddm1*, *drm1 drm2 cmt3* and *suvh4 suvh5 suvh6* mutants, draws attention to the self-reinforcing loop between non-CG methylation, H3K9me2 and 24-nt siRNAs [21,38]. H3K9me2 is mostly maintained by the three histone transferases SUVH4, SUVH5 and SUVH6 and is highly correlated with CHG methylation. In mutants defective in DNA methylation, such as *ddm1* and *cmt3*, decreased H3K9me2 is observed at certain loci [39-41]. Genome-wide chromatin immunoprecipitation (ChIP) studies have shown that H3K9me2 is highly associated with heterochromatic regions and relatively low on euchromatin [38]. At the DRM2 sites on euchromatin arms, many of which are short TEs and edges of TEs, the biogenesis of 24-nt siRNAs begins with SHH1 binding of H3K9me2 at a large number of DRM2 loci, which recruits Pol IV to initiate the transcription of siRNA precursors. At CMT2 loci close to

centromeric regions, mostly long TEs, H3K9me2 is recognized by readers other than SHH1 that similarly recruit Pol IV to generate 24-nt siRNAs [21,38]. Both pathways highlight the importance of H3K9me2 methylation for 24-nt siRNA production. The 24-nt hypo- and hyper-DSRs identified in *int51* seem to correspond to the 24-nt siRNAs produced at DRM2 and CMT2 sites, respectively, raising the question whether H3K9me2 and the 24-nt DSRs of *int51* are connected, and if so, how RCD1 acts in the self-reinforcing loop between DNA methylation, H3K9me2 and 24-nt siRNAs.

First, we examined the global abundance of H3K9me2 in wild-type and *int51* seedlings by western blotting. A reduction in global H3K9me2 levels in *int51* was consistently observed in different biological replicates (Fig 3.9A), suggesting that RCD1 may contribute to H3K9me2 maintenance, although the specific loci with altered H3K9me2 remain unclear. Since H3K9me2 is highly associated with heterochromatic regions, especially long transposons and repeats, from which many *int51* 24-nt hyper-DSRs were also derived, these hyper-DSRs were expected to share a similar distribution pattern with H3K9me2 across the genome. Bioinformatic analysis revealed that 24-nt hyper-DSR loci were indeed enriched for H3K9me2 methylation, along with LTR-Gypsy TEs that were strongly associated with 24-nt hyper-DSRs (Fig 3.9B). In contrast, neither 24-nt hypo-DSR loci nor any other type of TEs were enriched for H3K9me2. However, this overlap analysis could not identify the loci at which H3K9me2 was impaired and whether the changes were due to 24-nt siRNAs at the hyper-DSR loci.

To further investigate how RCD1 may influence H3K9me2 methylation and DNA methylation, and whether the regulation is mediated by 24-nt DSRs induced by the loss of RCD1, H3K9me2 levels were analyzed in the *suvh4 suvh5 suvh6* and *drm1 drm2 cmt2 cmt3* mutants, with a specific focus on several loci related to the *int51* mutant. These

mutants were analyzed because they exhibit similar changes, including elevated 24-nt siRNA accumulation at *int51* hyper-DSR loci, decreased CHG methylation at *int51* hypo-DSR loci and globally reduced H3K9me2 methylation. In both mutants, the analysis revealed dramatic reductions in H3K9me2 at *int51* 24-nt hyper-DSR (Fig 3.10A) and LTR-Gypsy TE loci (Fig 3.10B) and increased H3K9me2 at *int51* 24-nt hypo-DSR loci (Fig 3.10C) and gene bodies (Fig 3.10D). These findings suggest dual but opposite functions of these genes in H3K9me2 maintenance at different loci across the genome. Moreover, increased 24-nt siRNA accumulation in these mutants appears to consistently correspond with decreased H3K9me2, and vice versa. The same may also be true for the *int51* mutant, but it is difficult to draw conclusions about how H3K9me2 is affected and whether H3K9me2 is regulated by 24-nt siRNAs in *int51*.

Besides H3K9me2, the global levels of several other epigenetic marks were also examined in wild-type and *int51* seedlings. No major differences were detected except for increased H3K27ac in *int51* (Fig 3.11), indicating that transcription may be reactivated at some loci, although the exact loci remain unclear. Interestingly, bioinformatic analysis of the *suvh4 suvh5 suvh6* and *drm1 drm2 cmt2 cmt3* mutants revealed opposite distributions for H3K23ac and H3K9me2. H3K23ac was enriched at *int51* 24-nt hyper-DSR and LTR-Gypsy loci in both *suvh4 suvh5 suvh6* and *drm1 drm2 cmt2 cmt3* compared to wild type (Fig 3.10A, B). Thus, H3K23ac in *int51* may also warrant further study.

Discussion

As a major cellular hub, RCD1 protein plays an essential role in diverse development and response programs in plants. Although RCD1 does not appear to exhibit PARP activity, its interaction with many diverse transcription factors underlies the RCD1-mediated regulatory network. In this study, we focused on small RNAs and epigenetic

modifications in *int51*, a loss-of-function mutant of *RCD1*. miRNA and tasiRNA accumulation and activity were normal in *int51*, indicating that the pleiotropic developmental phenotype of *rcd1* mutants is not attributable to mis-regulation of miRNAs or tasiRNAs. However, many siRNAs, especially 24-nt siRNAs, were differentially generated and formed a unique distribution pattern across the genome in *int51*: while some 24-nt siRNAs over-accumulated at pericentromeric and centromeric regions, fewer 24-nt siRNAs were produced from euchromatic regions in *int51* compared to wild type. The abnormal accumulation of 24-nt siRNAs could be due to enhanced or repressed transcription of siRNA precursors and may further affect DNA methylation, particularly on euchromatin arms via the RdDM pathway. The 24-nt siRNAs identified at both hyper- and hypo-DSR loci in *int51* were Pol IV-, RDR2- and DCL3-dependent, and only siRNAs from hypo-DSR loci appeared to regulate DNA methylation at their respective loci, resembling 24-nt siRNAs in the RdDM pathway. DNA methylation in all sequence contexts was dramatically reduced at hypo-DSR loci in *int51*, but in general, no obvious changes were observed at hyper-DSR loci. These results suggest that RCD1 may be involved in the RdDM pathway by playing a dual but opposite role at different loci. At RdDM target sites, RCD1 may function like other RdDM components and may be required for the biogenesis of 24-nt siRNAs, presumably through its interaction with some specific TFs that activate Pol IV transcription of siRNA precursors. At pericentromeric and centromeric regions, RCD1 may repress the transcription of siRNA precursors by interacting with other specific TFs at these loci.

In addition to the general components of the RdDM pathway, the biogenesis of 24-nt siRNAs also requires the H3K9me2 histone modification mark. A self-reinforcing loop involving 24-nt siRNAs, DNA methylation and H3K9me2 methylation has been proposed

at both DRM2 sites and CMT2 sites. Global H3K9me2 was greatly reduced in the *int51* mutant. Considered alongside the similar changes in H3K9me2 reported in the *suvh4 suvh5 suvh6* and *drm1 drm2 cmt2 cmt3* mutants, it is possible that RCD1 participates in the same regulatory pathways involving these genes. Besides the similar impairment in H3K9me2, *int51* has other changes in common with these mutants, including enhanced enrichment of 24-nt siRNAs at *int51* hyper-DSR loci and decreased DNA methylation at *int51* hypo-DSR loci, further supporting our hypothesis proposed above. The specific loci at which H3K9me2 is affected in *int51* remain unclear, but ChIP-seq analysis will provide more information in this regard. The decreased level of the repressive mark H3K9me2 implies an up-regulation or reactivation of at least at some loci, if not genome-wide, in the *int51* mutant. Moreover, the global level of H3K27ac was elevated in *int51*, and H3K23ac may be another potential up-regulated active mark based on the analysis of *suvh4 suvh5 suvh6* and *drm1 drm2 cmt2 cmt3* mutants.

One interesting finding was the strong association of 24-nt siRNAs from *int51* hyper-DSR loci with LTR-Gypsy TEs, which are predominantly located at pericentromeric regions. Few functions of LTR-Gypsy TEs have been reported thus far, but some studies have linked them to organelles including chloroplasts and mitochondria [42,43], which possess their own genomes and communicate with the nucleus through retrograde signaling. Many stresses, such as high light, salinity and UV-B, trigger retrograde signaling, leading to the repression of genes required for normal growth and development and the activation of stress-response genes. As a result, affected plants exhibit abnormal morphological phenotypes and undergo leaf senescence or programed cell death, similar to the *rcd1* mutant phenotype. Previous yeast two-hybrid (Y2H) screening identified NAC013 as an RCD1-interacting partner [2], and it was later shown to function in

mitochondrial retrograde regulation under oxidative stress [44]. In addition, a recent study using a mutant of the nuclear-encoded organelle-targeted gene *MutS Homolog 1* (*MSH1*) identified thousands of down-regulated 24-nt siRNA clusters located at pericentromeric regions and up-regulated 24-nt siRNA clusters from euchromatic regions [45]. The down-regulated 24-nt siRNAs in *msh1* mainly derived from LTR-Gypsy TEs [45], which is opposite to our observations in *int51*. Nevertheless, the defective developmental phenotypes of the *msh1* mutant [46], such as dwarfism, altered leaf shape and delayed flowering, together with the altered CG methylation in the mutant [47], further suggest a connection between RCD1 and mitochondrial function.

Materials and Methods

Plant materials and growth conditions

The mutants used in this study are all in the Col background. *int51* harbors a point mutation in *RCD1* that causes a premature stop codon. Double mutants were generated by crossing *int51* with RdDM mutants including *sde4-3* (*pol4*) (SALK_128428) [48], *rdr2-1* (SAIL_1277_H08), *dcl3-1* (SALK_005512) [49], *nrpe1-11* (*pol5*) (SALK_029919) [50] and *ago4* (SALK_071772). The plant materials used in this study were 13-day-old seedlings or inflorescences from plants grown at 22°C under long day (16 h light/8 h darkness) conditions.

RNA extraction and RNA analysis

Total RNA was extracted from seedlings or inflorescences using TRI Reagent (TR 118, Molecular Research Center, Inc.). Northern blotting to detect small RNAs was performed as previously described [51]. Five microgram of total RNA was used for each miRNA or tasiRNA northern blot. For each siRNA locus, 30 µg small RNA, enriched from total RNA using 50% PEG8000 and 5M NaCl, was used. Antisense DNA oligonucleotides

were 5'-end labeled with γ32P-ATP to detect miRNAs or tasiRNAs. DNA fragments amplified from genomic DNA using primers targeting siRNA loci were randomly labeled with α^{32}P-dCTP to detect siRNAs. For the detection of miRNA or tasiRNA target transcripts, reverse transcription was performed with oligo d(T), and real-time PCR was performed as previously described [52] with primers corresponding to each target gene. *UBQ5* was used as an internal control. All oligonucleotides are listed in Table 3.2.

Small RNA library construction and bioinformatic analysis

Small RNA libraries were constructed as previously described [53]. Briefly, small RNA fragments around 15-40 nt were recovered from 15 μg total RNA by 15% urea-polyacrylamide gel electrophoresis, and 3' and 5' adapters were sequentially ligated according to the manufacturer's instructions for the NEBNext Small RNA Library Prep kit. Reverse transcription was performed, followed by a 14-cycle PCR reaction to obtain sufficient double-stranded DNA products for deep sequencing. The libraries were barcoded in one lane and sequenced on an Illumina HiSeq 2000 at the UCR Institute for Integrative Genome Biology (IIGB) Genomic Core Facility.

Western blotting

Thirteen-day-old seedlings were ground in liquid nitrogen and the powder was boiled in 1×SDS protein sample buffer for 5 min. Proteins were resolved in 12% (wt/vol) SDS/PAGE gels and transferred onto nitrocellulose membranes (Bio-Rad). After blocking in TBST buffer with 5% (wt/vol) nonfat milk for 1 h, the membranes were probed with anti-H3K9me2 (Abcam), anti-H3K27ac (Abcam), anti-H3 (Sigma-Aldrich), anti-H3K9ac (Abcam), anti-H3K4me3 (Abcam), anti-H3K27me (Millipore), anti-H2AZ (Abcam) and anti-H2AXS139P (Sigma-Aldrich) in TBST. HSC70 (Enzo Life Sciences) was used as an internal control.

McrBC treatment and BS-seq library construction

McrBc treatment was performed as described [54]. For McrBC-treated samples, 400 ng genomic DNA was digested by McrBC (New England Biolabs) at 37°C for 30 min in a 20 µl reaction system. The same procedure was used for the untreated negative control samples but without McrBC. For PCR, 1 µl of both digested and undigested genomic DNA were used as the templates to amplify the genomic regions corresponding to *int51* hyper-DSR loci. *At2g19920* was used as an unmethylated internal control. Primers for the amplification of genomic regions are listed in Table 3.2.

To construct whole genome bisulfate sequencing libraries, genomic DNA was extracted from the seedlings of Col and *int51* using the DNeasy Plant Mini Kit (Qiagen, Cat# 69104). 1 µg of genomic DNA was sonicated into 150~300 bp using the Diagenode Bioruptor, fragmented DNA was purified by PureLink® PCR Purification Kit (Life Sciences) and end-repaired using the End-It kit (Epicentre). After purification with Agencourt AMPure XP beads (Beckman Coulter), end-repaired DNA was adenylated with dATP using Klenow 3'-5' exo- (New England Biolabs) followed by purification with Agencourt AMPure XP beads. The purified DNA was ligated with genomic DNA adapters from Illumina Kit A (Illumina) using T4 DNA Ligase (New England Biolabs) and ligation products were purified with AMPure XP beads. Less than 400ng ligation product was subjected to bisulfite conversion using the MethylCode Kit (Invitrogen) following the manufacturer's instructions. PCR was then performed using PfuTurbo Cx Hotstart DNA Polymerase (Agilent, Cat# 600414) and PCR products were purified using AMPure XP beads. The final BS-seq libraries were barcoded and sequenced on an Illumina HiSeq 2000 at the UCR Institute for Integrative Genome Biology (IIGB) Genomic Core Facility.

Bioinformatic analysis

For small RNA-seq, raw reads were processed by first trimming 3' adapter sequence using custom Perl script. Reads without 3' adapter sequence or less than 18 nucleotides after trimming were discarded from further analysis. Trimmed reads were aligned against a custom database containing rRNA, tRNA, snoRNA, and snRNAs using Bowtie 0.12.8 [55] to filter out rRNA reads. Non-aligned reads were subsequently aligned to the *Arabidopsis* genome (TAIR10) using Bowtie 0.12.8. Genome-aligned reads were used for all downstream analysis. To identify differential small RNA regions (DSRs), the genome was first divided into 100bp bins. Small RNA reads in each bin were counted by size. To avoid over-counting reads overlapping two bins, we assigned the read based to the bin based on the 5' nucleotide position. Differentially enriched bins were calculated using the EdgeR package [56] with a corrected p-value < 0.05 and a fold-enrichment ≥ 2.

For BS-seq, read sequences were aligned to a reference genome using the BS Seeker program [57] allowing for up to two mismatches. The reference genome of TAIR10 Col consisted of 5 chromosomes, mitochondrion and chloroplast genomes. In addition, the 48,502 bp cI857 Sam7 Lambda genome (NC_001416) [58], and the 5,386 bp ϕ-X174 (PhiX) genome (NC_001422) [59] were used to map reads from the spiked-in Lambda and PhiX controls. Only reads that mapped uniquely to the reference genome were retained for further analysis. The BS-Seeker output was subjected to post-processing that consisted of two steps: (1) To reduce PCR amplification bias for each library, clonal reads (i.e. reads containing identical 5' mapped position and exact nucleotide sequence) were collapsed and all but one read was retained; (2) Reads containing three or more consecutive cytosines in the CHH context, that are likely not bisulfite converted [60], were removed. For each cytosine site in the reference genome, the total number of reads

identified as C (representing a methylated cytosine) and T (representing an unmethylated cytosine) were summarized using custom scripts. Cytosine sites with at least five mapped reads were used for downstream analysis.

Histone methylation raw data were downloaded from the NCBI Gene Expression Omnibus (GEO) site (http://ncbi.nlm.nih.gov/geo). H3K9me2 data came from geo series GSE51304 [38]. Reads were aligned to the TAIR 10 genome with Bowtie [55], allowing up to two mismatches and only uniquely mapped reads were kept for downstream analysis. Meta-analysis plots were generated using SeqPlots [61].

References

1. Ahlfors R, Lång S, Overmyer K, Jaspers P, Brosché M, et al. (2004) *Arabidopsis* RADICAL-INDUCED CELL DEATH1 belongs to the WWE protein–protein interaction domain protein family and modulates abscisic acid, ethylene, and methyl jasmonate responses. Plant Cell 16: 1925.

2. Jaspers P, Blomster T, Brosché M, Salojärvi J, Ahlfors R, et al. (2009) Unequally redundant RCD1 and SRO1 mediate stress and developmental responses and interact with transcription factors. Plant J 60: 268-279.

3. Teotia S, Lamb RS (2011) RCD1 and SRO1 are necessary to maintain meristematic fate in *Arabidopsis thaliana*. J Exp Bot 62: 1271-1284.

4. Jaspers P, Brosché M, Overmyer K, Kangasjärvi J (2010) The transcription factor interacting protein RCD1 contains a novel conserved domain. Plant Signal Behav 5: 78-80.

5. Zhu Y, Du B, Qian J, Zou B, Hua J (2013) Disease resistance gene-Induced growth inhibition is enhanced by *rcd1* independent of defense activation in *Arabidopsis*. Plant Physiol 161: 2005.

6. Overmyer K, Tuominen H, Kettunen R, Betz C, Langebartels C, et al. (2000) Ozone-sensitive *Arabidopsis rcd1* mutant reveals opposite roles for ethylene and jasmonate signaling pathways in regulating superoxide-dependent cell death. Plant Cell 12: 1849.

7. Katiyar-Agarwal S, Zhu J, Kim K, Agarwal M, Fu X, et al. (2006) The plasma membrane Na+/H+ antiporter SOS1 interacts with RCD1 and functions in oxidative stress tolerance in *Arabidopsis*. Proc Natl Acad Sci U S A 103: 18816-18821.

8. Teotia S, Lamb RS (2009) The Paralogous Genes *RADICAL-INDUCED CELL DEATH1* and *SIMILAR TO RCD ONE1* have partially redundant functions during *Arabidopsis* development. Plant Physiol 151: 180-198.

9. Fujibe T, Saji H, Arakawa K, Yabe N, Takeuchi Y, et al. (2004) A methyl viologen-resistant mutant of *Arabidopsis*, which is allelic to ozone-sensitive *rcd1* is tolerant to supplemental ultraviolet-B irradiation. Plant Physiol 134: 275.

10. Morales LO, BroschÉ M, Vainonen JP, Sipari N, Lindfors AV, et al. (2015) Are solar UV-B- and UV-A-dependent gene expression and metabolite accumulation in *Arabidopsis* mediated by the stress response regulator RADICAL-INDUCED CELL DEATH1? Plant Cell Environ 38: 878-891.

11. Vainonen Julia P, Jaspers P, Wrzaczek M, Lamminmäki A, Reddy Ramesha A, et al. (2012) RCD1–DREB2A interaction in leaf senescence and stress responses in *Arabidopsis thaliana*. Biochem J 442: 573.

12. Morimoto K, Mizoi J, Qin F, Kim J-S, Sato H, et al. (2013) Stabilization of *Arabidopsis* DREB2A is required but not sufficient for the induction of target genes under conditions of stress. PLoS ONE 8: e80457.

13. Overmyer K, Brosché M, Pellinen R, Kuittinen T, Tuominen H, et al. (2005) Ozone-Induced Programmed Cell Death in the *Arabidopsis radical-induced cell death1* Mutant. Plant Physiol 137: 1092.

14. Aravind L (2001) The WWE domain: a common interaction module in protein ubiquitination and ADP ribosylation. Trends Biochem Sci 26: 273-275.

15. Jaspers P, Overmyer K, Wrzaczek M, Vainonen JP, Blomster T, et al. (2010) The RST and PARP-like domain containing SRO protein family: analysis of protein structure, function and conservation in land plants. BMC Genomics 11: 170.

16. Briggs AG, Bent AF (2011) Poly(ADP-ribosyl)ation in plants. Trends Plant Sci 16: 372-380.

17. Riechmann JL, Meyerowitz EM (1998) The AP2/EREBP family of plant transcription factors. Biol chem 379: 633-646.

18. Song C-P, Agarwal M, Ohta M, Guo Y, Halfter U, et al. (2005) Role of an *Arabidopsis* AP2/EREBP-type transcriptional repressor in abscisic acid and drought stress responses. Plant Cell 17: 2384-2396.

19. Dietz KJ, Vogel MO, Viehhauser A (2010) AP2/EREBP transcription factors are part of gene regulatory networks and integrate metabolic, hormonal and environmental signals in stress acclimation and retrograde signalling. Protoplasma 245: 3-14.

20. Law JA, Jacobsen SE (2010) Establishing, maintaining and modifying DNA methylation patterns in plants and animals. Nat Rev Genet 11: 204-220.

21. Du J, Johnson LM, Jacobsen SE, Patel DJ (2015) DNA methylation pathways and their crosstalk with histone methylation. Nat Rev Mol Cell Biol 16: 519-532.

22. Choy M-K, Movassagh M, Goh H-G, Bennett MR, Down TA, et al. (2010) Genome-wide conserved consensus transcription factor binding motifs are hyper-methylated. BMC Genomics 11: 519.

23. Bannister AJ, Kouzarides T (2011) Regulation of chromatin by histone modifications. Cell Res 21: 381-395.

24. Cokus SJ, Feng S, Zhang X, Chen Z, Merriman B, et al. (2008) Shotgun bisulphite sequencing of the *Arabidopsis* genome reveals DNA methylation patterning. Nature 452: 215-219.

25. Lister R, O'Malley RC, Tonti-Filippini J, Gregory BD, Berry CC, et al. (2008) Highly integrated single-base resolution maps of the epigenome in *Arabidopsis*. Cell 133: 523-536.

26. Finnegan EJ, Dennis ES (1993) Isolation and identification by sequence homology of a putative cytosine methyltransferase from *Arabidopsis thaliana*. Nucleic Acids Res 21: 2383-2388.

27. Finnegan EJ, Peacock WJ, Dennis ES (1996) Reduced DNA methylation in *Arabidopsis thaliana* results in abnormal plant development. Proc Natl Acad Sci U S A 93: 8449-8454.

28. Bartee L, Malagnac F, Bender J (2001) *Arabidopsis* cmt3 chromomethylase mutations block non-CG methylation and silencing of an endogenous gene. Genes Dev 15: 1753-1758.

29. Lindroth AM, Cao X, Jackson JP, Zilberman D, McCallum CM, et al. (2001) Requirement of CHROMOMETHYLASE3 for maintenance of CpXpG methylation. Science 292: 2077-2080.

30. Bernatavichute YV, Zhang X, Cokus S, Pellegrini M, Jacobsen SE (2008) Genome-wide association of histone H3 lysine nine methylation with CHG DNA methylation in *Arabidopsis thaliana*. PLoS ONE 3: e3156.

31. Jackson JP, Lindroth AM, Cao X, Jacobsen SE (2002) Control of CpNpG DNA methylation by the KRYPTONITE histone H3 methyltransferase. Nature 416: 556-560.

32. Jackson JP, Johnson L, Jasencakova Z, Zhang X, PerezBurgos L, et al. (2004) Dimethylation of histone H3 lysine 9 is a critical mark for DNA methylation and gene silencing in *Arabidopsis thaliana*. Chromosoma 112: 308-315.

33. Ebbs ML, Bender J (2006) Locus-Specific Control of DNA methylation by the *Arabidopsis* SUVH5 histone methyltransferase. Plant Cell 18: 1166.

34. Chen X (2005) MicroRNA biogenesis and function in plants. FEBS Lett 579: 5923-5931.

35. Chen X (2009) Small RNAs and their roles in plant development. Annu Rev Cell Dev Biol 25: 21-44.

36. Marin E, Jouannet V, Herz A, Lokerse AS, Weijers D, et al. (2010) miR390, *Arabidopsis* TAS3 tasiRNAs, and their AUXIN RESPONSE FACTOR targets define an autoregulatory network quantitatively regulating lateral root growth. Plant Cell 22: 1104-1117.

37. Zemach A, Kim MY, Hsieh P-H, Coleman-Derr D, Eshed-Williams L, et al. (2013) The nucleosome remodeler DDM1 allows DNA methyltransferases to access H1-containing heterochromatin. Cell 153: 193-205.

38. Stroud H, Do T, Du J, Zhong X, Feng S, et al. (2014) Non-CG methylation patterns shape the epigenetic landscape in *Arabidopsis*. Nat Struct Mol Biol 21: 64-72.

39. Soppe WJJ, Jasencakova Z, Houben A, Kakutani T, Meister A, et al. (2002) DNA methylation controls histone H3 lysine 9 methylation and heterochromatin assembly in *Arabidopsis*. EMBO J 21: 6549-6559.

40. Zemach A, Li Y, Wayburn B, Ben-Meir H, Kiss V, et al. (2005) DDM1 binds *Arabidopsis* methyl-CpG binding domain proteins and affects their subnuclear localization. Plant Cell 17: 1549.

41. Du J, Zhong X, Bernatavichute Yana V, Stroud H, Feng S, et al. (2012) Dual binding of chromomethylase domains to H3K9me2-containing nucleosomes directs DNA methylation in plants. Cell 151: 167-180.

42. Knoop V, Unseld M, Marienfeld J, Brandt P, Sünkel S, et al. (1996) copia-, gypsy- and LINE-like retrotransposon fragments in the mitochondrial genome of *Arabidopsis thaliana*. Genetics 142: 579.

43. Liu Y, Zhang W, Zhang K, You Q, Yan H, et al. (2017) Genome-wide mapping of DNase I hypersensitive sites reveals chromatin accessibility changes in *Arabidopsis* euchromatin and heterochromatin regions under extended darkness. Sci Rep 7: 4093.

44. De Clercq I, Vermeirssen V, Van Aken O, Vandepoele K, Murcha MW, et al. (2013) The membrane-bound NAC transcription factor ANAC013 functions in mitochondrial retrograde regulation of the oxidative stress response in *Arabidopsis*. Plant Cell 25: 3472.

45. Shao MR, Kumar Kenchanmane Raju S, Laurie JD, Sanchez R, Mackenzie SA (2017) Stress-responsive pathways and small RNA changes distinguish variable developmental phenotypes caused by *MSH1* loss. BMC Plant Biol 17: 47.

46. Virdi KS, Wamboldt Y, Kundariya H, Laurie JD, Keren I, et al. (2016) MSH1 is a plant organellar DNA binding and thylakoid protein under precise spatial regulation to alter development. Mol Plant 9: 245-260.

47. Virdi KS, Laurie JD, Xu YZ, Yu J, Shao MR, et al. (2015) *Arabidopsis MSH1* mutation alters the epigenome and produces heritable changes in plant growth. Nat Commun 6: 6386.

48. Herr AJ, Jensen MB, Dalmay T, Baulcombe DC (2005) RNA Polymerase IV directs silencing of endogenous DNA. Science 308: 118-120.

49. Xie Z, Johansen LK, Gustafson AM, Kasschau KD, Lellis AD, et al. (2004) Genetic and functional diversification of small RNA pathways in plants. PLoS Biol 2: e104.

50. Pontier D, Yahubyan G, Vega D, Bulski A, Saez-Vasquez J, et al. (2005) Reinforcement of silencing at transposons and highly repeated sequences requires the concerted action of two distinct RNA polymerases IV in *Arabidopsis*. Genes Dev 19: 2030-2040.

51. Kurihara Y, Takashi Y, Watanabe Y (2006) The interaction between DCL1 and HYL1 is important for efficient and precise processing of pri-miRNA in plant microRNA biogenesis. RNA 12: 206-212.

52. Li S, Liu L, Zhuang X, Yu Y, Liu X, et al. (2013) MicroRNAs inhibit the translation of target mRNAs on the endoplasmic reticulum in *Arabidopsis*. Cell 153: 562-574.

53. Yu Y, Ji L, Le BH, Zhai J, Chen J, et al. (2017) ARGONAUTE10 promotes the degradation of miR165/6 through the SDN1 and SDN2 exonucleases in *Arabidopsis*. PLoS Biol 15: e2001272.

54. Dinh TT, O'Leary M, Won SY, Li S, Arroyo L, et al. (2013) Generation of a luciferase-based reporter for CHH and CG DNA methylation in *Arabidopsis thaliana*. Silence 4: 1-1.

55. Langmead B, Trapnell C, Pop M, Salzberg SL (2009) Ultrafast and memory-efficient alignment of short DNA sequences to the human genome. Genome Biol 10: R25.

56. Robinson MD, McCarthy DJ, Smyth GK (2010) edgeR: a Bioconductor package for differential expression analysis of digital gene expression data. Bioinformatics 26: 139-140.

57. Chen P-Y, Cokus SJ, Pellegrini M (2010) BS Seeker: precise mapping for bisulfite sequencing. BMC Bioinformatics 11: 203.

58. Sanger F, Coulson AR, Hong GF, Hill DF, Petersen GB (1982) Nucleotide sequence of bacteriophage lambda DNA. J Mol Biol 162: 729-773.

59. Sanger F, Air GM, Barrell BG, Brown NL, Coulson AR, et al. (1977) Nucleotide sequence of bacteriophage phi X174 DNA. Nature 265: 687-695.

60. Cokus SJ, Feng S, Zhang X, Chen Z, Merriman B, et al. (2008) Shotgun bisulphite sequencing of the *Arabidopsis* genome reveals DNA methylation patterning. Nature 452: 215-219.

61. Stempor P, Ahringer J (2016) SeqPlots - Interactive software for exploratory data analyses, pattern discovery and visualization in genomics. Wellcome Open Res 1:14.

Figures and Tables

Fig 3.1 Loss of *RCD1* does not affect the abundance or activity of miRNAs and tasiRNAs.

(A) The levels of several miRNAs and tasiRNAs in seedlings of wild type (Col) and the *int51* mutant as determined by northern blotting. Three biological repeats were included. U6 served as an internal control, and the numbers indicated the abundance of the miRNAs or tasiRNAs in *int51* relative to wild type. No change of miRNA or tasiRNA abundance was observed in *int51*. (B) Semi-quantitative RT-PCR to determine the transcript levels of miRNA and tasiRNA targets in wild type and *int51*. *UBQ5* was used as an internal control.

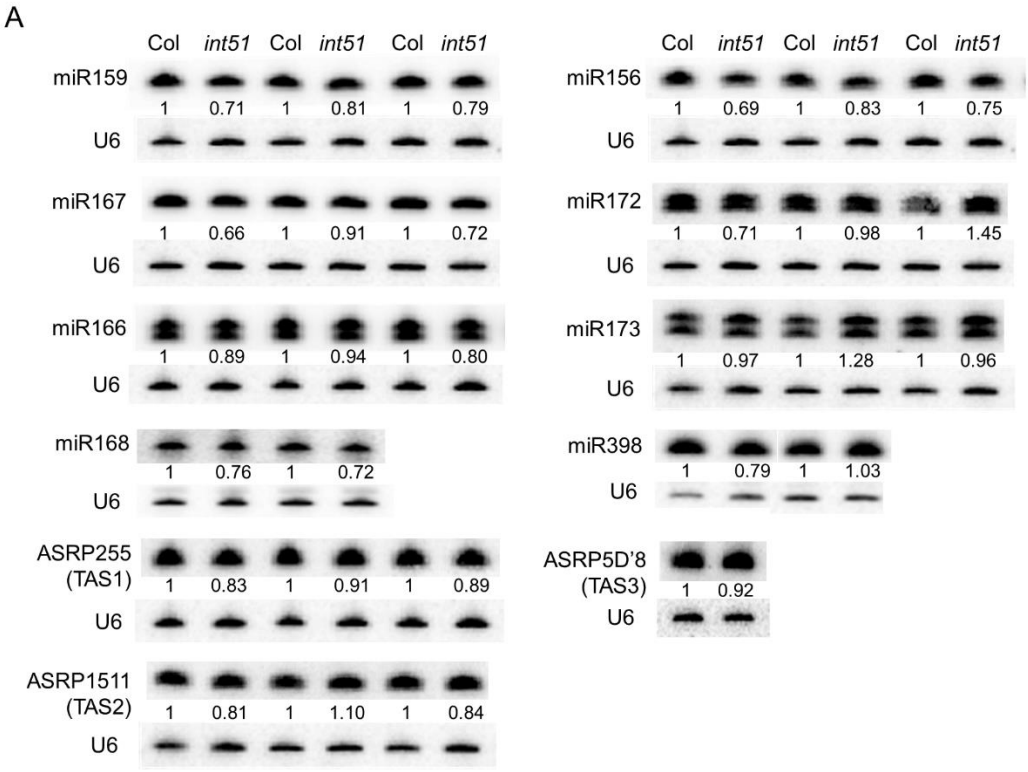
A
Col
int51
miR159
1 0.71 1 0.81 1 0.79
U6
miR167
1 0.66 1 0.91 1 0.72
U6
miR166
1 0.89 1 0.94 1 0.80
U6
miR168
1 0.76 1 0.72
U6
ASRP255 (TAS1)
1 0.83 1 0.91 1 0.89
U6
ASRP1511 (TAS2)
1 0.81 1 1.10 1 0.84
U6
miR156
1 0.69 1 0.83 1 0.75
U6
miR172
1 0.71 1 0.98 1 1.45
U6
miR173
1 0.97 1 1.28 1 0.96
U6
miR398
1 0.79 1 1.03
U6
ASRP5D'8 (TAS3)
1 0.92
U6

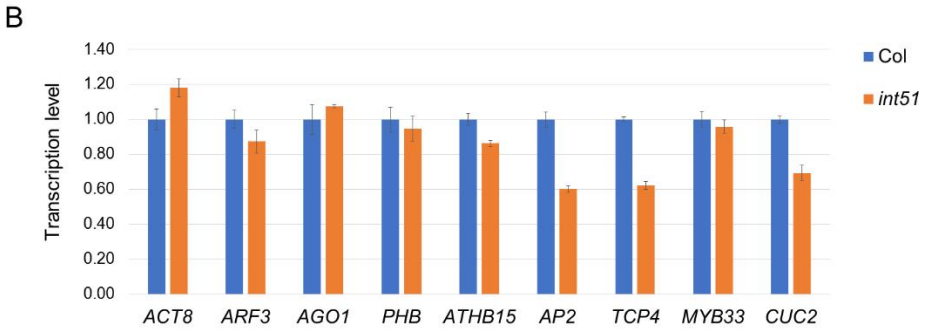
B
Transcription level
1.40
1.20
1.00
0.80
0.60
0.40
0.20
0.00
Col
int51
ACT8
ARF3
AGO1
PHB
ATHB15
AP2
TCP4
MYB33
CUC2

Fig 3.2 Loss of *RCD1* induces differential expression of siRNAs across the genome. (A) Genome-wide distribution of DSR loci in different sizes identified in the *int51* mutant. *int51* hyper-DSRs (red) are loci generating more siRNAs in *int51* than wild type (Col), *int51* hypo-DSRs (blue) are loci producing less siRNAs in *int51* than wild type (Col). Triangle (black) represents the position of centromere. *int51* hyper-DSRs are predominantly located to pericentromeric and centromeric regions, while hypo-DSRs spread throughout the euchromatic arms. Consistent distribution patterns were observed in both seedlings and inflorescences. (B) Northern blotting to validate the DSRs in inflorescences from wild type (Col) and *int51*. U6 served as an internal control, and the numbers indicated the abundance of the siRNAs in *int51* relative to wild type (Col). All the interrogated DSRs were validated.

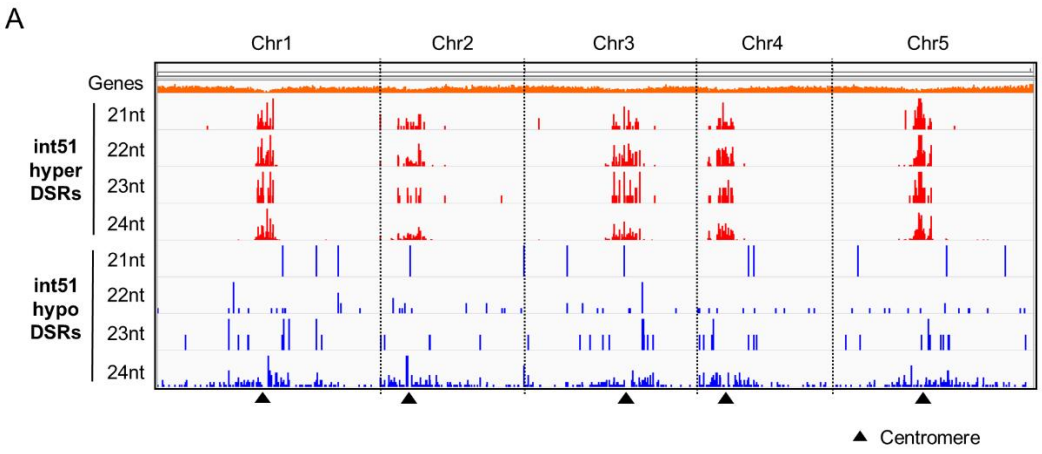
A
Chr1
Chr2
Chr3
Chr4
Chr5
Genes
int51 hyper DSRs
21nt
22nt
23nt
24nt
int51 hypo DSRs
21nt
22nt
23nt
24nt
Centromere

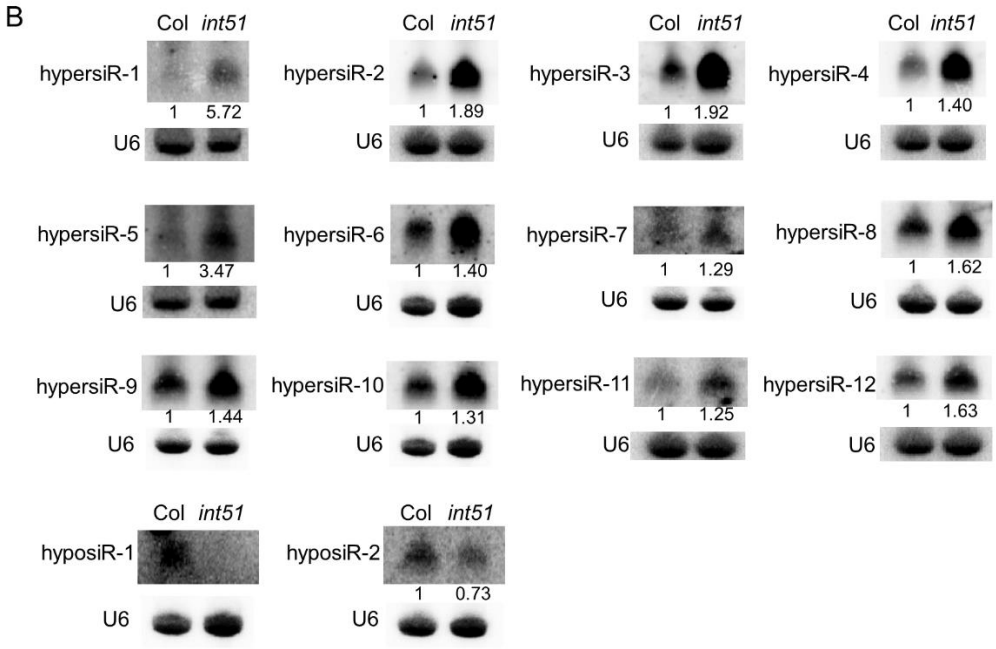
B
Col int51
hypersiR-1
1 5.72
U6
hypersiR-2
1 1.89
hypersiR-3
1 1.92
hypersiR-4
1 1.40
hypersiR-5
1 3.47
hypersiR-6
1 1.40
hypersiR-7
1 1.29
hypersiR-8
1 1.62
hypersiR-9
1 1.44
hypersiR-10
1 1.31
hypersiR-11
1 1.25
hypersiR-12
1 1.63
hyposiR-1
hyposiR-2
1 0.73

Fig 3.3 24-nt hyper-DSRs are mainly LTR-Gypsy TEs localized in the pericentromeric region.

(A) Genome-wide features of *int51* hyper- and hypo-DSRs. Features associated with hyper- and hypo-DSR loci were analyzed and the relative percentage of the features was calculated for each group of DSRs based on size differences. The X-axis represents the 8 groups of DSR loci, the Y-axis represents the relative percentage of features associated with the DSR loci. Around 90% of the hyper-DSR loci were TEs, and the features associated with hypo-DSR loci were diverse. (B) TE features associated with 24-nt *int51* hyper- and hypo-DSRs. The percentage of each type of TEs was calculated for 24-nt hyper- and hypo-DSRs, and the genome-wide TE distribution was used as a reference. The Y-axis represents the relative percentage of each type of TEs associated with the DSR loci. 24-nt hyper-DSRs are enriched for LTR-Gypsy TE family, and hypo-DSRs resemble the pattern of the control. (C) Genome-wide distribution of each type of TEs. Gene distribution was used as a reference. LTR/Gypsy TEs are localized in the centromere.

A

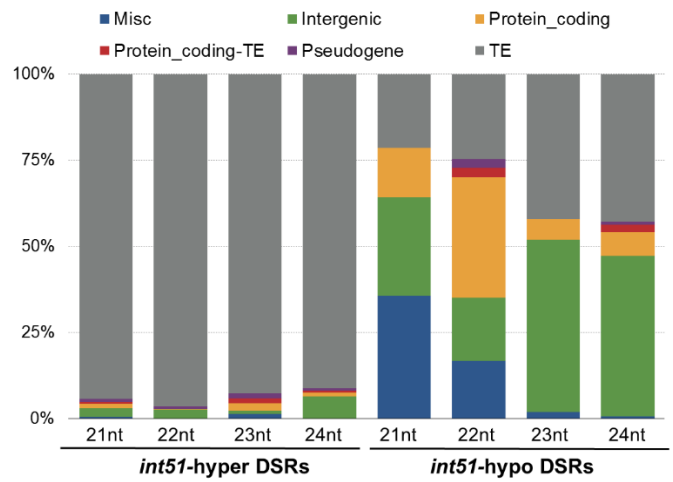
Misc
Intergenic
Protein_coding
Protein_coding-TE
Pseudogene
TE
100%
75%
50%
25%
0%
21nt
22nt
23nt
24nt
21nt
22nt
23nt
24nt
int51-hyper DSRs
int51-hypo DSRs

B

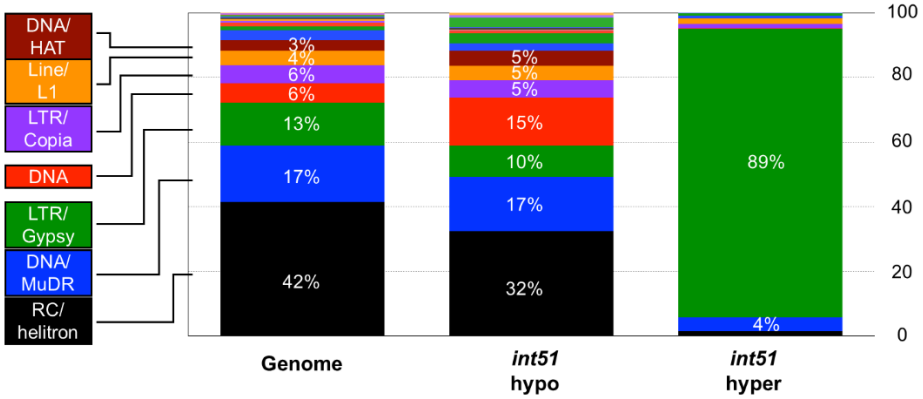
DNA/ HAT
Line/ L1
LTR/ Copia
DNA
LTR/ Gypsy
DNA/ MuDR
RC/ helitron
3%
4%
6%
6%
13%
17%
42%
5%
5%
5%
15%
10%
17%
32%
89%
4%
100
80
60
40
20
0
Genome
int51 hypo
int51 hyper

C

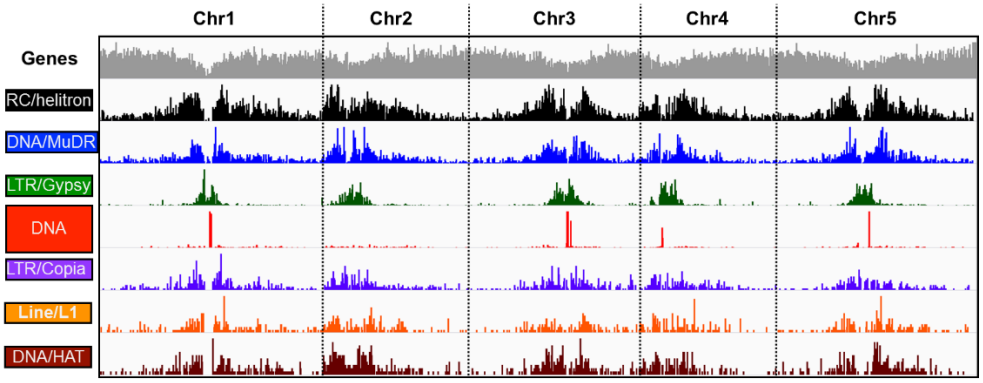
Chr1
Chr2
Chr3
Chr4
Chr5
Genes
RC/helitron
DNA/MuDR
LTR/Gypsy
DNA
LTR/Copia
Line/L1
DNA/HAT

Fig 3.4 The accumulation of 24-nt siRNAs within specific genomic locations.

Several specific genomic locations associated with the 24-nt DSRs were analyzed for 24-nt siRNA accumulation. The same relative length from the transcription start site (Start) to the transcription termination site (End) was assigned to each locus. 1 kb regions from both upstream of Start and downstream of End were used as the control. The Y-axis represents relative small RNA abundance. The loci are indicated below the black bar. (A) 24-nt siRNA accumulation at protein-coding genes. An overall reduction of 24-nt siRNA abundance was observed along gene bodies in *int51*. (B) 24-nt siRNA accumulation at repeat loci. 24-nt siRNAs were reduced in *int51* at all three types of repeat loci. (C) 24-nt siRNA accumulation at each DSR locus. The siRNAs at hypo-DSR loci were generally present at a higher level in wild type (Col) than in *int51* throughout a given DSR locus, whereas only some specific regions within hyper-DSR loci generated more siRNAs than other regions.

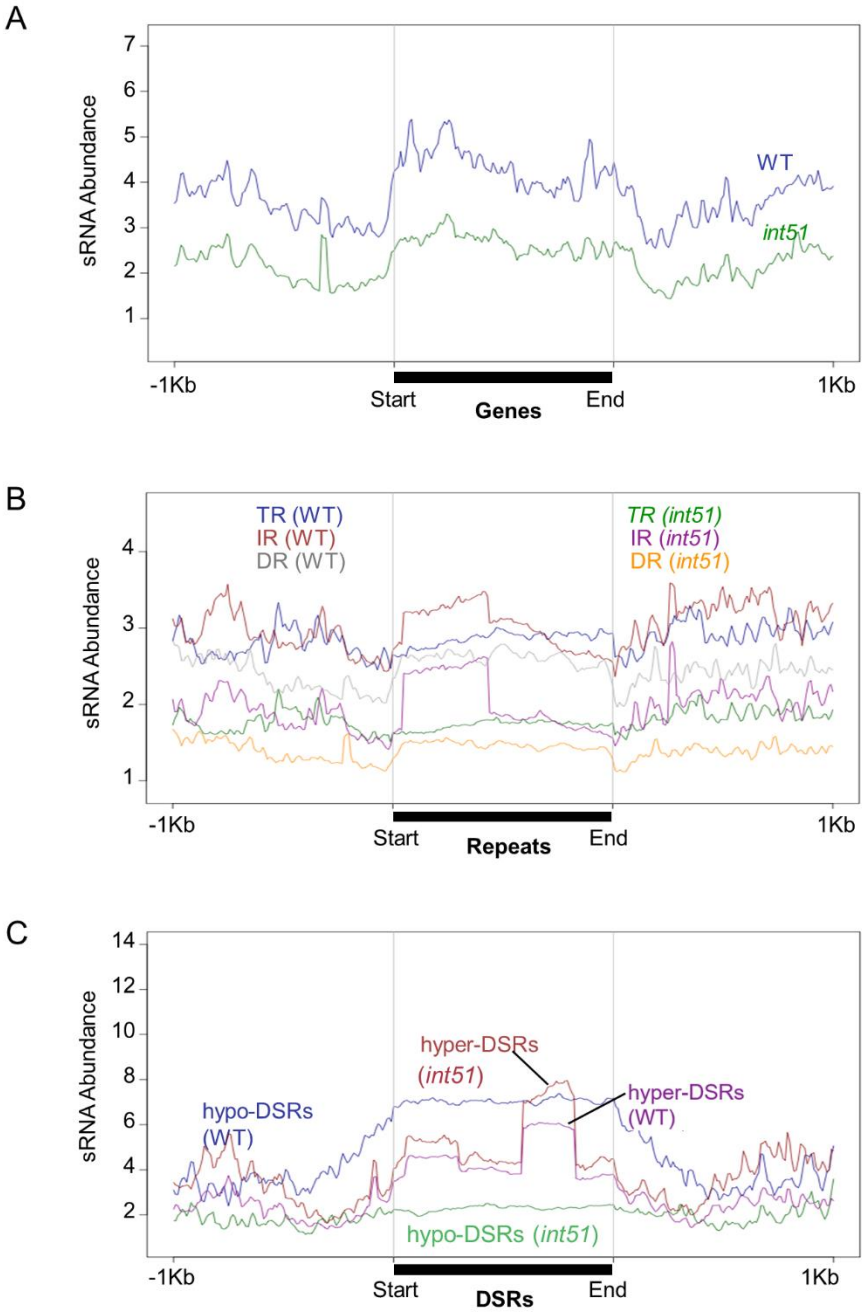
A
sRNA Abundance
7
6
5
4
3
2
1
WT
int51
-1Kb
Start
Genes
End
1Kb
B
sRNA Abundance
4
3
2
1
TR (WT)
IR (WT)
DR (WT)
TR (int51)
IR (int51)
DR (int51)
-1Kb
Start
Repeats
End
1Kb
C
sRNA Abundance
14
12
10
8
6
4
2
hyper-DSRs
(int51)
hyper-DSRs
(WT)
hypo-DSRs
(WT)
hypo-DSRs (int51)
-1Kb
Start
DSRs
End
1Kb

Fig 3.5 The biogenesis of 24-nt siRNAs at *int51* hyper-DSR loci requires components of diverse pathways.

The accumulation of 24-nt siRNAs at *int51* hyper-DSR loci was analyzed in various mutants by utilizing published small RNA-seq datasets. The X-axis lists the genotypes analyzed, the Y-axis refers to the normalized read count representing relative small RNA abundance. The abundance of 24-nt siRNAs was decreased in RdDM mutants (A), such as *pol4*, *dcl3* and *rdr2*, but was increased in the mutants defective in DNA methylation and H3K9me2 methylation (B), including *ddm1*, *drm1 drm2 cmt2 cmt3*, *drm1 drm2 cmt3* and *suvh4 suvh5 suvh6*.

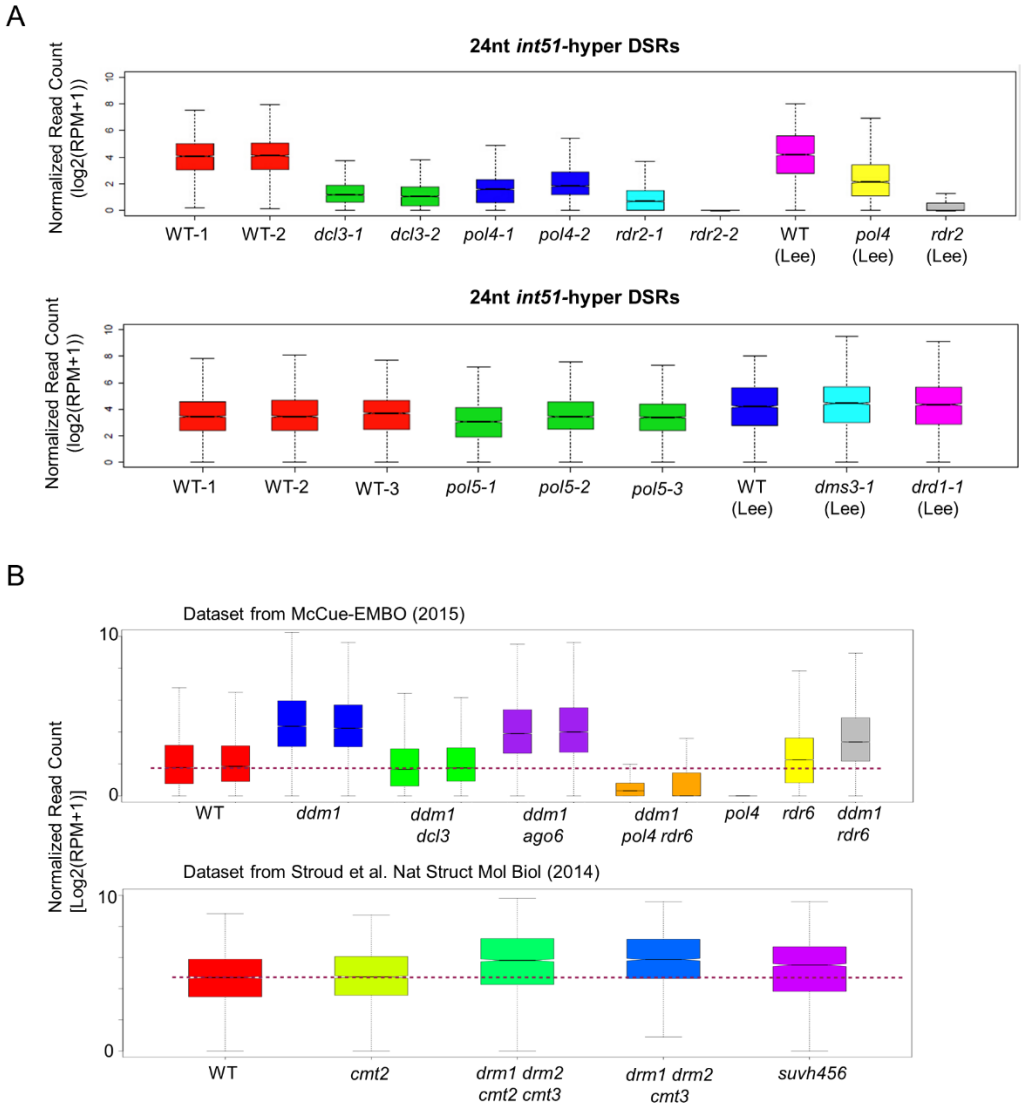
A
24nt int51-hyper DSRs
Normalized Read Count (log2(RPM+1))
WT-1
WT-2
dcl3-1
dcl3-2
pol4-1
pol4-2
rdr2-1
rdr2-2
WT (Lee)
pol4 (Lee)
rdr2 (Lee)
24nt int51-hyper DSRs
Normalized Read Count (log2(RPM+1))
WT-1
WT-2
WT-3
pol5-1
pol5-2
pol5-3
WT (Lee)
dms3-1 (Lee)
drd1-1 (Lee)
B
Dataset from McCue-EMBO (2015)
Normalized Read Count [Log2(RPM+1)]
WT
ddm1
ddm1 dcl3
ddm1 ago6
ddm1 pol4 rdr6
pol4
rdr6
ddm1 rdr6
Dataset from Stroud et al. Nat Struct Mol Biol (2014)
WT
cmt2
drm1 drm2 cmt2 cmt3
drm1 drm2 cmt3
suvh456

Fig 3.6 The biogenesis of 24-nt siRNAs at hyper-DSR loci requires components of the RdDM pathway.

Northern blotting to validate the 24-nt hyper-DSRs in inflorescences from wild type (Col), *int51* and RdDM pathway mutants. U6 served as an internal control, and the numbers indicats the abundance of siRNAs in *int51* and RdDM mutants relative to wild type (Col). The accumulation of 24-nt hyper-DSRs was reduced in single mutants of *pol4*, *dcl3* and *rdr2* (A), and double mutants of *int51 dcl3* (B).

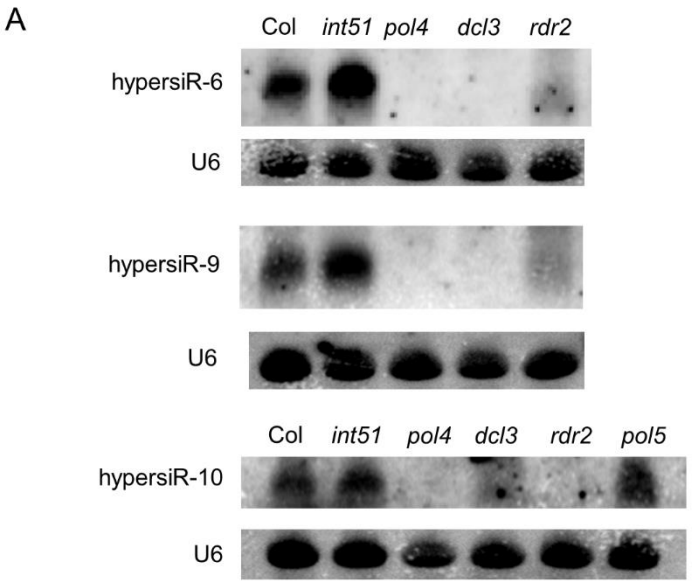
A
Col
int51
pol4
dcl3
rdr2
hypersiR-6
U6
hypersiR-9
U6
Col
int51
pol4
dcl3
rdr2
pol5
hypersiR-10
U6

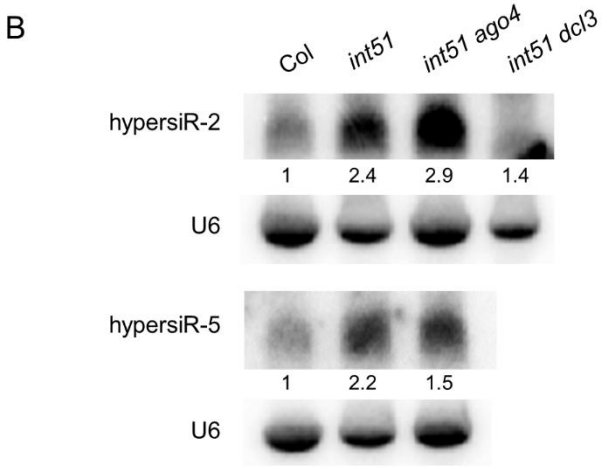
B
Col
int51
int51 ago4
int51 dcl3
hypersiR-2
1
2.4
2.9
1.4
U6
hypersiR-5
1
2.2
1.5
U6

Fig 3.7 Loss of function in *RCD1* does not affect DNA methylation at hyper-DSR loci. The level of DNA methylation in seedlings of wild type (Col) and the *int51* mutant as determined by McrBc assay. The X-axis lists the hyper-DSR loci detected, the Y-axis represents the relative abundance of undigested DNA fragments in McrBc-treated samples as normalized to untreated samples. *At2g19920* was used as an unmethylated internal control. DNA methylation level at hyper-DSR loci was comparable in wild type (Col) and the *int51* mutant.

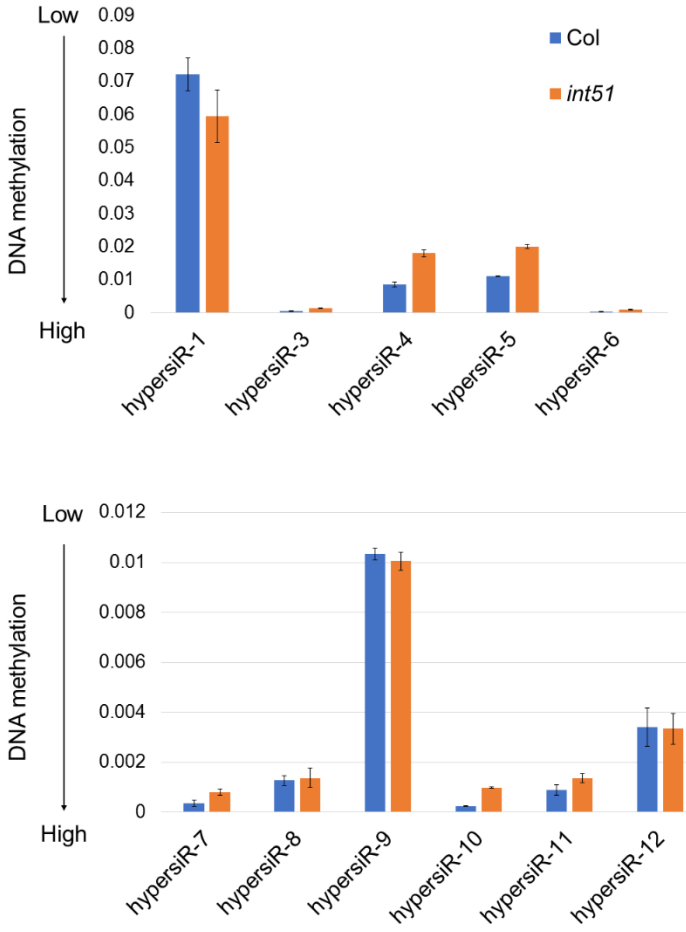
Low
High
DNA methylation
0.09
0.08
0.07
0.06
0.05
0.04
0.03
0.02
0.01
0
Col
int51
hypersiR-1
hypersiR-3
hypersiR-4
hypersiR-5
hypersiR-6
Low
High
DNA methylation
0.012
0.01
0.008
0.006
0.004
0.002
0
Col
int51
hypersiR-7
hypersiR-8
hypersiR-9
hypersiR-10
hypersiR-11
hypersiR-12

Fig 3.8 *int51* hypo-DSRs have reduced DNA methylation in all sequence contexts.

Whole genome bisulfite-sequencing to determine genome-wide DNA methylation in seedlings of wild type (Col) and the *int51* mutant. The same relative length from the transcription start site (Start) to the transcription termination site (End) was assigned to each locus. 1 kb regions from both upstream of Start and downstream of End were used as the control. The Y-axis represents the relative methylation level. The loci are indicated below the black bar. No changes in DNA methylation were detected for any sequence contexts at 24-nt hyper-DSR loci in *int51* (A). Slightly decreased CHH methylation, increased CHG methylation and unaltered CG methylation were detected in *int51* at LTR-Gypsy TE loci (B). Significant reductions in all CG, CHG and CHH methylation were observed at 24-nt hypo-DSR loci in *int51* (C). No obvious differences of DNA methylation at protein-coding genes or LTR-Copia TE loci were found between wild type (Col) and *int51* (D).

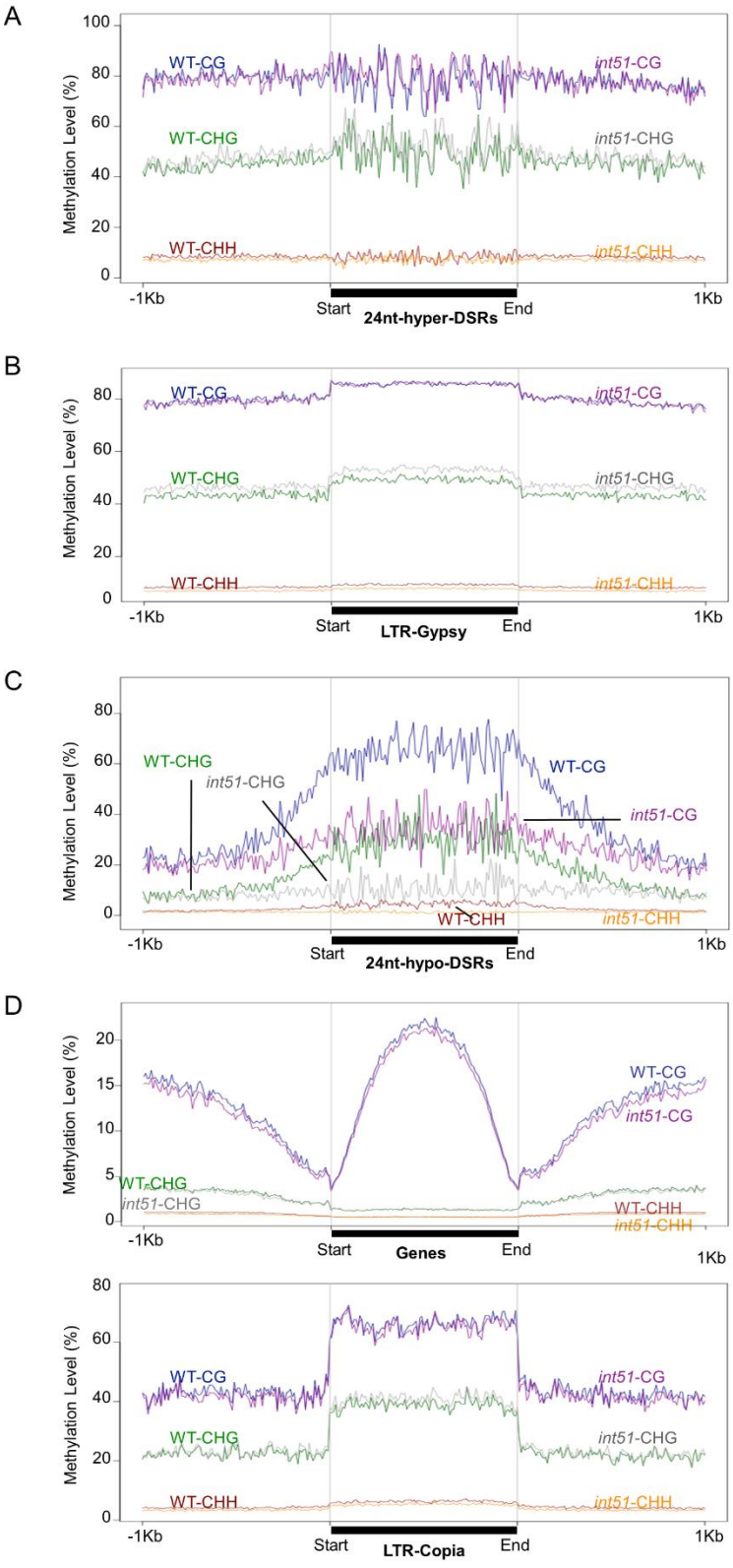
A
Methylation Level (%)
WT-CG
int51-CG
WT-CHG
int51-CHG
WT-CHH
int51-CHH
-1Kb
Start
24nt-hyper-DSRs
End
1Kb
B
LTR-Gypsy
C
24nt-hypo-DSRs
D
Genes
LTR-Copia

Fig 3.9 H3K9me2 methylation is impaired in the *int51* mutant.

(A) Global levels of H3K9me2 in seedlings of wild type (Col) and the *int51* mutant as determined by western blotting. HSC70 was used as an internal control, and the numbers indicate the level of H3K9me2 in *int51* relative to wild type (Col). A reduction in the H3K9me2 level in *int51* was consistently observed in different biological replicates. (B) Genome-wide distribution of H3K9me2 in wild type (Col). The same relative length from the transcription start site (Start) to the transcription termination site (End) was assigned to each locus. 1 kb regions from both upstream of Start and downstream of End were used as the control. The Y-axis represents the relative H3K9me2 methylation level. H3K9me2 is enriched at the LTR-Gypsy TE loci, which overlapped with 24-nt *int51*-hyper DSRs.

A

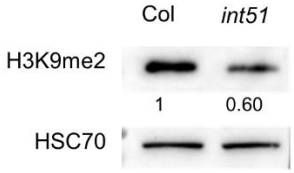
Col
int51
H3K9me2
1
0.60
HSC70

B

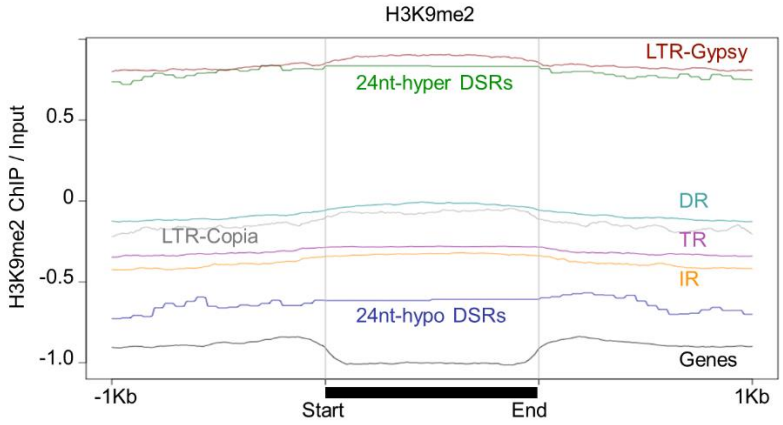
H3K9me2
LTR-Gypsy
24nt-hyper DSRs
DR
LTR-Copia
TR
IR
24nt-hypo DSRs
Genes
H3K9me2 ChIP / Input
0.5
0
-0.5
-1.0
-1Kb
Start
End
1Kb

Fig 3.10 Histone modification is altered in *drm1 drm2 cmt2 cmt3* and *suvh4 suvh5 suvh6* mutants.

Distribution of H3K9me2 methylation and H3K23ac acetylation at specific loci was analyzed in *drm1 drm2 cmt2 cmt3* and *suvh4 suvh5 suvh6* mutants. The same relative length from the transcription start site (Start) to the transcription termination site (End) was assigned to each locus. 1 kb regions from both upstream of Start and downstream of End were used as the control. The Y-axis represents the relative H3K9me2 methylation and H3K23ac acetylation levels. The loci are indicated below the black bar. In both mutants, H3K9me2 was dramatically reduced at *int51* 24-nt hyper-DSR (A) and LTR-Gypsy TE loci (B), and was increased at *int51* 24-nt hypo-DSR loci (C) and gene bodies (D). H3K23ac was enriched at *int51* 24-nt hyper-DSR (A) and LTR-Gypsy loci (B) in both *suvh4 suvh5 suvh6* and *drm1 drm2 cmt2 cmt3* as compared to wild type (Col).

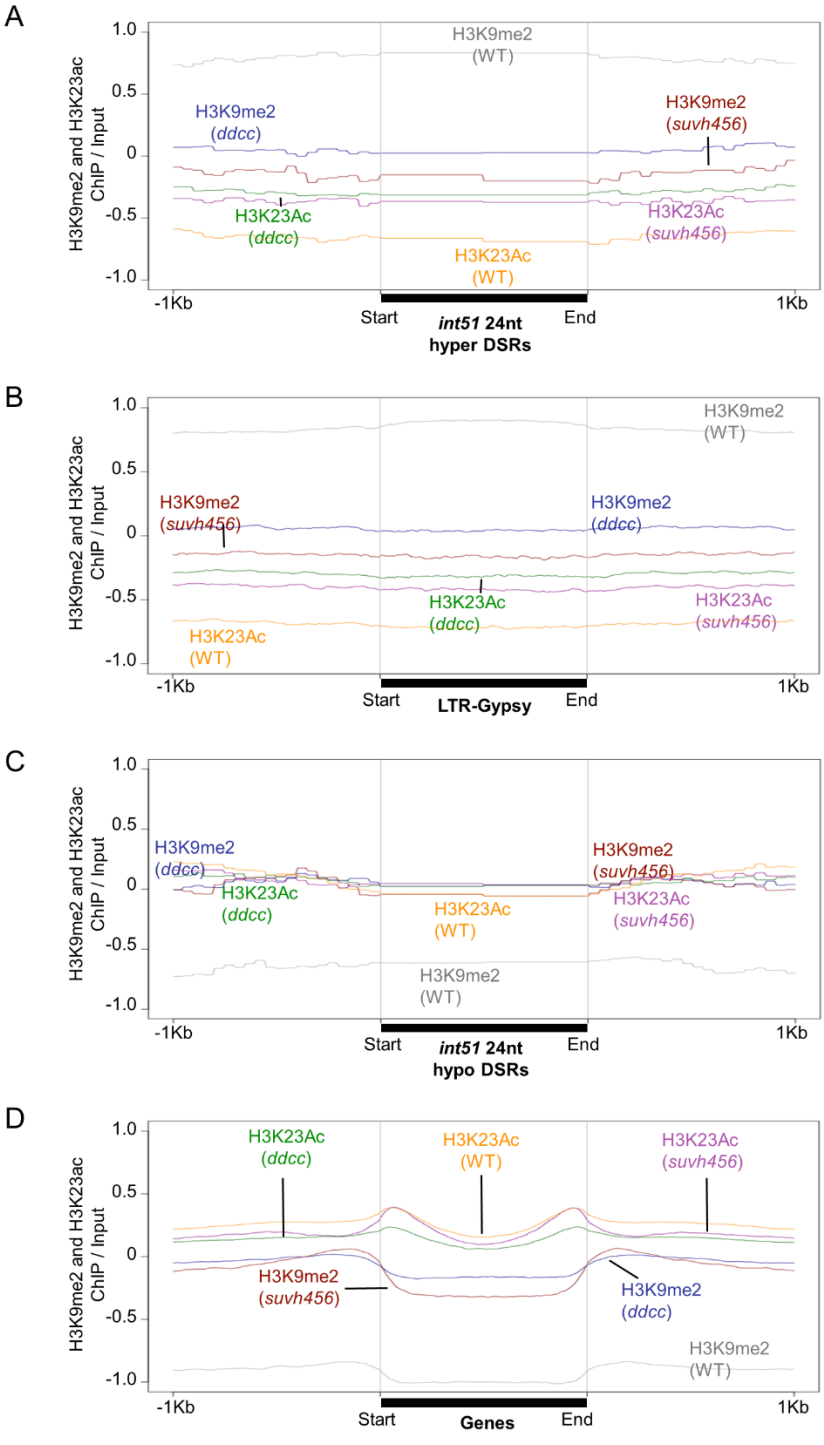
A
H3K9me2 and H3K23ac ChIP / Input
1.0
0.5
0
-0.5
-1.0
H3K9me2 (WT)
H3K9me2 (ddcc)
H3K9me2 (suvh456)
H3K23Ac (ddcc)
H3K23Ac (suvh456)
H3K23Ac (WT)
-1Kb
Start
int51 24nt hyper DSRs
End
1Kb
B
H3K9me2 and H3K23ac ChIP / Input
1.0
0.5
0
-0.5
-1.0
H3K9me2 (WT)
H3K9me2 (suvh456)
H3K9me2 (ddcc)
H3K23Ac (ddcc)
H3K23Ac (suvh456)
H3K23Ac (WT)
-1Kb
Start
LTR-Gypsy
End
1Kb
C
H3K9me2 and H3K23ac ChIP / Input
1.0
0.5
0
-0.5
-1.0
H3K9me2 (ddcc)
H3K9me2 (suvh456)
H3K23Ac (ddcc)
H3K23Ac (WT)
H3K23Ac (suvh456)
H3K9me2 (WT)
-1Kb
Start
int51 24nt hypo DSRs
End
1Kb
D
H3K9me2 and H3K23ac ChIP / Input
1.0
0.5
0
-0.5
-1.0
H3K23Ac (ddcc)
H3K23Ac (WT)
H3K23Ac (suvh456)
H3K9me2 (suvh456)
H3K9me2 (ddcc)
H3K9me2 (WT)
-1Kb
Start
Genes
End
1Kb

Fig 3.11 Global levels of histone marks in wild type (Col) and the *int51* mutant.

The global levels of several histone marks in seedlings of wild type (Col) and the *int51* mutant as determined by western blotting. HSC70 served as the internal control, and the numbers indicated the level of histone marks in *int51* relative to wild type (Col). Only the H3K27ac level was increased in the *int51* mutant.

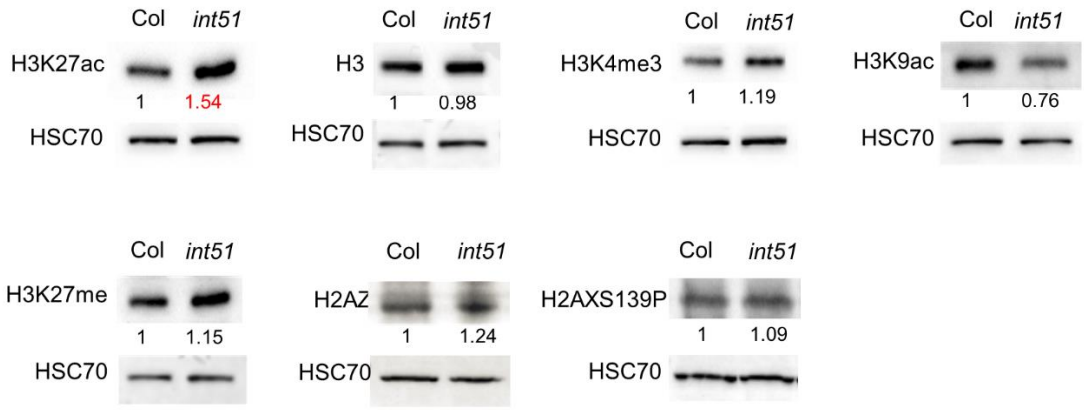
Col
int51
H3K27ac
1
1.54
HSC70
Col
int51
H3
1
0.98
HSC70
Col
int51
H3K4me3
1
1.19
HSC70
Col
int51
H3K9ac
1
0.76
HSC70
Col
int51
H3K27me
1
1.15
HSC70
Col
int51
H2AZ
1
1.24
HSC70
Col
int51
H2AXS139P
1
1.09
HSC70

Table 3.1 Number of hypo- and hyper-DSR loci identified in the *int51* mutant.

inflorescences			
Size	**hypo-DSRs**	**hyper-DSRs**	**Total**
21 nt	30	63	93
22 nt	156	102	258
23 nt	160	94	254
24 nt	891	675	1,566

seedlings			
Size	**hypo-DSRs**	**hyper-DSRs**	**Total**
21 nt	5	7	12
22 nt	3	11	14
23 nt	22	7	29
24 nt	237	115	352

Differential small RNA regions (DSRs) identified in *int51* inflorescences or seedlings as compared to wild type (Col) based on small RNA-seq. hypo-DSRs are regions generating less small RNAs in *int51* than wild type, while hyper-DSRs are regions generating more small RNAs in *int51* than wild type. Each 100 bp window along the genome was defined as one locus.

Table 3.2 Oligonucleotides used in this study.

oligo name	oligo sequence	purpose
miR156AS	GTGCTCTCTTTCTTCTGTCA	miR northern blot
miR159AS	TAGAGCTCCCTTCAATCCAAA	miR northern blot
miR166AS	GGGGAATGAAGCCTGGTCCGA	miR northern blot
miR167AS	TAGATCATGTTGGCAGTTTCA	miR northern blot
miR168AS	TTCCCGACCTGCACCAAGCGA	miR northern blot
miR172AS	ATGCAGCATCATCAAGATTCT	miR northern blot
miR173AS	GTGATTTCTCTCTGTAAGCGA	miR northern blot
miR398AS	AAGGGGTGACCTGAGAACACA	miR northern blot
TAS1 siR255AS	TACGCTATGTTGGACTTAGAA	tasiR northern blot
TAS2 siR1511AS	AAGTATCATCATTCGCTTGGA	tasiR northern blot
TAS3 siR5'D8AS	AAAGGTCTTACAAGGTCAAGA	tasiR northern blot
U6	AGGGGCCATGCTAATCTTCTCTG	miR northern blot
qACT8-F	CACATGCTATCCTCCGTCTC	real-time PCR
qACT8-R	CAATGCCTGGACCTGCTT	real-time PCR
qARF3-F	GGTGGCCTGGTTCAAAATGGAG	real-time PCR
qARF3-R	CGGAAGAGGGTGATGATGATAC	real-time PCR
qAGO1-F	TGGACCACCGCAGAGACAAT	real-time PCR
qAGO1-R	CATCATACGCTGGAAGACGAC	real-time PCR
qPHB-F	TGCTGTTGACTGGGTTCAGATG	real-time PCR
qPHB-R	GGCACGTGCTGCAATTCC	real-time PCR
qATHB15-F	ATCCTCAGAGAGATGCTAGTCCT	real-time PCR
qATHB15-R	TTGTAGGCTCAAGACCCACTAG	real-time PCR
qAP2-F	AGCGGAGGCGGATTCTCACTGTT	real-time PCR
qAP2-R	TCGTCGAGGCCCGACCATCAAA	real-time PCR
qTCP4-F	TAGAAAACGCAAGGAAATGA	real-time PCR
qTCP4-R	CACAATAAGAACAGGGAGCA	real-time PCR
qMYB33-F	AGTTGTTGTATCCTGGGTGTAGCA	real-time PCR
qMYB33-R	CCGTTGGTGGTGGTGGAGAC	real-time PCR
qCUC2-F	CTCACTCCCACCTCTCCT	real-time PCR
qCUC2-R	GAAAAGGGTCAAAGTCAAAC	real-time PCR
N_UBQ5	GGTGCTAAGAAGAGGAAGAA	real-time PCR
C_UBQ5	CTCCTTCTTTCTGGTAAACGT	real-time PCR
hypersiR1-F	ACAATCTCAAGATGGCAGCA	siR northern blot

hypersiR1-R	TCTGCTTAGTGGAAAGACGACA	siR northern blot
hypersiR2-F	TGACTCCCTTGCAATCTGAA	siR northern blot
hypersiR2-R	CACTGGTGGAGACAGGAGGT	siR northern blot
hypersiR3-F	AGCGGTACAACCGAAGAAGA	siR northern blot
hypersiR3-R	GCTGGTACCGCCTATCTCAC	siR northern blot
hypersiR4-F	TCCAGCTCTGGAAGGATGAT	siR northern blot
hypersiR4-R	CTTGAGCTGACACAGGGTGA	siR northern blot
hypersiR5-F	CAGCACCGCTCTGATGATAC	siR northern blot
hypersiR5-R	AAGGCCATCACGTTTCTGAC	siR northern blot
hypersiR6-F	GACCTCATCAGCTCTGTGGCGG	siR northern blot
hypersiR6-R	ATGAAGCGGAGTTTGACACGAG	siR northern blot
hypersiR7-F	TCCGTTTGTTCCCATTCTCCTT	siR northern blot
hypersiR7-R	GCTAAGAAGAATCCTGTCCAGC	siR northern blot
hypersiR8-F	GTCTCATCAATATCTTCTGTTGT	siR northern blot
hypersiR8-R	GAGATGATAGATTATGCGCTTA	siR northern blot
hypersiR9-F	GAATCCTAGTAGCGTCAATGCA	siR northern blot
hypersiR9-R	TCTAAGAGCAACCAAATCCAAA	siR northern blot
hypersiR10-F	CTATATCATCCGTCTCATCAA	siR northern blot
hypersiR10-R	ATGCGCTTACAGGGATTCTCC	siR northern blot
hypersiR11-F	TTACCGGAGGACGTACAGCAT	siR northern blot
hypersiR11-R	ACATTCTTTCCCTTCGTCCGGT	siR northern blot
hypersiR12-F	AGTCGCCAGCCATGTCAAACT	siR northern blot
hypersiR12-R	GGAACCAAACCCAGATTTGACA	siR northern blot
hyposiR1-F	GCGTTTGTACATGGAAAGATA	siR northern blot
hyposiR1-R	TCAGATCTCAAAGATTATCGC	siR northern blot
hyposiR2-F	TAGACATAACGAACCGACCGT	siR northern blot
hyposiR2-R	TCTCAAACGAGGGCTACTTAG	siR northern blot
At2g19920-F	TCACCCGAACAGTTGGAAGAA	McrBc PCR
At2g19920-R	GTGAGGAACCGGTCCATTATT	McrBc PCR

Conclusions and Perspectives

Plant small RNAs are a class of non-coding RNAs consisting of microRNAs (miRNAs) and small interfering RNAs (siRNAs) that mediate gene silencing at post-transcriptional level and transcriptional level. Previous studies have reported that abnormal accumulation or activity of small RNAs, even for a single small RNA, leads to severe developmental defects and failure in response to stress or disease. Research efforts have established the major molecular framework of small RNA biogenesis and modes of action, and are beginning to elucidate the mechanisms of small RNA degradation (reviewed in [1,2] [3-5]). In my thesis research, I have worked on two independent research projects to study the mechanism of small RNA metabolism in *Arabidopsis*.

The project reported in Chapter Two of this dissertation aimed to dissect the mechanism of miRNA degradation. In *Arabidopsis*, ARGONAUTE 10 (AGO10) is specifically associated with miR165/6 and represses the accumulation of this miRNA [6,7]. In this research, the loss of *AGO10* leads to increased level of miR165/6 without affecting its biogenesis, but causes a slight reduction of 3' truncated species. Consistently, *AGO10* overexpression results in a reduction of full-length miR165/6 species accompanied with elevated 3' truncation of miR165/6, which is rescued by losses of two exonucleases SMALL RNA DEGRADING NUCLEASE 1 (SDN1) and SDN2. *In vitro* enzymatic assay of SDN1 on AGO10 immunoprecipitates followed by small RNA sequencing confirms that AGO10 represses the accumulation of miR165/6 through promoting its degradation via SDN1. This finding furthers our knowledge on the function of AGO10: AGO10 promotes the degradation of miR165/6 to ensure normal expressions of miR165/6 targets that are essential for stem cell maintenance and leaf polarity.

AGO10 is the closest paralog of AGO1 among the ten Argonaute proteins in Arabidopsis. To address the question whether AGO1 also promotes the degradation of small RNAs, same enzymatic assay of SDN1 assay was performed on AGO1 immunoprecipitates. Based on small RNA-seq analysis, many miRNAs are truncated at their 3' ends after incubation with SDN1. A model of miRNA degradation is thereby proposed: SDNs initiate degradation by trimming the miRNA to result in a 3′ truncated and unmethylated miRNA that is subsequently uridylated by HEN1 SUPPRESSOR1 (HESO1) or URIDYLYLTRANSFERASE 1 (URT1). The tailed species are further degraded by an yet unknown enzyme. In addition, both SDN1 (this study) and the nucleotidyl transferases (HESO1 and URT1) [8,9] can act on AGO1-bound miRNAs, as well as free miRNAs.

Unlike miRNAs, the metabolism and activities of siRNAs are still ambiguous. The well-studied siRNAs are 24-nt in length and the canonical biogenesis pathway of these 24-nt siRNAs requires essential factors, including RNA POLYMERASE IV (Pol IV), RNA-DIRECTED RNA POLYMERASE 2 (RDR2) and DICER-LIKE 3 (DCL3). siRNA biogenesis starts with the initiation of transcription via Pol IV that is recruited by several cofactors, such as SAWADEE HOMEODOMAIN HOMOLOG 1 (SHH1) and CLASSY1 (CLSY1) (reviewed in [4,5]). However, the distribution of these cofactors is not completely overlapped with Pol IV loci [10], suggesting that some factors remain undiscovered. In addition, emerging studies have reported that the length of most siRNA precursors is 30-to-40 nt [11] or 26-to-45 nt [12], and have identified some novel siRNAs that are independent of Pol IV, RDR2 or DCL3 [13,14]. All these findings make the siRNA biogenesis mysterious. Further investigation on siRNA biogenesis is necessary. So are the functions of siRNAs, especially the 24-nt siRNAs generated from the pericentromeric and centromeric regions. In the Chapter Three of this dissertation, through small RNA

sequencing, many siRNAs were identified to be differentially expressed in the *RCD1* (RADICAL-INDUCED CELL DEATH 1) mutant *int51* compared to those in wild type. The whole-genome bisulfate-sequencing further reveals that DNA methylation in all sequence contexts is greatly reduced on euchromatin arms in *int51*, while is not changed at heterochromatic regions. The global level of H3K9me2 is also reduced in *int51*. These changes observed in *int51* resemble those of mutants defective in DNA or histone methylation, providing a novel link to further dissect the RCD1-mediated regulatory network. RCD1 is an important cellular hub that interacts with many transcription factors (TFs) to regulate gene expression. It is possible that RCD1 may interact with specific TFs at certain loci to activate or repress Pol IV transcription, which therefore leads to differential expressions of siRNAs.

References

1. Chen X (2005) MicroRNA biogenesis and function in plants. FEBS Lett 579: 5923-5931.

2. Chen X (2009) Small RNAs and their roles in plant development. Annu Rev Cell Dev Biol 25: 21-44.

3. Rogers K, Chen X (2013) Biogenesis, turnover, and mode of action of plant microRNAs. Plant Cell 25: 2383-2399.

4. Law JA, Jacobsen SE (2010) Establishing, maintaining and modifying DNA methylation patterns in plants and animals. Nat Rev Genet 11: 204-220.

5. Du J, Johnson LM, Jacobsen SE, Patel DJ (2015) DNA methylation pathways and their crosstalk with histone methylation. Nat Rev Mol Cell Biol 16: 519-532.

6. Liu Q, Yao X, Pi L, Wang H, Cui X, et al. (2009) The *ARGONAUTE10* gene modulates shoot apical meristem maintenance and establishment of leaf polarity by repressing miR165/166 in *Arabidopsis*. Plant J 58: 27-40.

7. Zhu H, Hu F, Wang R, Zhou X, Sze SH, et al. (2011) *Arabidopsis* Argonaute10 specifically sequesters miR166/165 to regulate shoot apical meristem development. Cell 145: 242-256.

8. Ren G, Xie M, Zhang S, Vinovskis C, Chen X, et al. (2014) Methylation protects microRNAs from an AGO1-associated activity that uridylates 5' RNA fragments generated by AGO1 cleavage. Proc Natl Acad Sci U S A 111: 6365-6370.

9. Wang X, Zhang S, Dou Y, Zhang C, Chen X, et al. (2015) Synergistic and independent actions of multiple terminal nucleotidyl transferases in the 3' tailing of small RNAs in *Arabidopsis*. PLoS Genet 11: e1005091.

10. Law JA, Du J, Hale CJ, Feng S, Krajewski K, et al. (2013) Polymerase-IV occupancy at RNA-directed DNA methylation sites requires SHH1. Nature 498: 385-389.

11. Zhai J, Bischof S, Wang H, Feng S, Lee T-f, et al. (2015) A one precursor one siRNA model for Pol IV-dependent siRNAs biogenesis. Cell 163: 445-455.

12. Blevins T, Podicheti R, Mishra V, Marasco M, Wang J, et al. (2015) Identification of Pol IV and RDR2-dependent precursors of 24 nt siRNAs guiding de novo DNA methylation in *Arabidopsis*. eLife 4: e09591.

13. Ye R, Chen Z, Lian B, Rowley MJ, Xia N, et al. (2016) A dicer-independent route for biogenesis of siRNAs that direct DNA methylation in *Arabidopsis*. Mol Cell 61: 222-235.

14. Yang DL, Zhang G, Tang K, Li J, Yang L, et al. (2016) Dicer-independent RNA-directed DNA methylation in *Arabidopsis*. Cell Res 26: 66-82.

Appendix A: Double-stranded RNA binding proteins in *Arabidopsis*

The *Arabidopsis* genome encodes five closely related double-stranded RNA binding (DRB) proteins [1,2]. DRB1, also known as HYPONASTIC LEAVES 1 (HYL1), interacts with the RNase III enzyme DICER-LIKE 1 (DCL1) to efficiently and accurately process the hairpin-structured primary-miRNAs in the miRNA biogenesis pathway [1,3,4]. DRB4 is required by DCL4 for the efficient and precise processing of long and perfectly double-stranded RNA substrates in the tasiRNA biogenesis pathway [5,6]. However, little is known about the functions of DRB2, DRB3 and DRB5. Recent study has suggested that DRB2 may play a role in the biogenesis of a subset of miRNAs in the shoot apex meristem (SAM) region due to its specific expression pattern [7]. DRB3 and DRB5 may assist the DRB2-dependent miRNAs to function at steps downstream of miRNA biogenesis [8]. While the *drb2* plant displays subtle morphological defects in the form of serrated and dark green rosette leaves, *drb3*, *drb5*, and *drb3/5* double mutants are essentially normal in appearance. In *drb2/3* or *drb2/5* double mutants, the *drb2* phenotype is only weakly enhanced. Intriguingly, the *drb2/3/5* triple mutants display a severe developmental phenotype resembling that in *hyl1* [7,8]. Moreover, both *hyl1* and *drb2/3/5* triple mutants are resistant to the artificial miRNA-directed silencing of the endogenous Phytoene desaturase (PDS) gene [8]. This evidence indicates that DRB2, DRB3 and DRB5 function redundantly in the miRNA pathway. One of my PhD projects is to investigate the function of Arabidopsis DRB2 in miRNA pathway.

To examine whether *DRB2* is essential for miRNA pathway, the accumulations of several miRNAs were measured in the inflorescences of wild type (Col) and the *drb2* mutant. It was found that the levels of all the miRNAs detected were comparable between the *drb2* mutant and wild type (Figure A.1). To figure out whether activities of miRNAs are

affected in *drb2*, qPCR and western blotting were carried out separately. In brief, no changes were observed on transcript levels of miRNA targets, but the protein levels of two miRNA targets AGO1 and AP2 were slightly increased (Figure A.2). All these results indicate that DRB2 may affect miRNA-directed translational repression. This hypothesis will need further confirming through the use of miRNA resistant reporter lines. In addition, transcript and protein levels of several other players involved in miRNA biogenesis were also investigated, and no abnormal expressions of them were found (Figure A.3). However, it was reported that DRB2 is required for miRNA-mediated translational inhibition and repression of HYL1 expression, which allows the selection of miRNA mode of action [9]. As such, research on DRB2 in miRNA pathway has not been preceded further.

Many studies have shown that small RNAs are mobile [10]. However, the proteins guiding small RNA movement remain uncovered and it is still unknown in which form small RNAs move. One possibility is that small RNAs move in the form of duplex or double-stranded precursor. To examine whether DRB proteins play a role in small RNA movement, crosses between *drb2*, *drb3* and *drb5* single mutants to *SUC2::amiR-SUL* and *SUC2::siR-SUL* were generated in this research, respectively. *SUC2::amiR-SUL* (*amiRsul*) and *SUC2::siR-SUL* (*sucsul*) are two reporter lines using artificial miRNA or RNAi to knock down *CHLORINA42* (*CH42*), the *Arabidopsis* homolog of tobacco *SULPHUR (SUL*), in *SUC2* expressing cells [11]. The photobleached phenotype observed in the vein of transgenic plants suggests that small RNAs are able to move. Loss of *DRB2* or *DRB3* resulted in enhanced photobleached phenotype of *sucsul*, but not *amiRsul* (Figure A.4), indicating that *DRB2* and *DRB3* may be involved in siRNA

biogenesis or movement. Nevertheless, loss of *DRB5* had no effect on changing the photobleached phenotype of either *sucsul* or *amiRsul* (Figure A.4).

Further investigation was carried out in *drb2 sucsul* and *drb3 sucsul* plants. By qPCR analysis, reduced levels of *SUL* mRNA were found in both (Figure A.5). Northern blotting was also performed to examine the levels of *SUL* siRNAs, and increased levels of *SUL* siRNAs were observed in both *drb2 sucsul* and *drb3 sucsul* plants by comparing to *sucsul* (Figure A.6), implying that the enhanced phenotype could be attributed to the elevated productions of *SUL* siRNAs when *DRB2* or *DRB3* was lost, and in conclusion, both proteins may play a negative role in siRNA biogenesis.

This project is still ongoing and many questions remain to be addressed. Further insightful studies need to figure out how DRB2 or DRB3 represses the biogenesis of siRNAs, whether DRB2 or DRB3 guides small RNA movement, what kind of double-stranded RNAs are associated with DRB2 or DRB3, and what are the specific features of these RNAs. The completion of this project may lead to novel understanding of DRB proteins in siRNA pathway and small RNA movement.

References

1. Hiraguri A, Itoh R, Kondo N, Nomura Y, Aizawa D, et al. (2005) Specific interactions between Dicer-like proteins and HYL1/DRB-family dsRNA-binding proteins in *Arabidopsis thaliana*. Plant Mol Biol 57: 173-188.

2. Curtin SJ, Watson JM, Smith NA, Eamens AL, Blanchard CL, et al. (2008) The roles of plant dsRNA-binding proteins in RNAi-like pathways. FEBS Lett 582: 2753-2760.

3. Vazquez F, Gasciolli V, Crete P, Vaucheret H (2004) The nuclear dsRNA binding protein HYL1 is required for microRNA accumulation and plant development, but not posttranscriptional transgene silencing. Curr Biol 14: 346-351.

4. Han MH, Goud S, Song L, Fedoroff N (2004) The *Arabidopsis* double-stranded RNA-binding protein HYL1 plays a role in microRNA-mediated gene regulation. Proc Natl Acad Sci U S A 101: 1093-1098.

5. Adenot X, Elmayan T, Lauressergues D, Boutet S, Bouche N, et al. (2006) DRB4-dependent TAS3 trans-acting siRNAs control leaf morphology through AGO7. Curr Biol 16: 927-932.

6. Nakazawa Y, Hiraguri A, Moriyama H, Fukuhara T (2007) The dsRNA-binding protein DRB4 interacts with the Dicer-like protein DCL4 in vivo and functions in the trans-acting siRNA pathway. Plant Mol Biol 63: 777-785.

7. Eamens AL, Kim KW, Curtin SJ, Waterhouse PM (2012) DRB2 is required for microRNA biogenesis in *Arabidopsis thaliana*. PLoS One 7: e35933.

8. Eamens AL, Wook Kim K, Waterhouse PM (2012) DRB2, DRB3 and DRB5 function in a non-canonical microRNA pathway in *Arabidopsis thaliana*. Plant Signal Behav 7: 1224-1229.

9. Reis RS, Hart-Smith G, Eamens AL, Wilkins MR, Waterhouse PM (2015) Gene regulation by translational inhibition is determined by Dicer partnering proteins. Nat Plants 1: 14027.

10. Chitwood DH, Nogueira FT, Howell MD, Montgomery TA, Carrington JC, et al. (2009) Pattern formation via small RNA mobility. Genes Dev 23: 549-554.

11. de Felippes FF, Ott F, Weigel D (2011) Comparative analysis of non-autonomous effects of tasiRNAs and miRNAs in *Arabidopsis thaliana*. Nucleic Acids Res 39: 2880-2889.

Figures and Tables

Figure A.1 Loss of *DRB2* does not affect the accumulation of miRNAs.

The accumulation of miRNAs in the inflorescences of wild type (Col) and *drb2* mutant was determined by northern blotting. U6 served as the internal control, and the numbers indicated the abundance of miRNAs in *drb2* relative to wild type (Col). No change of miRNA abundance was observed in *drb2*.


Col
drb2
miR156
1
0.76
U6
miR164
1
0.87
U6
miR166
1
1.01
U6
miR173
1
0.83
U6
miR390
1
0.87
U6
miR168
1
1.02
U6
miR398
1
0.85
U6

Figure A.2 DRB2 may play a role in miRNA-mediated translational repression.

Semi-quantitative qPCR and western blotting were used to determine the transcript levels and protein levels of miRNA targets, respectively, in the inflorescences of wild type (Col) and *drb2*. Two biological replicates were shown. UBQ5 was used as the internal control for qPCR, and HSC70 was the internal control for western blotting. The transcript levels of miRNA targets were comparable in wild type (Col) and *drb2*. The protein levels of AGO1 and AP2 were slightly increased in *drb2* compared to those in wild type (Col) in both biological replicates.

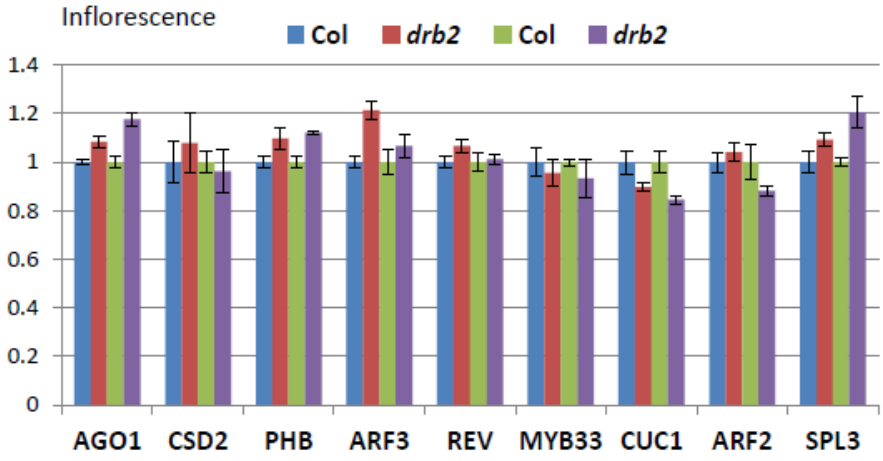
Inflorescence
Col
drb2
Col
drb2
1.4
1.2
1
0.8
0.6
0.4
0.2
0
AGO1
CSD2
PHB
ARF3
REV
MYB33
CUC1
ARF2
SPL3

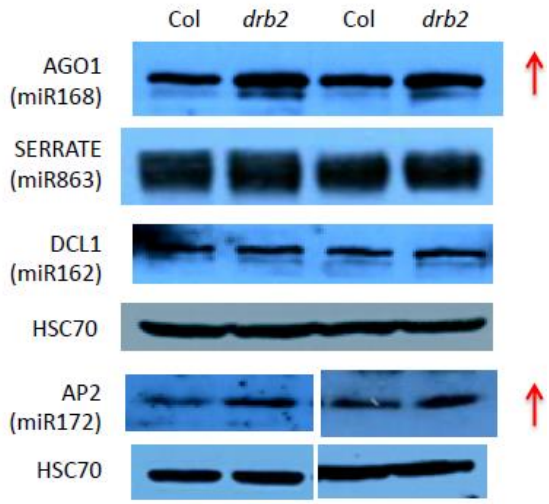
Col
drb2
Col
drb2
AGO1
(miR168)
SERRATE
(miR863)
DCL1
(miR162)
HSC70
AP2
(miR172)
HSC70

Figure A.3 DRB2 has no effect on the expression of players involved in miRNA biogenesis.

Semi-quantitative qPCR and western blotting were employed to determine the transcript levels and protein levels of players involved in miRNA biogenesis, respectively, in the inflorescences of wild type (Col) and *drb2*. Two biological replicates were shown. UBQ5 was used as the internal control for qPCR, and HSC70 was the internal control for western blotting. No changes of either transcript levels or protein levels of these players were observed in *drb2* compared to those in wild type (Col) in both biological replicates.

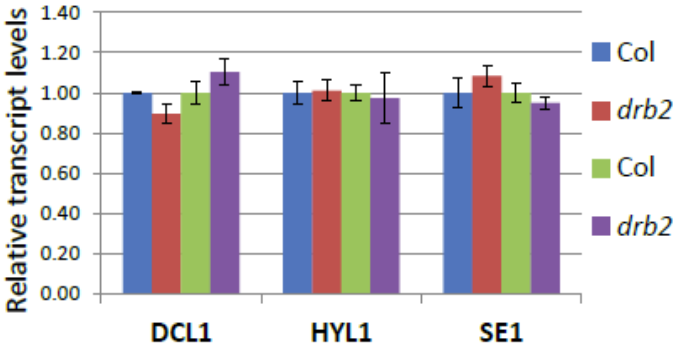
Relative transcript levels
1.40
1.20
1.00
0.80
0.60
0.40
0.20
0.00
DCL1
HYL1
SE1
Col
drb2
Col
drb2

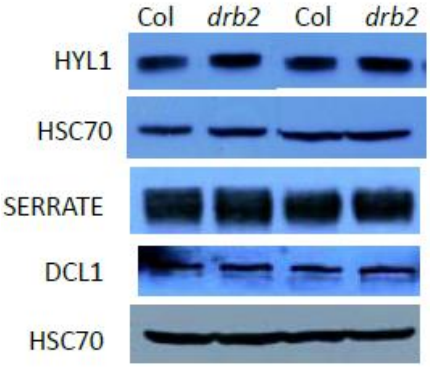
Col
drb2
Col
drb2
HYL1
HSC70
SERRATE
DCL1
HSC70

Figure A.4 Losses of *DRB2* and *DRB3* enhance the photobleached phenotype of *SUC2::siR-SUL* reporter line.

Photobleached phenotype of the *drb sucsul* and *drb amiRsul* plants was exhibited. Losses of *DRB2* and *DRB3* enhance the phenotype of *sucsul*. No differences were found in other double mutants.


sucsul
drb2 sucsul
drb3 sucsul
drb5 sucsul
amiR SUL
drb2 amiR SUL
drb3 amiR SUL
drb5 amiR SUL

Figure A.5 *SUL* mRNA level is impaired in both *drb2 sucsul* and *drb3 sucsul* plants. Semi-quantitative qPCR was used to determine the transcript level of *SUL* gene in the mature leaves of *sucsul*, *drb2 sucsul* and *drb3 sucsul* plants. Two independent lines of *drb2 sucsul* (*L1* and *L2*) were shown. UBQ5 was used as the internal control. The sequence of *SUL* cDNA used for the *SUC::siR-SUL* construct was shown and two pairs of primers detecting *SUL* mRNA level (*SUL-1* and *SUL-2*) were highlighted with red bar. The transcript level of *SUL* was decreased in both *drb2 sucsul* and *drb3 sucsul* plants.

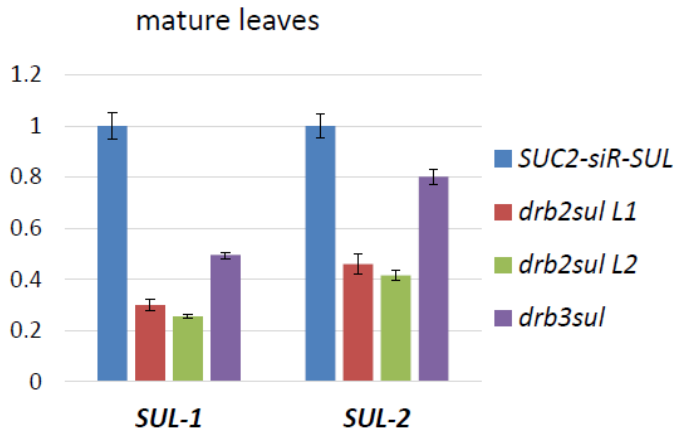
mature leaves
1.2
1
0.8
0.6
0.4
0.2
0
SUL-1
SUL-2
SUC2-siR-SUL
drb2sul L1
drb2sul L2
drb3sul

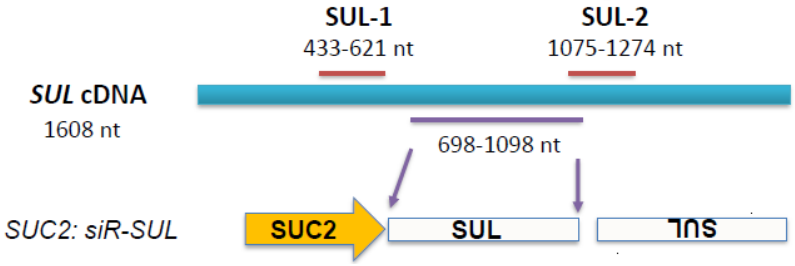
SUL-1
433-621 nt
SUL-2
1075-1274 nt
SUL cDNA
1608 nt
698-1098 nt
SUC2: siR-SUL
SUC2
SUL
TNS

Figure A.6 DRB2 and DRB3 repress the accumulation of *SUL* siRNAs.

The abundance *of SUL* siRNAs in the mature leaves of *sucsul*, *drb2 sucsul* and *drb3 sucsul* plants was determined by northern blotting. Two independent lines of *drb2 sucsul* (*L1* and *L2*) were shown. U6 served as the internal control, and the numbers indicated the abundance of *SUL* siRNAs in the mutants relative to that of wild type (Col). *SUL* siRNA levels of both 21-nt and 24-nt were elevated in *drb2 sucsul* and *drb3 sucsul* plants. The sizes of siRNAs were indicated.

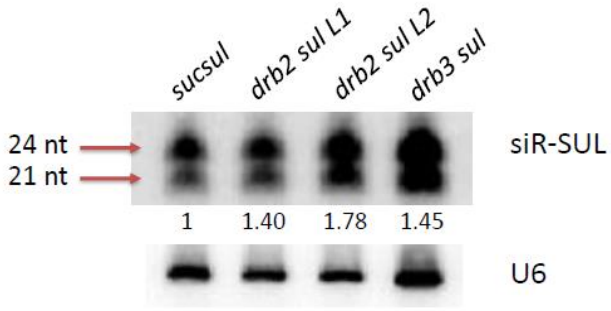
sucsul
drb2 sul L1
drb2 sul L2
drb3 sul
24 nt
21 nt
siR-SUL
1
1.40
1.78
1.45
U6

Table A Oligonucleotides used in this study.

oligo name	oligo sequence	purpose
miR156AS	GTGCTCTCTTTCTTCTGTCA	miR northern blot
miR164AS	TGCACGTGCCCTGCTTCTCCA	miR northern blot
miR166AS	GGGGAATGAAGCCTGGTCCGA	miR northern blot
miR168AS	TTCCCGACCTGCACCAAGCGA	miR northern blot
miR172AS	ATGCAGCATCATCAAGATTCT	miR northern blot
miR173AS	GTGATTTCTCTCTGTAAGCGA	miR northern blot
miR398AS	AAGGGGTGACCTGAGAACACA	miR northern blot
TAS1 siR255AS	TACGCTATGTTGGACTTAGAA	tasiR northern blot
TAS2 siR1511AS	AAGTATCATCATTCGCTTGGA	tasiR northern blot
TAS3 siR5'D8AS	AAAGGTCTTACAAGGTCAAGA	tasiR northern blot
U6	AGGGGCCATGCTAATCTTCTCTG	miR northern blot
qCSD2-F	ACAGGACCACATTTCAACCCTAA	real-time PCR
qCSD2-R	CATCGGCATTGGCATTTATG	real-time PCR
qARF3-F	GGTGGCCTGGTTCAAAATGGAG	real-time PCR
qARF3-R	CGGAAGAGGGTGATGATGATAC	real-time PCR
qAGO1-F	TGGACCACCGCAGAGACAAT	real-time PCR
qAGO1-R	CATCATACGCTGGAAGACGAC	real-time PCR
qPHB-F	TGCTGTTGACTGGGTTCAGATG	real-time PCR
qPHB-R	GGCACGTGCTGCAATTCC	real-time PCR
qREV-F	ATCTGTGGTCACAACTCC	real-time PCR
qREV-R	TAGCGACCTCTCACAAAC	real-time PCR
qARF2-F	TTCGATGCTTACCAGAGAAGGT	real-time PCR
qARF2-R	TTGAGTCTGTCCCATTCATGTTG	real-time PCR
qSPL3-F	CTGGACACAACGAGAGAAG	real-time PCR
qSPL3-R	TGGAGAAACAGACAGAGACA	real-time PCR
qMYB33-F	AGTTGTTGTATCCTGGGTGTAGCA	real-time PCR
qMYB33-R	CCGTTGGTGGTGGTGGAGAC	real-time PCR
qCUC1-F	CCAACGGGACTGAGAACGAACA	real-time PCR
qCUC1-R	CGGTGGAGCGGGAAGGAAT	real-time PCR
qDCL1-F	CAGAGTTCGCGATTCTTTTTG	real-time PCR
qDCL1-R	AGGGTTCAACATCAACATCCA	real-time PCR
qHYL1-F	TCCACTGATGTTTCCTCTGG	real-time PCR
qHYL1-R	GATCTCATAAACAGGCGTTGG	real-time PCR

qSE1-F	CTGATTCCGTCGATAACCGTCTCC	real-time PCR
qSE1-R	CAGGCCTCCCACCCATTTCAC	real-time PCR
N_UBQ5	GGTGCTAAGAAGAGGAAGAA	real-time PCR
C_UBQ5	CTCCTTCTTTCTGGTAAACGT	real-time PCR
qSUL-1-F	GATCCAAAGATTGGTGGTGTTATG	real-time PCR
qSUL-1-R	AACTTGCTCTCCTTTCTCAACTCT	real-time PCR
qSUL-2-F	AGCATCCACACACACTTTGAATGC	real-time PCR
qSUL-2-R	GAGATCGTTCTTGAACATGGTGAG	real-time PCR
SUL-siR-F	TACGCTATAGACACAGCTCTGT	SUL-siR northern
SUL-siR-R	TGTAAGTGTCACGGAAATCCT	SUL-siR northern

Appendix B: Collaborated projects and publications

During my PhD study, I participated in several other projects investigating the mechanism of miRNA degradation and activities, in particular, translational repression and biogenesis of secondary siRNAs. We identified two nucleotidyl transderases HEN1 SUPPRESSOR1 (HESO1) [1] and URIDYLYLTRANSFERASE 1 (URT1) [2] which are responsible for 3' uridylation of unmethylated miRNAs toward their degradation. We also identified an ER-localized protein ALTERED MERISTEM PROGRAM 1 (AMP1) which is essential for miRNA-guided translational repression, which is the first report showing that translation repression guided by miRNAs occurs on ER membrane [3]. We later demonstrated that the biogenesis of secondary siRNAs triggered by miRNAs takes place on membrane-bound polysomes [4].

I also performed many small RNA analyses for our collaborators, including a lot of small RNA library constructions, northern blotting, and beta-elimination assay. All information can be found in the following published articles [5-9].

Publications

1. Zhao Y,* Yu Y*, Zhai J, Ramachandran V, Dinh TT, et al. (2012) The *Arabidopsis* nucleotidyl transferase HESO1 uridylates unmethylated small RNAs to trigger their degradation. Curr Biol 22: 689-694. (*equal contributions)

2. Tu B, Liu L, Xu C, Zhai J, Li S, et al. (2015) Distinct and cooperative activities of HESO1 and URT1 nucleotidyl transferases in microRNA turnover in *Arabidopsis*. PLoS Genet 11: e1005119.

3. Li S, Liu L, Zhuang X, Yu Y, Liu X, et al. (2013) MicroRNAs inhibit the translation of target mRNAs on the endoplasmic reticulum in *Arabidopsis*. Cell 153: 562-574.

4. Li S, Le B, Ma X, Li S, You C, et al. (2016) Biogenesis of phased siRNAs on membrane-bound polysomes in *Arabidopsis*. Elife 5: e22750.

5. Kim YJ, Zheng B, Yu Y, Won SY, Mo B, et al. (2011) The role of Mediator in small and long noncoding RNA production in *Arabidopsis thaliana*. EMBO J 30: 814.

6. Wong J, Gao L, Yang Y, Zhai J, Arikit S, et al. (2014) Roles of small RNAs in soybean defense against *Phytophthora sojae* infection. Plant J 79: 928-940.

7. Lam P, Zhao L, Eveleigh N, Yu Y, Chen X, et al. (2015) The Exosome and Trans-Acting Small Interfering RNAs Regulate Cuticular Wax Biosynthesis during *Arabidopsis* Inflorescence Stem Development. Plant Physiol 167: 323.

8. Johnson KCM, Yu Y, Gao L, Eng RC, Wasteneys GO, et al. (2016) A partial loss-of-function mutation in an *Arabidopsis* RNA polymerase III subunit leads to pleiotropic defects. J Exp Bot 67: 2219-2230.

9. Feng B, Ma S, Chen S, Zhu N, Zhang S, et al. (2016) PARylation of the forkhead‐associated domain protein DAWDLE regulates plant immunity. EMBO Rep 17:1799-1813.

Appendix C: Approval of using the published article in PLoS Biology

PLOS Biology <plosbiology@plos.org> Mon, Jul 17, 2017 at 2:58 AM
To: "yuyu1@ucr.edu" <yuyu1@ucr.edu>

Dear Yu,

Thank you very much for your email, you are welcome to use your PLOS article "ARGONAUTE10 promotes the degradation of miR165/6 through the SDN1 and SDN2 exonucleases in Arabidopsis" in your PhD thesis and defence.

The article was published under a Creative Commons Attribution license (CC BY), further information about the terms of the license can be found at: http://journals.plos.org/plosbiology/s/content-license.

All of our articles are available (through our websites) for anyone to download, reuse, reprint, modify, distribute, and/or copy so long as the original authors and source are cited.
The appropriate citation is:
Yu Y, Ji L, Le BH, Zhai J, Chen J, Luscher E, et al. (2017) ARGONAUTE10 promotes the degradation of miR165/6 through the SDN1 and SDN2 exonucleases in Arabidopsis. PLoS Biol 15(2): e2001272. https://doi.org/10.1371/journal.pbio.2001272

Please let me know if you have any further questions or concerns.

Best wishes,

Georgie

PLOS I OPEN FOR DISCOVERY
Georgina Field I Publications Assistant, PLOS Biology
Carlyle House, Carlyle Road, Cambridge CB4 3DN | United Kingdom
plosbiology@plos.org I Phone +44 (0) 1223 442810
plos.org I plosbiology.org I Facebook I @PLOSBiology I Blog

California (U.S.) corporation #C2354500, based in San Francisco

Case Number: 05312594